ORNL/TM-8381/V1

Health and Safety Research Division

SPECIFIC ABSORBED FRACTIONS OF ENERGY AT VARIOUS AGES FROM INTERNAL PHOTON SOURCES. I. METHODS.

M. Cristy and K. F. Eckerman
Metabolism and Dosimetry Research Group

Date Completed: February 1987
Date Published: April 1987

NOTICE This document contains information of a preliminary nature. It is subject to revision or correction and therefore does not represent a final report.

Prepared by the
OAK RIDGE NATIONAL LABORATORY
Oak Ridge, Tennessee 37831
operated by
MARTIN MARIETTA ENERGY SYSTEMS, INC.
for the
U.S. DEPARTMENT OF ENERGY
Contract No. DE-AC05-840R21400

CONTENTS

VOLUME I. METHODS

LIST OF FIGURES v

LIST OF TABLES vii

ACKNOWLEDGMENTS ix

ABSTRACT xi

I. INTRODUCTION 1
REFERENCES FOR CHAPTER I 2

II. METHODS OF CALCULATING Φ 3
Monte Carlo Radiation Transport Computer Program 3
Point-source Kernel Method 3
Special Case: Active Marrow and Endosteal Tissues
as Target Organs 4
REFERENCES FOR CHAPTER II 7

III. THE RECIPROCAL DOSE PRINCIPLE, CORRECTION FACTORS FOR CONVERSE MONTE CARLO ESTIMATES OF a, AND CORRECTION FACTOR FOR POINT-SOURCE KERNEL ESTIMATES OF Φ 9
The Reciprocal Dose Principle 9
Correction Factors for Converse Monte Carlo Estimates of Φ 10
One organ is the whole skeleton 10
One organ is the lungs 10
One organ is the whole body 12
One organ is near the tissue-vacuum boundary 14
Correction Factors for Point-source Kernel Estimates of Φ 14
REFERENCES FOR CHAPTER III 18

IV. RECOMMENDED VALUES OF Φ 19
Procedures 19
Examples 21
Approximate Methods for Remaining Tissue Compartment
(Used for Muscle) 33
Special Problems 33
REFERENCES FOR CHAPTER IV35 . . . . . .

APPENDIX A DESCRIPTION OF THE MATHEMATICAL PHANTOMS 37

APPENDIX B SUMMARY OF ORGAN MASSES IN ALL PHANTOMS 77

APPENDIX C CENTROIDS OF ORGANS IN ALL PHANTOMS 85

APPENDIX D DOSE-RESPONSE FUNCTIONS FOR SOFT TISSUES OF THE SKELETON 91

LIST OF FIGURES

VOLUME I. METHODS

Figure Page

III-1. Mean ratio Φ(source←target) : Φ(target←source plotted against initial photon energy for source = whole skeleton 11

III-2. Mean ratio Φ(source←target) : Φ(target←source) plotted against initial photon energy for source =lungs 11

III-3. Mean ratio Φ(source←target) : Φ(target←source) plotted against initial photon energy for source = wholebody 12

III-4. Φ(target↔source) estimated by the point-source kernel method vs Φ(target←source) estimated by the Monte Carlo radiation transport method for selected organ pairs 15

III-5. Mean of ratio Φ(point-source kernel method) toΦ (Monte Carlo method) vs initial photon energy for selected data 16

IV-1. Φ vs energy for source organ = kidneys and target organ = spleen in the age 5 phantom 21

IV-2. Φ vs energy for source = spleen and target = uterus in the age-l 5-male/adult-female phantom 22

IV-3. Φ vs energy for source = upper large intestine contents and target = ovaries in the age 5 phantom 23

IV-4. Φ vs energy for source = adrenals and target = ovaries in the age 1 phantom 24

IV-5. Φ vs energy for source = pancreas and target = testes in the age l0 phantom 25

IV-6. Φ vs energy for source = lungs and target = breasts in the age-l5-male/adult-female phantom 26

IV-7. Φ vs energy for source = lungs and target = adrenals in the age 1 phantom 27

IV-8. Φ vs energy for source = whole skeleton and target = liver in the age l0 phantom 28

IV-9. Φ vs energy for source = active marrow and target = adrenals in the age 1 phantom 29

IV-10. Φ vs energy for source = whole skeleton and target = ovaries in the age-l 5-male/adult-female phantom 30

IV-11. Φ vs energy for source = urinary bladder contents and target = stomach wall in the age 1 phantom 31

IV-12. Φ vs energy for source = lower large intestine wall and target = urinary bladder wall in the age 5 phantom 32

IV-13. Φ vs energy for source = stomach contents and target = pancreas in the age-l 5-male/adult-female phantom 34

A-1. The "Adult male" phantom 40

A-2. External views of the phantoms and superimposed cross-sections within the middle trunk of the newborn and adult male phantoms, depicting the space from the bottom of the liver to the top of the liver 41

A-3. Anterior view of the principal organs in the head and trunk of the adult phantom developed by Snyder et al. (1974) 46

A-4. For the adult phantom of Snyder et al. (1974), the idealized model of the skeleton for computer calculations is shown on the left and a more realistic representation is shown on the right 49

D-1. Absorbed fractions in active marrow AM from a source of monoenergetic electrons distributed uniformly in the trabeculae TB or the active marrow of the lumbar vertebra and parietal bone of the adult 95

D-2. Components of the absorbed dose in marrow from photon radiations 99

D-3. Illustration of the effects of the microstructure of trabecular bone on energy deposition in active marrow for various bones of the adult skeleton 101

LIST OF TABLES

VOLUME I. METHODS

Table Page

II-1. Summary of descriptive parameters for the skeleton 5

III-1. Correction factors to be used when the reciprocity principle is invalid (for all phantoms except the newborn) 13

III-2. Correction factors to be used when the reciprocity principle is invalid (for the newborn phantom only) 13

III-3. Correction factors to be applied to point-source kernel estimates of Φ when Monte Carlo estimates are statistically unreliable (for all phantoms except the newborn) 17

III-4. Correction factors to be applied to point-source kernel estimates of Φ when Monte Carlo estimates are statistically unreliable (for the newborn phantom only) 17

IV-1. Organs defined as source and target regions in the Monte Carlo radiation transport and the point-source kernel computer codes 20

A-1. Elemental composition of the tissues for all phantoms except the newborn 42

A-2. Elemental composition of the newborn skeleton 43

A-3. Elemental composition of the newborn and adult whole body 44

A-4. Elemental composition of the tissues of the newborn 45

A-5. Weights of total marrow, active marrow, and inactive marrow in the body as a function of age 54

A-6. Active marrow in individual bones, parts of bones, or bone groups expressed as the percentage of active marrow in the body 55

A-7. Inactive marrow in individual bones, parts of bones, or bone groups expressed as the percentage of inactive marrow in the body 56

B-1. Tissue densities in g/cm^3 79

B-2. Comparison of whole-body masses 80

B-3. Summary of organ masses in all phantoms 81
C-1. Trunk heights of phantoms 87
C-2. Centroids of organs 88

D-1. Mean chord- and ray-lengths (µm) for trabeculae and marrow cavities in various bones 94

D-2. Absorbed fraction, φ, in active marrow, *AM*, and bone surface, *BS*, from a uniformly distributed source of monoenergetic electrons in trabeculae, *TB*, and marrow of the parietal bone and lumbar vertebra of a 44-year-old male 96

D-3. Absorbed fraction, φ, in active marrow, *AM*, and in bone surface, *BS*, from a uniformly distributed source of monoenergetic electrons in trabeculae, *TB*, and marrow space of the parietal bone and lumbar vertebra of a 20-month-old child 97

D-4. Absorbed dose in active marrow, *D(AM)*, per unit fluence, $\Psi(E)$, of monoenergetic photons in trabecular bones of the skeleton of a 44-year-old male 98

D-5. Absorbed dose in active marrow, *D(AM)*, and in bone surface, *D(BS)*, per unit fluence, $\Psi(E)$, of monoenergetic photons in the skeleton 100

ACKNOWLEDGMENTS

We would like to thank Dr. J. C. Ryman for assistance with the computer programming and Drs. R. W. Leggett, G. D. Kerr, and G. G. Killough for useful discussions throughout this investigation. This research was sponsored primarily by the Office of Health and Environmental Research, U.S. Department of Energy, under contract DE-AC05-840R21400 with Martin Marietta Energy Systems, Inc. Earlier work on the phantoms (see Appendix A of Volume 1 of these reports) was sponsored by the Office of Nuclear Regulatory Research, U.S. Nuclear Regulatory Commission; this and additional support from the U.S. Environmental Protection Agency, the U.S. Food and Drug Administration, the U.S. Department of Transportation, and other offices within the Nuclear Regulatory Commission have been critical to the development of our research program and are also gratefully acknowledged.

ABSTRACT

This report is the second volume of a series in which specific absorbed fractions (Φ's) in various organs of the body ("target organs") from sources of monoenergetic photons in various other organs ("source organs") are tabulated. This volume outlines various methods used to compute the Φ-values and describes how the "best" estimates recommended by us are chosen. In companion volumes Φ-values are tabulated for the newborn, for ages 1, 5, 10, and 15 years, for an adult female, and for an adult male. These Φ-values can be used in calculating the photon component of the dose-equivalent rate in a given target organ from a given radionuclide that is present in a given source organ. The methods used to calculate Φ are similar to those used by Snyder et al. (1974) for an adult. However, an important difference involves the dosimetry for radiosensitive tissues in the skeleton. The International Commission on Radiological Protection recognizes, in the radiation protection system of its Publication 26 (1977), that the endosteal, or "bone surface," cells are the tissue at risk for bone cancer. We have applied the dosimetry methods that Spiers and co-workers developed for beta-emitting radionuclides deposited in bone to follow the transport of secondary electrons (freed by photon interactions) through the microscopic structure of the skeleton. With these methods we can estimate Φ in the endosteal cells and can better estimate Φ in the active marrow; the latter is overestimated with the methods of Snyder et al. at photon energies below 200 keV.

CHAPTER I. INTRODUCTION

This report outlines the methods used to compute specific absorbed fractions (Φ's) in various organs of the body ("target organs") from sources of monoenergetic photons in various other organs ("source organs"). These Φ-values can be used in calculating the photon component of the dose-equivalent rate in a given target organ from a given radionuclide that is present in a given source organ. In addition, this report describes the procedures used in choosing the "best" estimate of Φ from the estimates generated by several methods for a given source-target pair. The Φ-values calculated by these methods and the "best" estimates recommended by us will be published in companion volumes (Cristy and Eckerman 1987a-f) for the newborn, for ages 1, 5, 10, and 15 years, for an adult female, and for an adult male.

The methods used to calculate Φ are similar to those used by Snyder, Ford, Warner, and Watson (1974) for an adult. Simple equations describing the geometry of the body and its organs ("mathematical phantoms") are used (1) with a computer program that simulates radiation transport with Monte Carlo methods or (2) with a computer program that integrates the point-source kernel equation (including buildup) over the volumes of the source and target organs. The source of the photons is assumed to be distributed uniformly in a given source organ, and Φ is averaged over the volume of the target organ. The most important difference between our work and that of Snyder et al. involves the dosimetry for radiosensitive tissues in the skeleton. The International Commission on Radiological Protection recognizes, in the radiation protection system of its Publication 26 (1977), that the endosteal, or "bone surface," cells are the tissue at risk for bone cancer. We have applied the dosimetry methods that Spiers and co-workers developed for beta-emitting radionuclides deposited in bone to follow the transport of secondary electrons (freed by photon interactions) through the microscopic structure of the skeleton. With these methods we can estimate Φ in the endosteal cells and can better estimate Φ in the active marrow; the latter is overestimated with the methods of Snyder et al. at photon energies below 200 keV. Also, we have made more use of the converse Monte Carlo estimate, Φ(source organ$\leftarrow$target organ), as an approximation to the direct Monte Carlo estimate, Φ(target organ$\leftarrow$source organ), sometimes in conjunction with a correction factor; and we have made more extensive use of empirical correction factors for the estimates generated by the point-source kernel method. These methods are discussed in chapters II and III.

The mathematical phantoms used in our work are designed like the adult phantom of Snyder et al. (1974) and have different densities and chemical compositions for lung, skeletal, and soft tissues. (The term "soft tissues" will be used herein for all near-unit-density tissues, i.e., density $\simeq$ 1 g/cm^3.) These phantoms have been described by Cristy (1980), but several changes have been made in our phantoms since the 1980 report: (1) the age 15 phantom of Cristy (1980) has been redesigned so that it now represents both a 15-year-old male and an adult female; (2) the adult phantom of Cristy (1980) has been modified slightly and is now labeled "adult male," although it is hermaphroditic and could also represent a larger than average adult female; (3) the densities and chemical compositions of the tissues have been changed in all of the phantoms; and (4) the densities and compositions of the skeletal and soft tissues of the newborn phantom are now different from those at other ages. The equations describing the phantoms, as amended, and the newer data on densities and compositions are given in Appendix A. The masses of the organs and their centroids are given in Appendices B and C, respectively.

REFERENCES FOR CHAPTER I

Cristy, M. 1980. *Mathematical phantoms representing children of various ages for use in estimates of internal dose*. U.S. Nuclear Regulatory Commission Rep. NUREG/CR-1159 (also Oak Ridge National Laboratory Rep. ORNL/NUREG/TM-367).

Cristy, M., and Eckerman, K.F. 1987a. *Specific absorbed fractions of energy at various ages from internal photon sources. II. One-year-old.* Oak Ridge National Laboratory Rep. ORNL/TM-8381:Vol. 2.

—1987b. *Specific absorbed fractions of energy at various ages from internal photon sources. III. Five-year-old.* Oak Ridge National Laboratory Rep. ORNL/TM-8381:Vol. 3.

—1987c. *Specific absorbed fractions of energy at various ages from internal photon sources. IV. Ten-year-old.* Oak Ridge National Laboratory Rep. ORNL/TM-8381:Vol. 4.

—1987d. *Specific absorbed fractions of energy at various ages from internal photon sources. V. Fifteen-year-old male and adult female.* Oak Ridge National Laboratory Rep. ORNL/TM-8381:Vol. 5.

—1987e. *Specific absorbed fractions of energy at various ages from internal photon sources. VI. Newborn.* Oak Ridge National Laboratory Rep. ORNL/TM-8381:Vol. 6.

—1987f. *Specific absorbed fractions of energy at various ages from internal photon sources. VII. Adult male.* Oak Ridge National Laboratory Rep. ORNL/TM-8381:Vol. 7.

ICRP 1977. Recommendations of the International Commission on Radiological Protection. ICRP Publication 26. *Annals of the ICRP* 1: No. 3.

Snyder, W.S., Ford, M.R., Warner, G.G., and Watson, S.B. 1974. *A tabulation of dose equivalent per microcurie-day for source and target organs of an adult for various radionuclides: Part 1*. Oak Ridge National Laboratory Rep. ORNL-5000.

CHAPTER II. METHODS OF CALCULATING Φ

Three methods are used to calculate the specific absorbed fraction for a given source organ-target organ pair at a given initial photon energy: (1) Φ(target←source) is calculated with the Monte Carlo radiation transport computer program; (2) Φ(source←target) is calculated with the Monte Carlo computer program, and this value is used to estimate Φ(target←source), sometimes after applying a correction factor as explained in Chapter III; and (3) Φ(target↔source) is calculated with the point-source kernel method, and a correction factor may also be applied to this estimate (see Chapter III). For the special case of the active marrow or the endosteal cells as the target organ, another method is employed, which is a refinement of method (1).

Monte Carlo Radiation Transport Computer Program

A computer program, employing Monte Carlo techniques similar to that of Snyder et al. (1974), simulates the transport of photons of any given initial energy originating in a given organ (source organ). The source of the photons is assumed to be uniformly distributed in the source organ. The specific absorbed fraction, i.e., the energy absorbed in another organ (target organ), normalized as the fraction of emitted energy and per kilogram of target organ, is calculated, and the statistical reliability of the Φ-value is calculated as a coefficient of variation. The details of the method and the computer program may be found in Ryman, Warner, and Eckerman (1987a).

For a given source-target pair, we obtain two numbers: the direct estimate, Φ(target←source), obtained when the photons originate in the organ labeled "source," and the converse estimate, Φ(source←target), obtained when the photons originate in the organ labeled "target." Each of these numbers is from a Monte Carlo computer run: what is labeled the direct estimate and what is labeled the converse estimate depend upon which organ we label the target organ. For most source-target pairs, the converse estimate is a good approximation to the direct estimate; and for those pairs in which it is not, we have developed correction factors (see Chapter III).

Point-source Kernel Method

In this method, the equation describing the absorption of energy at a distance r from a point source of monoenergetic photons in an infinite homogeneous medium (water) is employed:

$$\Phi(r) = \frac{\mu_{en}}{\rho} \bullet \frac{1}{4\pi r^2} \bullet e^{-\mu r} \bullet B(\mu r),$$

where

$\Phi(r)$ = point isotropic specific absorbed fraction at r,
μ_{en} = linear energy-absorption coefficient at the source energy,
μ = linear attenuation coefficient at the source energy,
ρ = density of medium,
$B(\mu r)$ = buildup factor, a factor representing the contribution of the scattered radiation to the energy absorption.

The $B(\mu r)$ formulation for point photon sources in water have been published by Spencer and Simmons (1973).

This equation is integrated over the volumes of the source and target organs, using numerical methods, to yield Φ(target↔source). Note the double-ended arrow: the conditions of the reciprocal dose theorem (Loevinger 1969) are met, and the reciprocal doses are exactly equal.

In this method, the phantoms are composed of water throughout and are embedded in an infinite water medium. In the Monte Carlo radiation transport method, the phantoms have different densities and chemical compositions for lung, skeletal, and soft tissue and are embedded in vacuum. Thus there may be systematic errors in the point-source kernel estimates of Φ. These errors may be reduced by applying empirical correction factors, developed in Chapter III. Point-source kernel estimates are necessary only when the Monte Carlo estimates are statistically unreliable.

Details of the point-source kernel computer program are given in Ryman, Warner, and Eckerman (1987b).

Special Case:
Active Marrow and Endosteal Tissues as Target Organs

In calculating the specific absorbed fraction in a target organ, we assume that the energy transferred to electrons by the photon interactions is absorbed by the organ in which the interaction occurred, i.e., the transport of energy by secondary electrons is not treated. This approach is reasonable if the amount of energy transported by secondary electrons out of the region of interest is balanced by transport into the region, i.e., electronic equilibrium exists. However, in the vicinity of discontinuities in tissue compositions, electronic equilibrium is not established and significant error in dose estimation may be introduced in assuming equilibrium. Examples of discontinuities in the body are the boundaries between skin and the surrounding air, between tissue and air voids within the respiratory tract, and between bone and soft tissue regions of the skeleton. It is this latter boundary we address here.

In each phantom the skeleton is represented as a uniform mixture of its component tissues, namely cortical bone, trabecular bone, fatty marrow, active (hematopoietic) marrow, and various connective tissues (see Table II-l). The tissues of interest for dosimetric purposes (target regions) are the active marrow, which lies within the cavities of trabecular bone, and osteogenic cells adjacent to the surfaces of both cortical and trabecular bone; this latter target is referred to as endosteal tissue or "bone surfaces". To estimate the energy deposited in these targets, one must consider the energy transported by secondary electrons arising from photon interactions within the target and from electrons entering the target from interactions occurring in the immediate vicinity, e.g., bone adjacent to the active marrow.

A number of investigators (Spiers 1949, 1951; Woodard and Spiers 1953; Charlton and Cormack 1962; Aspin and Johns 1963; Howarth 1965), using simple geometrical models (e.g., thin slabs, cylinders, and spherical cavities) to approximate the geometry, have demonstrated that for photon energies less than about 200 keV electronic equilibrium does not exist and electrons liberated in bone mineral contribute substantially to the absorbed dose in soft tissues of the skeleton. Snyder, Ford, and Warner (1978) encountered the intractable geometry of the skeleton in their Monte Carlo studies of photon transport and formulated their calculation of absorbed dose in marrow in a conservative manner. They partitioned the energy deposited in the skeleton to various skeletal tissues, including active marrow, according to the fraction of the skeletal mass attributed to the tissue. The potential for an overestimate of absorbed dose in the active marrow was noted by them (p. 20):

> “ . . . it is assumed that the marrow absorbs energy per gram as efficiently as does bone. This assumption is not grossly wrong at energies of 200 keV or more, but is increasingly inaccurate at energies below 100 keV. The effect is to somewhat overestimate the dose to marrow and to somewhat underestimate the dose to bone. This difficulty results from the failure to find ways to program the intricate mixture of bone and marrow spaces in a more realistic fashion.”

Table II-1. Summary of descriptive parameters for the skeleton

Descriptive parameter	Age (yr) 0	1	5	10	15	Adult
Skeleton[a]						
Volume (cm^3)	288	813	1935	3309	5466	7155
Mass (kg)	0.351	1.140	2.710	4.630	7.650	10.0
Density (g/cm^3)	1.22	1.40	1.40	1.40	1.40	1.40
Bone mineral						
Calcium[b] (g)	28	99.8	219	396	806	1000
Mass[c] (kg)	0.140	0.499	1.095	1.980	4.030	5.000
Fraction[d]	0.399	0.438	0.404	0.427	0.527	0.500
Active marrow						
Mass[a] (kg)	0.047	0.150	0.320	0.610	1.050	1.120
Fraction[d]	0.134	0.132	0.118	0.132	0.137	0.112
Inactive marrow						
Mass[a] (kg)	—	0.020	0.140	0.590	1.550	2.380
Fraction[d]	—	0.018	0.052	0.127	0.203	0.238
Other tissues[e]						
Mass (kg)	0.164	0.469	1.154	1.453	1.022	1.5
Fraction[d]	0.467	0.412	0.426	0.314	0.133	0.150
Trabecular bone[f]						
Mass (kg)	0.140	0.200	0.219	0.396	0.806	1.000
Fraction[d]	0.176	0.438	0.081	0.085	0.105	0.100
S/V[g] (cm^2/cm^3)	—	220	—	225	—	190
Cortical bone[e]						
Mass (kg)	—	0.299	0.875	1.584	3.224	4.000
Fraction[d]	—	0.263	0.323	0.342	0.421	0.400
Surface area (m^2)						
Trabecular[h]	1.5	2.1	2.3	4.2	8.5	6.0
Cortical[i]	—	0.45	1.3	2.4	4.8	6.0
Total	1.5	2.6	3.6	6.6	13	12

[a]See Appendix B; data for ages 15 and adult are for males.
[b]See Leggett et al. 1982.
[c]Computed assuming 0.2 grams of calcium per gram bone mineral.
[d]Mass fraction in the skeleton.
[e]Difference between skeletal mass and identified tissues.
[f]All bone is assumed to be trabecular at birth; 40% at one year, 20% thereafter.
[g]Surface to volume ratio (from Table 5 of Beddoe 1978).
[h]Based on trabecular bone mass and *S/V* ratio of 220 through age 10, 190 at age 15, and 120 for the adult.
[i]The adult *S/V* ratio for cortical bone was applied to all ages.

The overestimate of the dose to active marrow with this assumption can be as much as 300-400% for photon energies less than 100 keV.

The consideration of osteogenic cells as the target tissue for bone cancer (ICRP 1977) and the overestimate of the dose to the active marrow required a new computational approach which formulated the absorbed dose in terms of the relevant physical and anatomical variables governing the energy deposition. The geometry problem, noted by Snyder and co-workers, is also encountered in the dosimetry of beta-emitting radionuclides incorporated in bone, for which Spiers and co-workers reduced the intractable three-dimensional geometry to one dimension through use of measured distributions of chord lengths in trabeculae and marrow cavities of trabecular bone (Spiers 1969; Beddoe, Darley, and Spiers 1976; Beddoe 1977). We have applied Spiers' methodology to secondary electrons liberated by photon interactions in the skeleton. Although the new computational approach uses information on the microscopic structure of bone to follow **electron transport**, it was possible to retain the homogeneous representation of the skeleton in the Monte Carlo calculations of **photon transport**. Thus, only minor revisions were made to the Monte Carlo transport code.

The absorbed dose from photon radiation varies, of course, with the number of photons passing through the region. In the discussion below we refer to the "dose per unit fluence" as a response function, *R*, and assume that such functions can be constructed to define the absorbed dose in the active marrow (or in the endosteal tissue) per unit fluence of photons in the skeleton. The derivation of the response functions is presented in Appendix D. The Monte Carlo transport code was modified to estimate the photon fluence and to score the absorbed dose in the active marrow and endosteal tissues based on the fluence and the response functions. The photon fluence $\Psi(E)$ in a region of volume V can be related to the number $N(E)$ of interactions occurring at energy E, calculated for the region;

$$\Psi(E) = \frac{N(E)}{\mu(E)V} \quad . \tag{1}$$

For an individual photon history *i*, the contribution to the absorbed dose is scored as

$$D_i = \frac{1}{V} \sum_{j=1}^{N_i} \frac{wt_j}{\mu(E_j)} = R(E_j) \quad , \tag{2}$$

where

j indexes the collisions in region V experienced by the ith photon,
V is the volume of the region over which the fluence is averaged,
wt_j is the statistical weight* of the photon entering the $_j$th collision,
$\mu(E_j)$ is the linear attentuation coefficient at energy E_j, and
$R(E_j)$ is the absorbed dose per unit fluence.

The specific absorbed fraction in the target region T is calculated from the computed absorbed dose for the emission of m monoenergetic photons within source organ S as

$$\Phi(T \leftarrow S) = \frac{1}{mE_S} \sum_i D_i \tag{3}$$

where E_s is the initial energy of each photon emitted from S. If D is expressed in gray and E_s in joule, then Φ has units of kg $^{-1}$.

In developing the above procedure we found it necessary to consider two response functions for the active marrow. One function pertains to marrow within the skull (a somewhat atypical trabecu-

---

* In simulating the transport of photons it is useful to allow photons to continue undergoing scattering events rather than be absorbed. A statistical weight of one is initially assigned to the photon and at each collision the weight is reduced by the probability that the collision was a scattering event. Thus the statistical weight after j collisions may be thought of as the probability of that particular photon existing. The number of collisions in region V for the ith photon history is simply $\sum_j wt_j$.

lar bone) and the other addresses all other active marrow sites. A single response function was found to be adequate for the endosteal tissue.

REFERENCES FOR CHAPTER II

Aspin, N., and Johns, H.E. 1963. The absorbed dose in cylindrical cavities within irradiated bone. *Brit. J. Radiol*. 36: 350-362.

Beddoe, A.H. 1977. Measurements of the microscopic structure of cortical bone. *Phys. Med. Biol*. 22: 298-308.

Beddoe, A.H. 1978. A quantitative study of the structure of trabecular bone in man, rhesus monkey, beagle, and miniature pig. *Calcif Tiss. Res*. 25: 273-28 1.

Beddoe, A.H., Darley, P.J., and Spiers, F.W. 1976. Measurements of trabecular bone structure in man. *Phys. Med. Biol*. 21: 589-607.

Charlton, D.E., and Cormack, D.V. 1962. Energy dissipation in finite cavities. *Radiat. Res*. 17: 34-49.

Howarth, J.L. 1965. Calculation of the absorbed dose in soft-tissue cavities in bone irradiated by X-rays. *Radiat. Res*. 24: 158-183.

ICRP 1977. Recommendations of the International Commission on Radiological Protection. ICRP Publication 26. *Annals of the ICRP* 1: No. 3.

Leggett, R.W., Eckerman, K.F., and Williams, L.R. 1982. Strontium-90 in bone: A case study in age-dependent dosimetric modelling. *Health Phys*. 43: 307-322.

Loevinger, R. 1969. Distributed radionuclide sources. In *Radiation dosimetry*, 2nd edition, Vol. III, eds. F.H. Attix and E. Tochilin, pp. 51-90. New York: Academic Press.

Ryman, J.C., Warner, G.G., and Eckerman, K.F. 1987a. *ALGAMP—a Monte Carlo radiation transport code for calculating specific absorbed fractions of energy from internal or external photon sources. Oak* Ridge National Laboratory Rep. ORNL/TM-8377 (in preparation).

—— 1987b. *Computer codes for calculating specific absorbed fractions of energy from internal photon sources by the point-source kernel method*. Oak Ridge National Laboratory Rep. ORNL/TM-8378 (in preparation).

Snyder, W.S., Ford, M.R., and Warner, G.G. 1978. *Estimates of specific absorbed fractions for photon sources uniformly distributed in various organs of a heterogeneous phantom*. MIRD Pamphlet No. 5, Revised. New York: Society of Nuclear Medicine.

Snyder, W.S., Ford, M.R., Warner, G.G., and Watson, S.B. 1974. *A tabulation of dose equivalent per microcurie-day for source and target organs of an adult for various radionuclides: Part 1*. Oak Ridge National Laboratory Rep. ORNL-5000.

Spencer, L.V., and Simmons, G.L. 1973. Improved moment method calculations of gamma-ray transport: application to point isotropic sources in water. *Nucl. Sci. Eng*. 50: 20-31.

Spiers, F.W. 1949. The influence of energy absorption and electron range on dosage in irradiated bone. *Brit. J. Radiol*. 22: 521-533.

Spiers, F.W. 1951. Dosage in irradiated soft tissue and bone. *Brit. J. Radiol*. 24: 365-369.

Spiers, F.W. 1969. Beta dosimetry in trabecular bone. In: *Delayed effects of bone-seeking radionuclides*, eds. C.W. Mays et al., pp. 95-108. Salt Lake City: Univ. Utah Press.

Woodard, H.Q., and Spiers, F.W. 1953. The effect of X-rays of different qualities on the alkaline phosphates of living mouse bone. *Brit. J. Radiol*. 26: 38-46.

CHAPTER III. THE RECIPROCAL DOSE PRINCIPLE, CORRECTION FACTORS FOR CONVERSE MONTE CARLO ESTIMATES OF Φ, AND CORRECTION FACTORS FOR POINT-SOURCE KERNEL ESTIMATES OF Φ

As mentioned in the preceding chapters, we have made more use of the reciprocal dose principle [i.e., use of the converse Monte Carlo estimate, Φ(source organ←target organ), as an approximation to the direct Monte Carlo estimate, Φ(target organ←source organ)] than did previous workers (e.g., Snyder et al. 1974). We have also made more extensive use of correction factors for the converse Monte Carlo estimate (when the reciprocal dose principle does not apply) and correction factors for point-source kernel estimates of Φ (when the Monte Carlo estimates are statistically unreliable).

The Reciprocal Dose Principle

According to a review by Loevinger (1969), a reciprocity theorem holds rigorously for certain sets of conditions (models) under which absorbed dose calculations may be done. He states (p. 66): "For any pair of regions in a uniform isotropic or uniform scatterless model, the specific absorbed fraction is independent of which region is designated source and which is designated target. In symbols,

$$\Phi_i\,(r_1 \leftarrow r_2) = \Phi_i(r_2 \leftarrow r_1) = \Phi_i(r_1 \leftrightarrow r_2),\text{"}$$

where $\Phi_i(r_1 \leftarrow r_2)$ is the specific absorbed fraction in region r_1 from emissions of radiation type i in region r_2. The double-ended arrow indicates that either region can be target or source.

Loevinger defined these models as follows (p. 61): In **the uniform isotropic model**, the "source activity is assumed uniformly distributed in regions of an infinite, homogeneous material of constant mass density." In **the uniform scatterless model**, the "source concentration is assumed uniform (i.e., constant) throughout the source regions of a material in which the radiation is absorbed without scatter or buildup;" the size, composition, and mass density of the material are arbitrary, and the mass density may vary within the material as long as the elemental composition is the same throughout. He also defined another model, **the uniform homogeneous model of finite size**, for which the reciprocity theorem does not hold rigorously but is used in many absorbed dose calculations. In this model, the "source activity is assumed uniformly distributed in a volume of homogeneous material of constant mass density, the volume being surrounded by empty space." Scattering is allowed in the uniform isotropic model and the uniform homogeneous model of finite size.

The long-known reciprocity relationships due to Mayneord (1945) and King (1912) are a special case of the uniform scatterless model (i.e., with constant source and target densities). The reciprocity theorem has often been stated in terms of absorbed dose (e.g., Loevinger, Japha, and Brownell, 1956), but is now commonly stated in terms of the specific absorbed fraction because of the formalism currently used in absorbed dose calculations (see Loevinger and Berman, 1976; ICRU, 1979).

The potential usefulness of the reciprocity theorem in estimating Φ in body organs from photon radiation is great: for small target organs like the ovaries, a Monte Carlo estimate of Φ(target←source) is often statistically unreliable, whereas a similar estimate of the converse value, Φ(source←target), may be reliable. In general, the use of a weighted average of the two Φ-estimates, each weighted according to the inverse of its variance, should improve the reliability of the estimated Φ.

For the human body and for our representation of the human body, the conditions of the theorem are not completely satisfied. The phantoms contain different absorbing media representing skeleton, lungs, and soft tissues, and in the Monte Carlo transport calculations (which include scattering) the phantoms are embedded in a vacuum, so that there is a tissue-vacuum boundary. Hence the reciprocity **theorem** does not apply. However, Cristy (1983) has shown that for most organ pairs in these heterogeneous phantoms the reciprocal Φ-values from photon radiation are approximately equal, and in these cases we speak of the reciprocity **principle**. Cristy concluded: (1) when both source and target organs are soft-tissue (near-unit-density) organs the reciprocity principle is probably valid within 10% and may even be substantially better than that; (2) when one of the organs is near the tissue-vacuum boundary (skin, breasts, or testes) the reciprocal Φ-values may differ by as much as 10% or so when scattering is marked (e.g., initial photon energy of 100 keV) but appear to differ substantially less than this at photon energies where there is less scattering; (3) when one of the organs is the lungs or the whole body, a difference of up to 12% may occur at some energies; and (4) when one of the organs is the skeleton, the principle is invalid at energies of 10-200 keV, with reciprocal Φ-values differing by as much as a factor of 4.

Correction Factors for Converse Monte Carlo Estimates of Φ

For organ pairs where the reciprocity principle does not apply and where the expected difference between the direct and the converse Monte Carlo estimates of Φ is well documented, we have developed correction factors to be applied to the converse estimate (Tables III-1 and III-2). The following shows how these correction factors were derived.

One organ is the whole skeleton

In Fig. III-1 is shown the mean of the ratio Φ(source←target) : Φ(target←source) and its 95% confidence limits as a function of initial photon energy for the whole skeleton as the source organ and all soft-tissue organs as targets. Data from four phantoms were combined (ages 1, 5, and 10 phantoms and the age-15-male/adult-female phantom; results from the adult male phantom were not available when this analysis was done, and the newborn phantom has different elemental compositions and densities for skeletal and soft tissues-see Appendix A). The data include only those organ pairs for which the coefficent of variation (C.V.) of each Φ-estimate was less than 10% (using data with a larger C.V. gave similar results, except that the confidence limits were wider). Note that the reciprocity principle holds well at energies of 500-4000 keV, but not at energies of 10-200 keV.

The Φ-values at the lower energies differ because of the differences in the mass absorption coefficients of skeletal tissue and soft tissue. The ratio of these (μ_a/ρ)-values as a function of energy are also plotted in Fig. III-1. At energies of 10-50 and 500-4000 keV the ratios of Φ-values are in good agreement with the ratios of the mass absorption coefficients. At **initial** photon energies of 100-200 keV, they diverge because the ratio of mass absorption coefficients is changing rapidly at energies just below 100-200 keV and thus the contribution to Φ from lower-energy scattered photons causes a breakdown in this simple comparison. Thus for correction factors we have adopted the ratio of absorption coefficients at initial energies of 10-50 and 500-4000 keV and the mean Φ-ratios at 100-200 keV; they are given in Table III-1. Correction factors for the newborn phantom were derived in a similar way and are given in Table III-2.

One organ is the lungs

In Fig. III-2 is shown a similar plot for the lungs as the source organ. Here the reciprocity principle seems to hold well at energies of 100-4000 keV. There is a systematic error at energies below

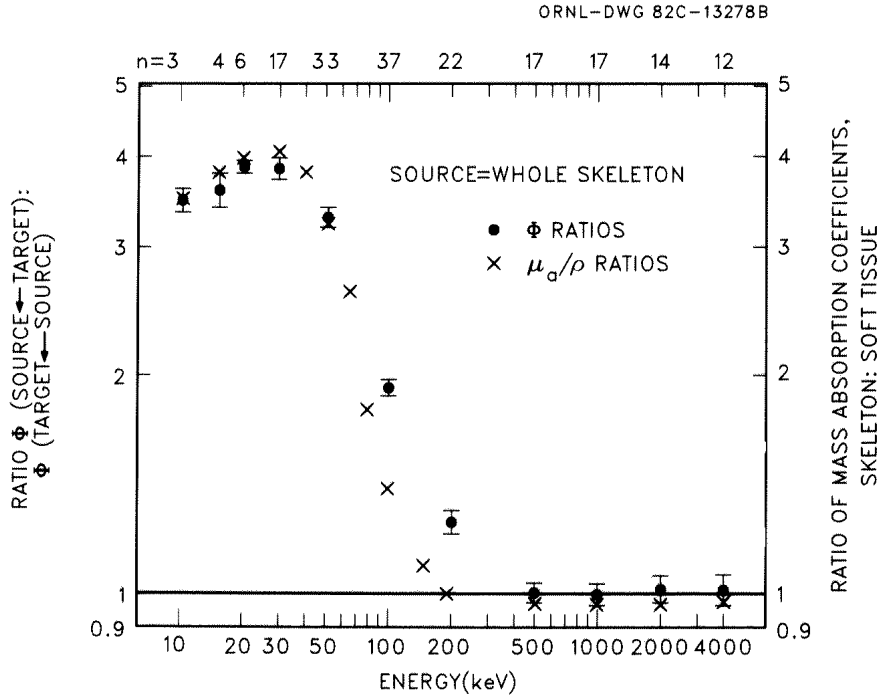

Fig. III-l. Mean ratio Φ(source→target) : Φ(target→source) plotted against initial photon energy for source = whole skeleton. Error bars indicate 95% confidence limits. Target organs are all soft-tissue organs. Data from four phantoms (age 1, 5, and 10 phantoms and the age-15-male/adult-female phantom) are combined. Data include only those organ pairs for which the C.V. of both Φ-estimates were less than 10%. The number of data meeting this criterion at each energy (n) is indicated. Also plotted for comparison is the ratio of the mass absorption coefficients, $(\mu_a/\rho)_{\text{skeletal tissue}}$: $(\mu_a/\rho)_{\text{soft tissue}}$. From Cristy (1983).

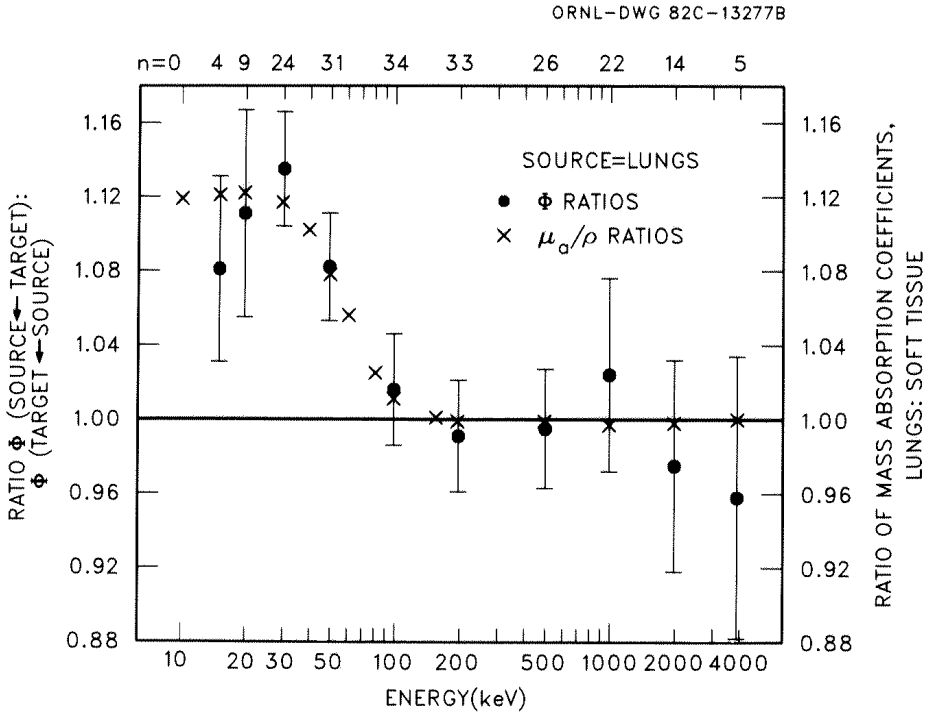

Fig. III-2. Mean ratio Φ(source→target) : Φ(target→source) plotted against initial photon energy for source = lungs. Target organs are all soft-tissue organs. Also plotted is the ratio of the mass absorption coefficient for lung tissue to that for soft tissue. See legend of Fig. III-1 for further explanation. From Cristy (1983).

100 keV because of the difference between the absorption coefficients of lung and soft tissue, but it is small (<15%).

Thus for initial energies of 500-4000 keV, the body is like the uniform homogeneous model of finite size, and the principle holds well when either the whole skeleton or the lungs is one of the organs considered. For initial energies below about 30 keV, the photoelectric effect dominates and the body is like the uniform scatterless model except for the differences in the absorption coefficients.

Correction factors for the lungs are based on the ratio of absorption coefficients and are given in Table III-1. Similarly derived correction factors for the newborn are given in Table III-2.

One organ is the whole body

In Fig. III-3 is shown a similar plot for the whole body as the source organ. The reciprocity principle seems to hold well at energies of 200-4000 keV. There is a systematic error at energies of 20-100 keV, but again it is small (<15%). Here the comparison with the ratio of absorption coefficients is misleading at low energies. The absorption coefficient for “whole body” is a weighted average of the coefficients for soft tissue, lungs, and skeleton, i.e., a homogenized whole body. At low energies, a disproportionate amount of the energy absorbed in the whole body from photons originating in a soft-tissue organ is absorbed in that organ itself and surrounding soft tissues. At 10-15 keV both Φ-values are approaching the limiting value of 1/(mass of whole body). Thus use of a "whole body absorption coefficient" below about 100 keV would lead to erroneous results. Correction factors for whole body are based on the mean Φ-ratios only and are given in Table III-1. The mean Φ-ratios for the newborn phantom were within statistical error of those for the other phantoms, and so the same correction factors are used (Table III-2).

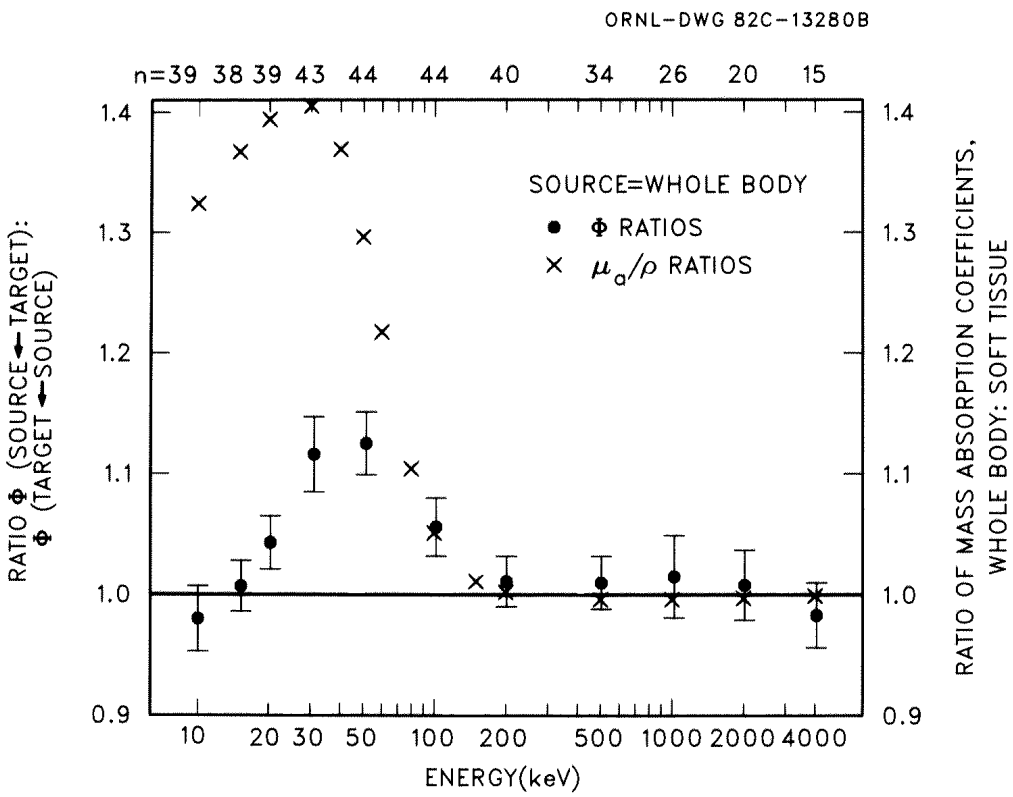

Fig. III-3. Mean ratio Φ(source→target) : Φ(target→source) plotted againat initial photon energy for = whole body. Target organs are all soft-tissue organs. Also plotted is the ratio of the mass absorption coefficient for a homogenized whole body to that for soft tissue. See legend of Fig. III-1 for further explanation. From Cristy (1983).

Table III-1. Correction factors to be used when the reciprocity principle is invalid (for all phantoms except the newborn). Organ *X* is a soft-tissue organ.

Energy (keV)	Φ(skeleton←*X*) / Φ(*X*←skeleton)	Φ(lungs←*X*) / Φ(*X*←lungs)	Φ(whole body←*X*) / Φ(*X*←whole body)
10	3.5[a]	1.12	1.00
15	3.8	1.12	1.00
20	4.0	1.12	1.04
30	4.1	1.12	1.12
50	3.3	1.08	1.12
100	2.0	1.00	1.06
200	1.3	1.00	1.00
500	1.0	1.00	1.00
1000	1.0	1.00	1.00
2000	1.0	1.00	1.00
4000	1.0	1.00	1.00

[a]Correction factors derived for the whole skeleton and for the active marrow were almost identical. The correction factors in this column are averages of the two, and they may also be used for the inactive marrow. In practice, these correction factors are useful only when the whole skeleton, the active marrow, or the inactive marrow is considered the source organ, since other methods are use to compute Φ's for the endosteal cells of the skeleton and the active marrow as target organs. Note: for active marrow the numerator, Φ(active marrow←*X*), is the value calculated by the old way in the Monte Carlo computer program, i.e., by the way done by Snyder et al. (1974), rather than by the special methods outlined in the section "Special Case: Active Marrow and Endosteal Cells as Target Organs" in Chapter II. Wherever data for active marrow as a target organ are tabulated in the companion volumes (Cristy and Eckerman 1987a-f), the values of Φ are those calculated by the old way in the **tables of raw data** (because it is useful in estimating the converse Φ-value) but the values of Φ in the **tables of recommended values** are those calculated by the special methods.

Table III-2. Correction factors to be used when the reciprocity principle is invalid (for the newborn phantom only). Organ *X* is a soft-tissue organ.

Energy (keV)	Φ(skeleton←*X*) / Φ(*X*←skeleton)	Φ(lungs←*X*) / Φ(*X*←lungs)	Φ(whole body←*X*) / Φ(*X*←whole body)
10	2.8[a]	1.05	1.00[b]
15	3.1	1.05	1.00
20	3.2	1.05	1.04
30	3.3	1.05	1.12
50	2.8	1.03	1.12
100	1.6	1.00	1.06
200	1.1	1.00	1.00
500	1.0	1.00	1.00
1000	1.0	1.00	1.00
2000	1.0	1.00	1.00
4000	1.0	1.00	1.00

[a]Correction factors derived for the whole skeleton and for the active marrow were almost identical. The correction factors in this column are averages of the two. See footnote in Table III-1 for further explanation.

[b]The correction factors for whole body were within statistical error of those for the other phantoms, so the latter were adopted.

One organ is near the tissue-vacuum boundary

No correction factors are used when one of the organs is near the tissue-vacuum boundary, for two reasons: (1) the error is at most about 10% and this occurs only at energies where scattering is substantial, and (2) the quality of the data estimating the error is not as good at most energies as in the cases above (see Cristy, 1983).

Correction Factors for Point-source Kernel Estimates of Φ

When neither of the two reciprocal Monte Carlo estimates of Φ is statistically reliable for a given source-target pair, the estimate of Φ by the point-source kernel method must be used. This occurs in general when the target organ is small and distant from the source organ, and more often at the lower and higher photon energies.

For the point-source kernel method, each phantom is composed of water throughout and embedded in the same medium of infinite extent. Therefore systematic differences between the Monte Carlo and point-source kernel estimates are to be expected, and the magnitude of the difference may depend on the distance of separation of the two organs.

Snyder et al. (1974) developed "rule-of-thumb" correction factors to be applied to the point-source kernel estimate if the source organ was the whole skeleton or the lungs or if the target organ was the whole skeleton. These correction factors were not rigorous, but they did "generally improve the correspondence of the two estimates" (p. 64). We develop here a more extensive set of correction factors by methods also not completely rigorous, but which are improvements over those developed by Snyder and co-workers.

In Fig. III-4 is shown a plot of Φ(target↔source) estimated by the point-source kernel method against Φ(target←source) estimated by the Monte Carlo method for selected soft-tissue organ pairs. For all organ pairs the target organ was a small organ (adrenals, gall bladder wall, ovaries, thymus, thyroid, or uterus), chosen to be typical of cases where the statistics of the Monte Carlo estimate are likely to be poor. The initial photon energy was 100 keV, and data from four phantoms were combined.

The point-source kernel estimate tended to be greater than the Monte Carlo estimate. The difference was larger for smaller Φ-values; it is probably a function of distance.

The C.V.'s of the point-source kernel estimates were always less than 1.2%, and the symbols in Fig. III-4 indicate the magnitude of the C.V.'s of the Monte Carlo estimates. The magnitude of the difference between the two Φ-estimates was also correlated with the C.V. of the Monte Carlo estimate, since this C.V. is correlated with Φ and distance of separation for small target organs. For example, the ratio Φ(point-source kernel method) : Φ(Monte Carlo method) had a mean of 1.15 (95% confidence interval 1.11-1.18; n=64) for the more reliable Monte Carlo estimates (C.V. <10%), and the ratio had a mean of 1.75 (95% confidence interval 1.59-1.93; n=58) for the less reliable Monte Carlo estimates (C.V. between 30% and 50%). This phenomenon was seen at all energies, but it was most pronounced at 100 and 200 keV.

As a correction factor, the larger of the two ratios above would be more appropriate for our purpose, since it is the less reliable Monte Carlo estimates that will be replaced. In fact, this larger ratio itself may underestimate the difference between the point-source kernel and Monte Carlo estimates when the C.V. of the latter is greater than 50%.

In Fig. III-5 is shown the ratio Φ(point-source kernel method) : Φ(Monte Carlo method) as a function of initial photon energy for the same set of small target organs as in Fig. III-4. Only the less reliable Monte Carlo estimates were used (C.V. between 30 and 50%). The largest difference between the Φ-values estimated by the two methods occurred at 100-200 keV.

It was surprising that the point-source kernel estimate was smaller than the Monte Carlo estimate at 10 keV. However, we have less confidence in the physical data upon which the point-source kernel method is based at this energy than at higher energies (see Ryman, Warner, and Eckerman 1987). Also, the amount of data was meager at this energy, and the 95% confidence limits were

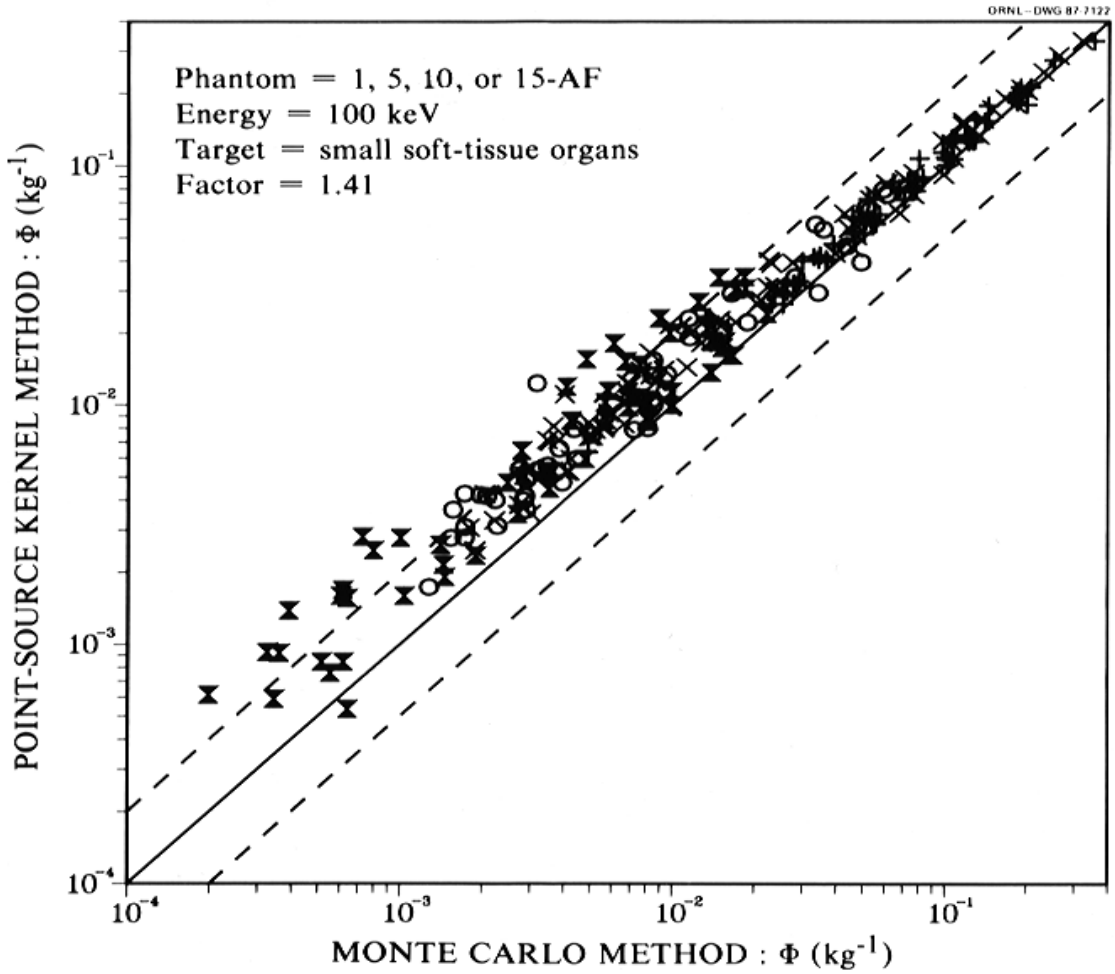

Fig. III-4. Φ(target←source) estimated by the point-source kernel method vs Φ(target←source) estimated by the Monte Carlo radiation transport method for selected organ pairs. The target organs are small soft-tissue organs (adrenals, gall bladder wall, ovaries, thymus, thyroid, or uterus). Source organs are soft-tissue organs, excluding those near the outside of the body (breasts, testes, and skin) and the brain, which is surrounded by bone. The initial photon energy is 100 keV, and data from four phantoms (ages 1, 5, and 10 phantoms and the age-15-male/adult-female phantom) are combined. Thus one datum will represent the source-target pair liver-to-ovaries in the age 5 phantom, another will represent small intestine-to-uterus in the age 10 phantom, and so on. The solid diagonal line is the line ordinate = abscissa, and the dashed diagonal lines are ordinate = 2 x abscissa and ordinate = 0.5 x abscissa. The symbols indicate the magnitude of the coefficient of variation (C.V.) of the Monte Carlo estimate—C.V. < 10% for the plus symbols, C.V. = l0-20% for the plain X's, C.V. = 20-30% for the circles, and C.V. = 30-50% for the filled X's. The C.V. of the point-source kernel estimate is always small (< 1.2%) for these data. "Factor" is the mean of the ratio of Φ(point-source kernel method) to Φ(Monte Carlo method) for all the data. Note, however, that as Φ becomes smaller (i.e., source and target are more widely separated), the ratio becomes larger.

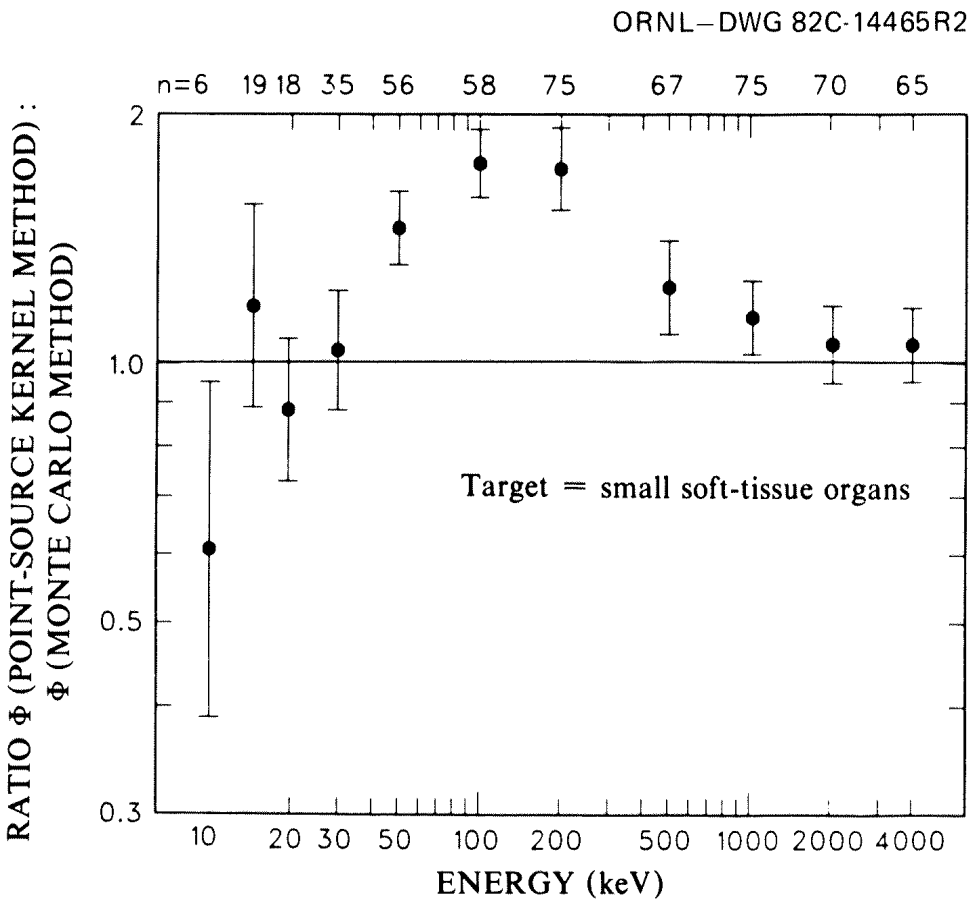

Fig. III-5. Mean of ratio Φ(point-source kernel method) to Φ(Monte Carlo method) vs initial photon energy for selected data. Error bars indicate 95% confidence intervals of the means. The target and source organs and the phantoms selected are as in Fig. III-4, but only the "worst" data from that set have been included—i.e., the C.V. of the Monte Carlo estimate must have been between 30-50% for the datum to have been selected. The number of data meeting this criterion at each energy (*n*) is indicated. See text for explanation.

large. On the other hand, using data on self-dose in 14 organs in four phantoms (n=56), we got a similar result: the mean ratio was 0.64, with a 95% confidence interval of 0.61-0.67. Thus this difference appears not to be a statistical artifact.

In Table III-3 are listed correction factors to be applied to those point-source kernel Φ-estimates which are used to replace unreliable Monte Carlo Φ-estimates. These correction factors were derived from the data in Fig. III-5 and similar data for the other source-target combinations. However, for these latter combinations, the data were less numerous and the confidence intervals were wider, especially at energies of 10-20 keV.

For the newborn phantom, the compositions of the tissues are different from those of the other phantoms (see Appendix A). Correction factors based on similar data for the newborn phantom are given in Table III-4.

The correction factors for the lungs as a source organ and the lungs as a target organ were adjusted slightly to make them consistent with the reciprocity correction factors for the lungs (Table III-1 or III-2, as appropriate). Similar adjustments were made for the skeleton.

It should be remembered that while these correction factors do improve the correspondence between the point-source kernel and the Monte Carlo estimates of Φ, their limitations should be kept in mind, especially for the correction factors at energies of 10-20 keV.

Table III-3. Correction factors to be applied to point-source kernel estimates of Φ when Monte Carlo estimates are statistically unreliable (for all phantoms except the newborn). The correction factor is the ratio Φ(point-source kernel metbod):Φ(Monte Carlo method) and thus is a divisor. Organs *X* and *Y* are soft-tissue organs.

Energy (keV)	Correction factors						
	Y↔*X*	Skin↔*X*	Brain↔*X*	*X*←Skeleton	Skeleton←*X*	*X*←Lungs	Lungs←*X*
10	0.65	0.65	0.65	2.0[a]	0.60[a]	0.15	0.13
15	1.0	1.0	1.0	3.4	0.90	0.35	0.31
20	1.0	1.3	1.0	2.6	0.65	0.45	0.40
30	1.1	1.5	1.4	1.8	0.45	0.63	0.56
50	1.5	1.8	2.0	1.5	0.45	1.3	1.2
100	1.8	1.9	3.8	1.4	0.70	1.8	1.8
200	1.6	1.6	3.6	1.3	1.0	1.6	1.6
500	1.3	1.3	2.7	1.1	1.1	1.3	1.3
1000	1.2	1.2	2.1	1.1	1.1	1.2	1.2
2000	1.1	1.1	1.6	1.1	1.1	1.1	1.1
4000	1.1	1.1	1.3	1.1	1.1	1.1	1.1

[a]The correction factors in this column are used for the whole skeleton, the active marrow, or the inactive marrow. See footnote in Table III-I regarding the Monte Carlo estimate of Φ(active marrow←X).

Table III-4. Correction factors to be applied to point-source kernel estimates of Φ when Monte Carlo estimates are statistically unreliable (for the newborn phantom only). The correction factor is the ratio Φ(point-source kernel metbod):Φ(Monte Carlo method) and thus is a divisor. Organs X and Y are soft-tissue organs.

Energy (keV)	Correction factors						
	Y↔*X*	Skin↔*X*	Brain↔*X*	*X*←Skeleton	Skeleton←*X*	*X*←Lungs	Lungs←*X*
10	0.65[a]	0.65[a]	0.65	2.5[b]	0.90[b]	0.25	0.24
15	1.0	1.0	1.0	2.2	0.72	0.52	0.31
20	1.0	1.3	1.0	1.6	0.53	0.69	0.40
30	1.1	1.5	1.1	1.4	0.44	0.95	0.56
50	1.5	1.8	2.0	1.4	0.50	1.3	1.2
100	1.8	1.9	3.5	1.4	0.90	1.8	1.8
200	1.6	1.6	2.6	1.3	1.2	1.6	1.6
500	1.3	1.3	1.7	1.1	1.1	1.3	1.3
1000	1.2	1.2	1.3	1.1	1.1	1.2	1.2
2000	1.1	1.1	1.2	1.1	1.1	1.1	1.1
4000	1.1	1.1	1.1	1.1	1.1	1.1	1.1

[a]The values in this column are the same as those in the corresponding column in Table III-3 for the other phantoms.

[b]The correction factors in this column are used for the whole skeleton or the active marrow. See footnote in Table III-1 regarding the Monte Carlo estimate of Φ(active marrow←X).

REFERENCES FOR CHAPTER III

Cristy, M. 1983. Applying the reciprocal dose principle to heterogeneous phantoms: practical experience from Monte Carlo studies. *Phys. Med. Biol.* 28: 1289-1303.

Cristy, M., and Eckerman, K.F. 1987a. *Specific absorbed fractions of energy at various ages from internal photon sources. II. One-year-old.* Oak Ridge National Laboratory Rep. ORNL/TM-8381:Vol. 2.

—- 1987b. *Specific absorbed fractions of energy at various ages from internal photon sources. III. Five-year-old.* Oak Ridge National Laboratory Rep. ORNL/TM-838 1 :Vol. 3.

—1987c. *Specific absorbed fractions of energy at various ages from internal photon sources. IV. Ten-year-old.* Oak Ridge National Laboratory Rep. ORNL/TM-8381:Vol. 4.

— 1987d. *Specific absorbed fractions of energy at various ages from internal photon sources. V. Fifteen-year-old male and adult female.* Oak Ridge National Laboratory Rep. ORNL/TM-8381:Vol. 5.

— 1987e. *Specific absorbed fractions of energy at various ages from internal photon sources. VI. Newborn.* Oak Ridge National Laboratory Rep. ORNL/TM-8381:Vol. 6.

— 1987f. *Specific absorbed fractions of energy at various ages from internal photon sources. VII. Adult male.* Oak Ridge National Laboratory Rep. ORNL/TM-8381:Vol. 7.

ICRU 1979. *Methods of assessment of absorbed dose in clinical use of radionuclides.* ICRU Report 32. Washington: International Commission on Radiation Units and Measurements.

King, L.V. 1912. Absorption problems in radioactivity. *Philosophical Magazine* 23: 242-250.

Loevinger, R. 1969. Distributed radionuclide sources. In *Radiation dosimetry*, 2nd edition, Vol. III, eds. F. H. Attix and E. Tochilin, pp. 51-90. New York: Academic Press.

Loevinger, R., and Berman, M. 1976. *A revised schema for calculating the absorbed dose from biologically distributed radionuclides.* MIRD Pamphlet No. 1, Revised. New York: Society of Nuclear Medicine.

Loevinger, R., Japha, E.M., and Brownell, G.L. 1956. Discrete radioisotope sources. In *Radiation dosimetry*, eds. G.J. Hine and G.L. Brownell, pp. 693-799. New York: Academic Press.

Mayneord, W.V. 1945. Energy absorption. IV. The mathematical theory of integral dose in radium therapy. *Brit. J. Radiol.* 18: 12-19.

Ryman, J.C., Warner, G.G., and Eckerman, K.F. 1987. *Computer codes for calculating specific absorbed fractions of energy from internal photon sources by the point-source kernel method.* Oak Ridge National Laboratory Rep. ORNL/TM-8378 (in preparation).

Snyder, W.S., Ford, M.R., Warner, G.G., and Watson, S.B. 1974. *A tabulation of dose equivalent per microcurie-day for source and target organs of an adult for various radionuclides: Part 1.* Oak Ridge National Laboratory Rep. ORNL-5000.

CHAPTER IV. RECOMMENDED VALUES OF Φ

This chapter describes the procedures used to obtain the "best" estimates of Φ from the Φ-values estimated by the various methods. These procedures were used for all organ pairs, except when the target organ was the active marrow or the endosteal cells of the skeleton. For the latter case, see the section "Special Case: Active Marrow and Endosteal Cells as Target Organs" in Chapter II.

The Monte Carlo computer program was not run for all possible source organs. The organs routinely run as source organs are indicated in Table IV-l.

Procedures

The procedures used to obtain the recommended values of Φ for a given source-target pair were as follows:

(1) If the coefficient of variation (C.V.) of the direct Monte Carlo estimate, Φ(target←source), the C.V. of the converse Monte Carlo estimate, Φ(source←target), or the C.V. of the point-source kernel estimate, Φ(target↔source), was greater than 50%, that estimate was rejected as unreliable. This criterion is the same as that used by Snyder et al. (1974).

(2) At a given energy, the weighted average of the direct and converse Monte Carlo estimates was taken (each weighted according to the inverse of its variance). This operation and all subsequent operations were performed on the logarithm-transformed variables. Correction factors given in Tables III-1 and III-2 were used as appropriate. The C.V. of the weighted average was computed with the formula

$$\frac{1}{ln(1+c^2)} = \frac{1}{ln(1+c_1^2)} + \frac{1}{ln(1+c_2^2)} \quad ,$$

where c_1 and c_2 are the C.V.'s of the Monte Carlo estimates and c is the C.V. of the weighted average. If there was only one Monte Carlo estimate, that value was taken as the "weighted average" in the following steps.

(3) If the C.V. of the weighted average was greater than 30%, then a new weighted average was taken of this value and the point-source kernel estimate, modified with correction factors given in Table III-3 or III-4, as appropriate. This new weighted average was taken as the "weighted average" in the following step. (Except at low energies, where the C.V. of the point-source kernel estimate may be high, this procedure has the practical effect of substituting the corrected point-source kernel estimate for the old weighted average.)

(4) The plot of *ln*(Φ--*weighted average*) vs *ln*(*energy*) was smoothed with a cubic spline technique (de Boor 1978). The smoothed variate was taken as the "best" or recommended value.

(5) If there were no acceptable Monte Carlo estimates at certain energies (outside the above smoothing interval), then the corrected point-source kernel estimates were taken as the recommended values. No smoothing was done on these values.

(6) If neither organ was employed as a source organ in the Monte Carlo computer runs, no recommendation is made, because correction factors for the point-source kernel estimates have not been developed for this situation. However, these point-source kernel estimates are tabulated in the companion volumes (see Cristy and Eckerman 1987a-f).

Adjustments to the smoothing procedure (procedure 4, above) were made empirically. The smoothing spline often did not fit well at low energies, where the curve may bend steeply downward. Additional weight was given the first two data points to correct this problem. When the C.V.

Table IV-l. Organs defined as source and target regions in the Monte Carlo radiation transport and the point-source kernel computer codes. Those organs run as source organs with the Monte Carlo code are indicated in the right column.

Organ	Run as source organ in Monte Carlo code?
Adrenals	Yes
Brain	Yes
Breasts	Yes
Gall bladder contents	Yes
Gall bladder wall	No[a]
Gastrointestinal tract:	
Lower large intestine contents	Yes
Lower large intestine wall	No[a]
Small intestine	Yes
Stomach contents	Yes
Stomach wall	No[a]
Upper large intestine contents	Yes
Upper large intestine wall	No[a]
Heart contents	Yes
Heart wall	Yes
Kidneys	Yes
Liver	Yes
Lungs	Yes
Ovaries	Yes
Pancreas	Yes
Remaining tissue	No
Skeleton:	
Active marrow	Yes
Inactive marrow	No[b]
Whole skeleton	Yes
Skin	No[a]
Spleen	Yes
Testes	Yes
Thymus	Yes
Thyroid	Yes
Urinary bladder contents	Yes
Urinary bladder wall	No[a]
Uterus	Yes
Whole body	Yes

[a]For the newborn and the adult male phantoms, this organ was also run as a source organ in the Monte Carlo code.

[b]The inactive marrow was run as a source organ for the adult male phantom.

of the weighted average at 4000 keV was greater than 10% the smoothing spline technique also frequently gave poor results at 4000 keV, where the curve is usually bending gently downward. To correct this problem, we substituted the weighted average of the Monte Carlo weighted average and the uncorrected point-source kernel estimate at 4000 keV if the C.V. of the former was between 10 and 30%. The point-source kernel estimate was reliable at this energy, and this procedure gave

additional weight to this data point, since the C.V. of the point-source kernel estimate was nearly always small. These empirical adjustments served to “tie down” or restrain the Φ-values at the ends of the smoothing interval.

Occasionally the smoothing spline did not work well, even with these adjustments (e.g., Fig. IV-11). Graphs of *ln*(Φ) vs *ln*(*energy*) were plotted for all source-target pairs for all phantoms; the Φ-values by the various methods, the weighted average as defined above, and the smoothing spline fit were all plotted. If the smoothing was poor, smoothing was done by hand. This occurred in about 2% of the organ pairs and was usually the result of an oscillation in the smoothed curve, an artifact of the smoothing spline technique.

Examples

The following examples are given to clarify the procedures. In the following figures, only Φ-estimates with C.V.’s less than 50% are plotted.

In Fig. IV-1 the kidneys are the source organ and the spleen is the target organ in the age 5 phantom. The C.V.’s of both Monte Carlo estimates were small at all energies except 10 keV, and the reciprocal estimates were close to each other. The advantages of averaging and smoothing are

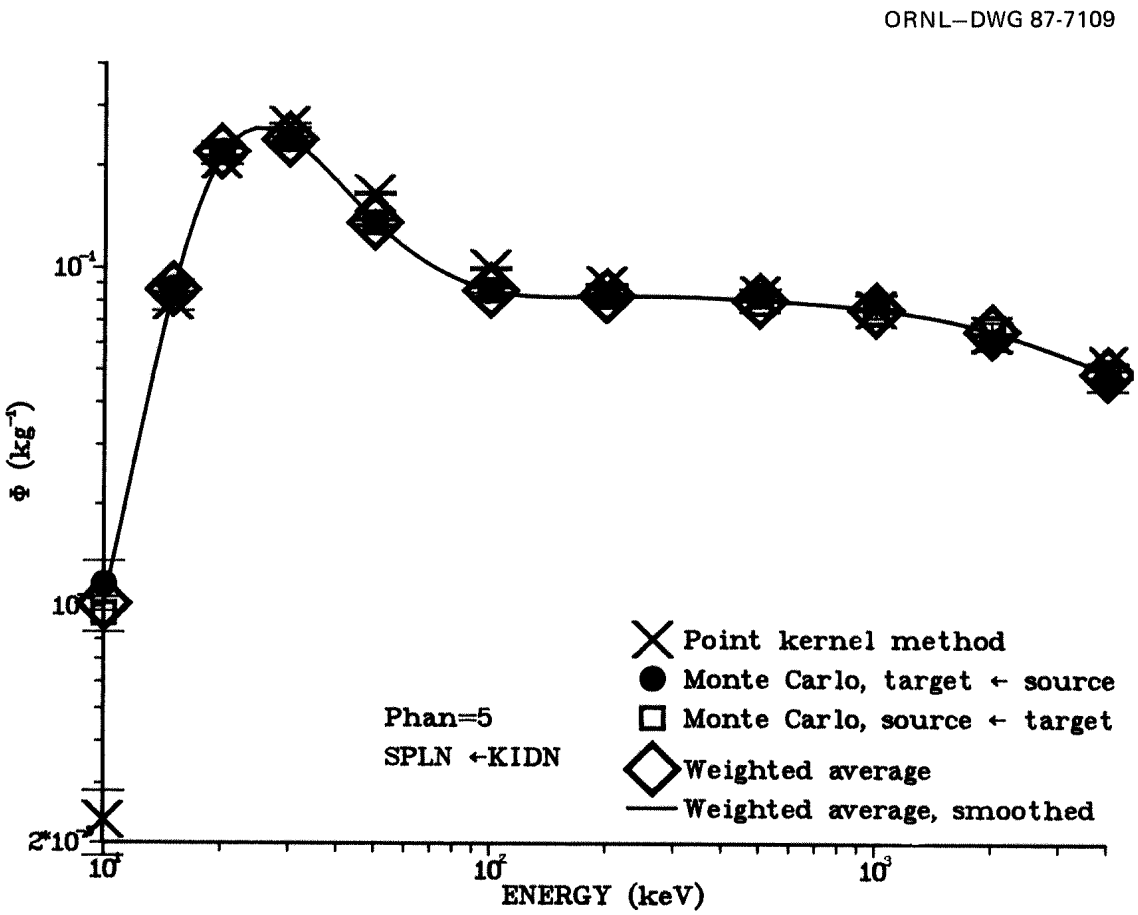

Fig. IV-l. Φ vs energy for source organ = kidneys and target organ = spleen in the age 5 phantom. Error bars (± one S.D.) are plotted for the point-source kernel estimate and the two Monte Carlo estimates but are omitted from the weighted average. The "weighted average" is defined in the text. The smoothing spline fit of the weighted average is drawn with a solid line.

small in this example. Note that for the converse case (kidneys as target organ), the weighted average and the smoothing would be identical, since no correction factors are used for the converse Monte Carlo estimate here.

In Fig. IV-2 the spleen is the source and the uterus is the target in the age-15-male/adult-female phantom. At energies below 50 keV, there were no acceptable Monte Carlo estimates, direct or converse, and the corrected point-source kernel estimate is recommended. In the interval 50-4000 keV, acceptable Monte Carlo estimates were available. The C.V.'s of both Monte Carlo estimates are larger than in the previous example, and the advantages of averaging and smoothing are more apparent.

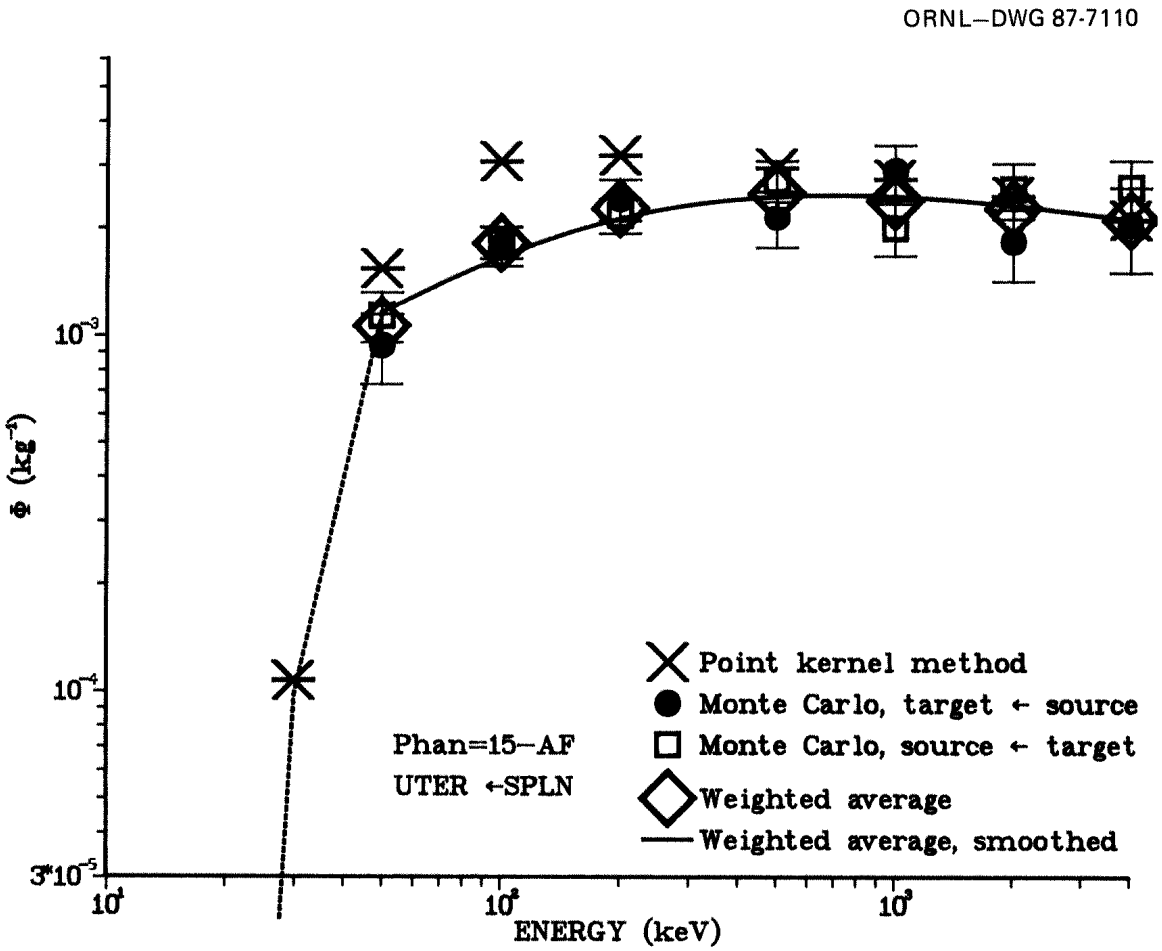

Fig. IV-2. Φ vs energy for source = spleen and target = uterus in the age-15male/adult-female phantom. The dashed line connects corrected point-source kernel estimates to the smoothed curve (the data points indicated by "X" on this and all other graphs have not been adjusted by the correction factors). Data at energies below 30 keV (point-source kernel estimates only) are off-scale.

In Fig. IV-3 the upper large intestine contents is the source and the ovaries are the target. Here the converse Monte Carlo estimate was more reliable than the direct estimate and largely determined the weighted average. At 10 keV, only the converse estimate had an acceptable C.V.

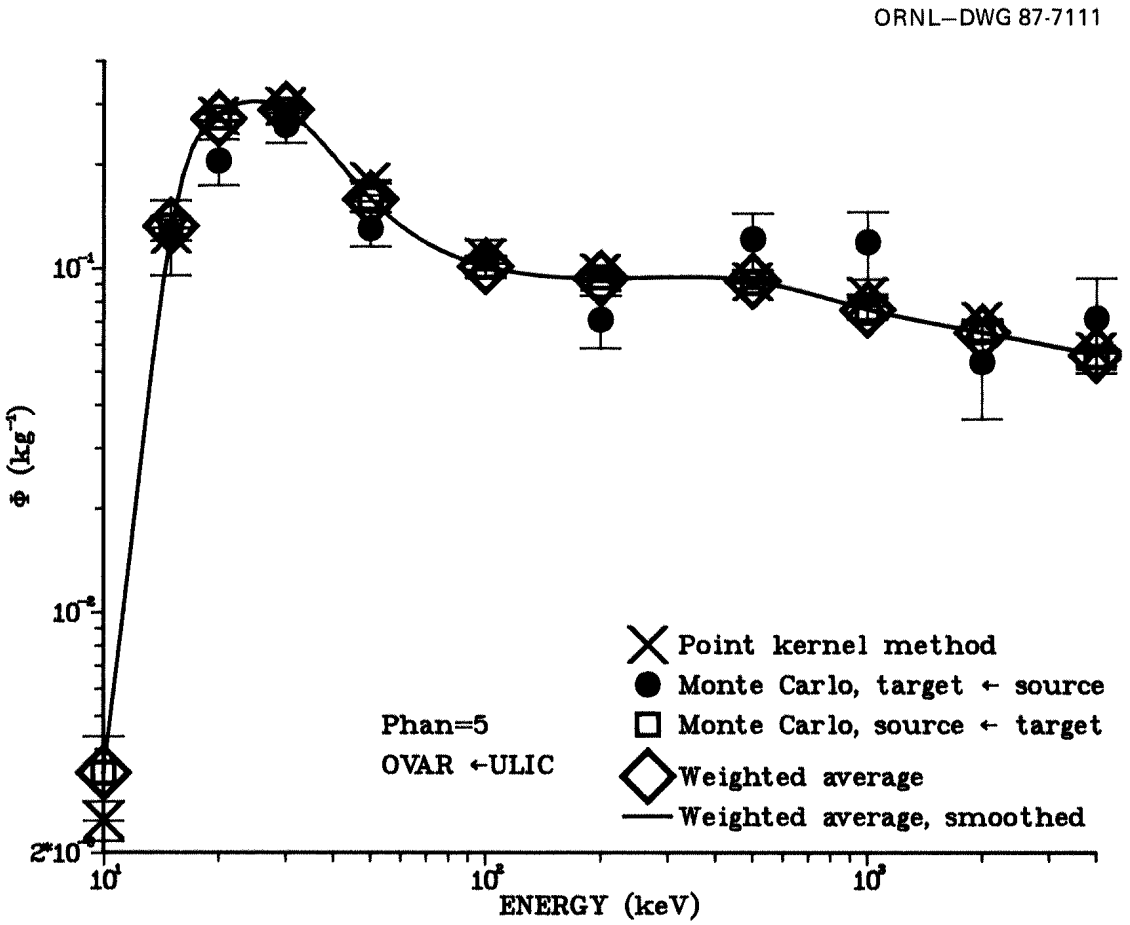

Fig. IV-3. Φ vs energy for source = upper large intestine contents and target = ovaries in the age 5 phantom.

In Fig. IV-4 acceptable Monte Carlo estimates were available only in the interval 30-1000 keV. Outside this interval (l0-20 keV and 2000-4000 keV), the corrected point-source kernel estimate is recommended. At 30, 500, and 1000 keV, the C.V. of the weighted average was greater than 30%, and procedure 3 was invoked. The unreliability of Monte Carlo estimates with C.V.'s greater than 30% is apparent in this figure.

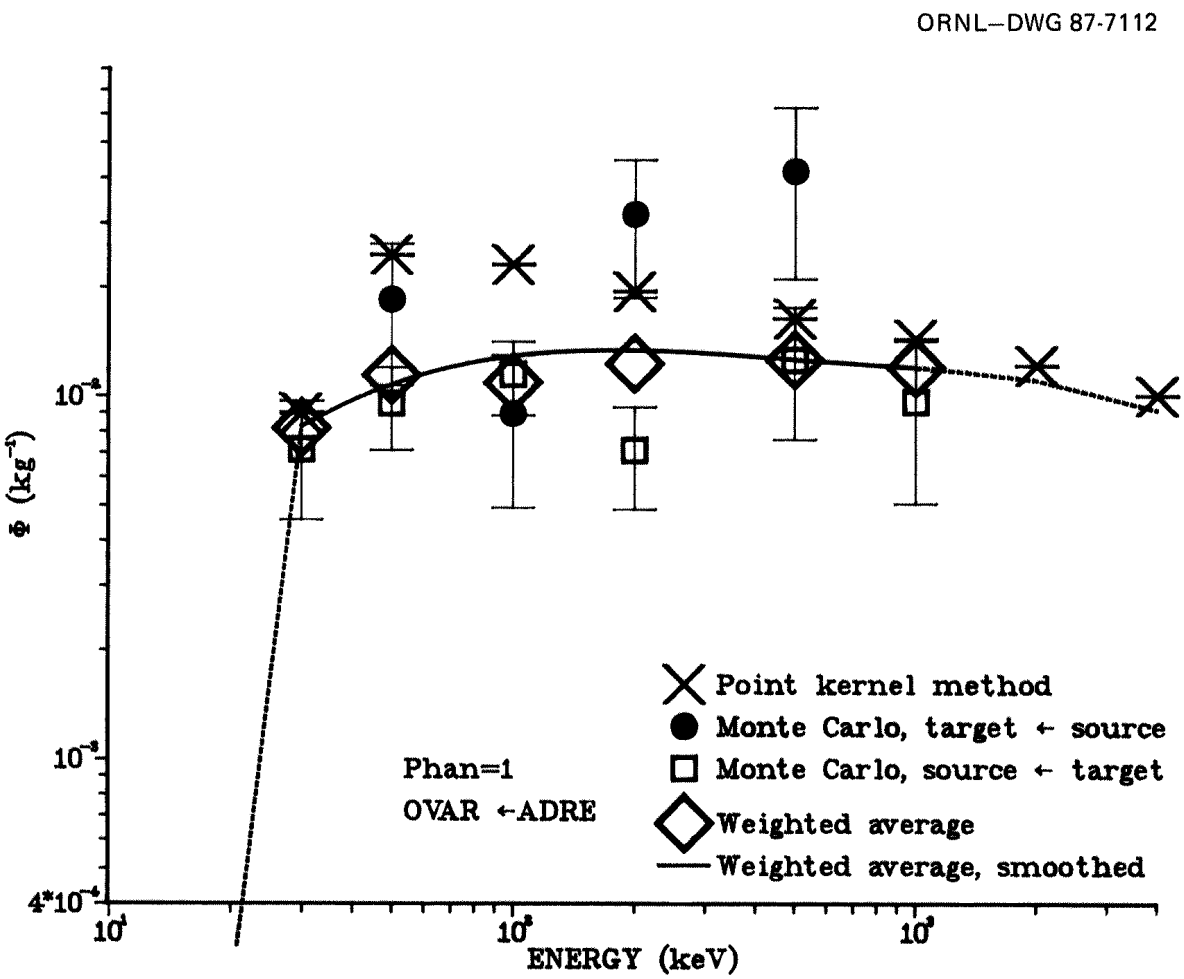

Fig. IV-4. Φ vs energy for source = adrenals and target = ovaries in the age 1 phantom.

In Fig. IV-5 procedure 3 was invoked uniformly in the smoothing interval. There were no acceptable direct Monte Carlo estimates, and all five of the acceptable converse estimates had C.V.'s greater than 30%. Practically, the corrected point-source kernel estimate was used at all energies.

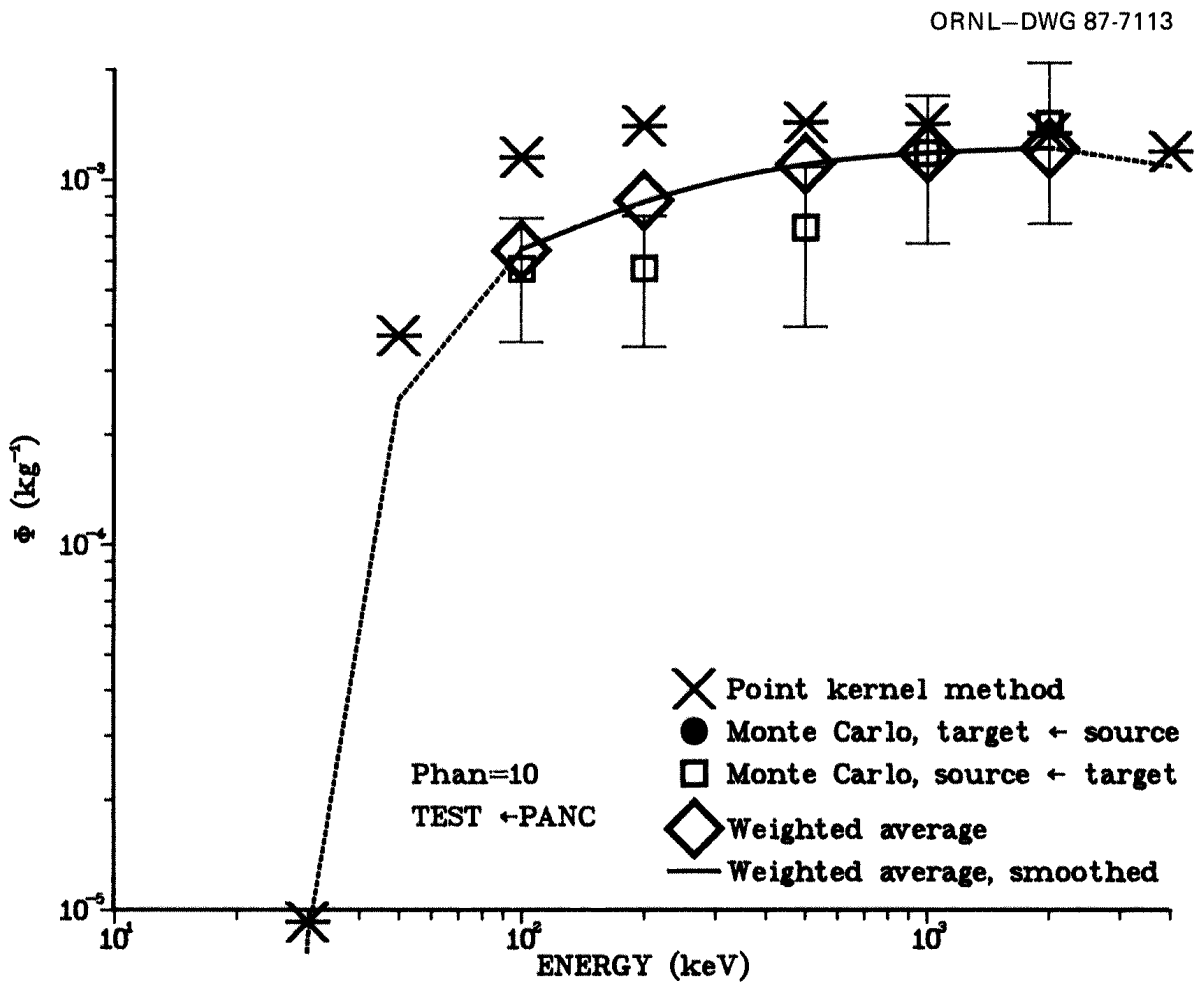

Fig. IV-5. Φ vs energy for source = pancreas and target = testes in the age 10 phantom.

In Fig. IV-6 the source organ is the lungs, and here correction factors were applied to the converse Monte Carlo estimates at energies below 100 keV (see Table III-l). The data plotted are the uncorrected estimates, but the correction factors were employed in calculating the weighted average. The C.V.'s of both Monte Carlo estimates were small at most energies, but the converse estimate was the smaller of the two and contributed more to the weighted average. In this case, if the source and target were reversed, the weighted average would be different at energies below 100 keV.

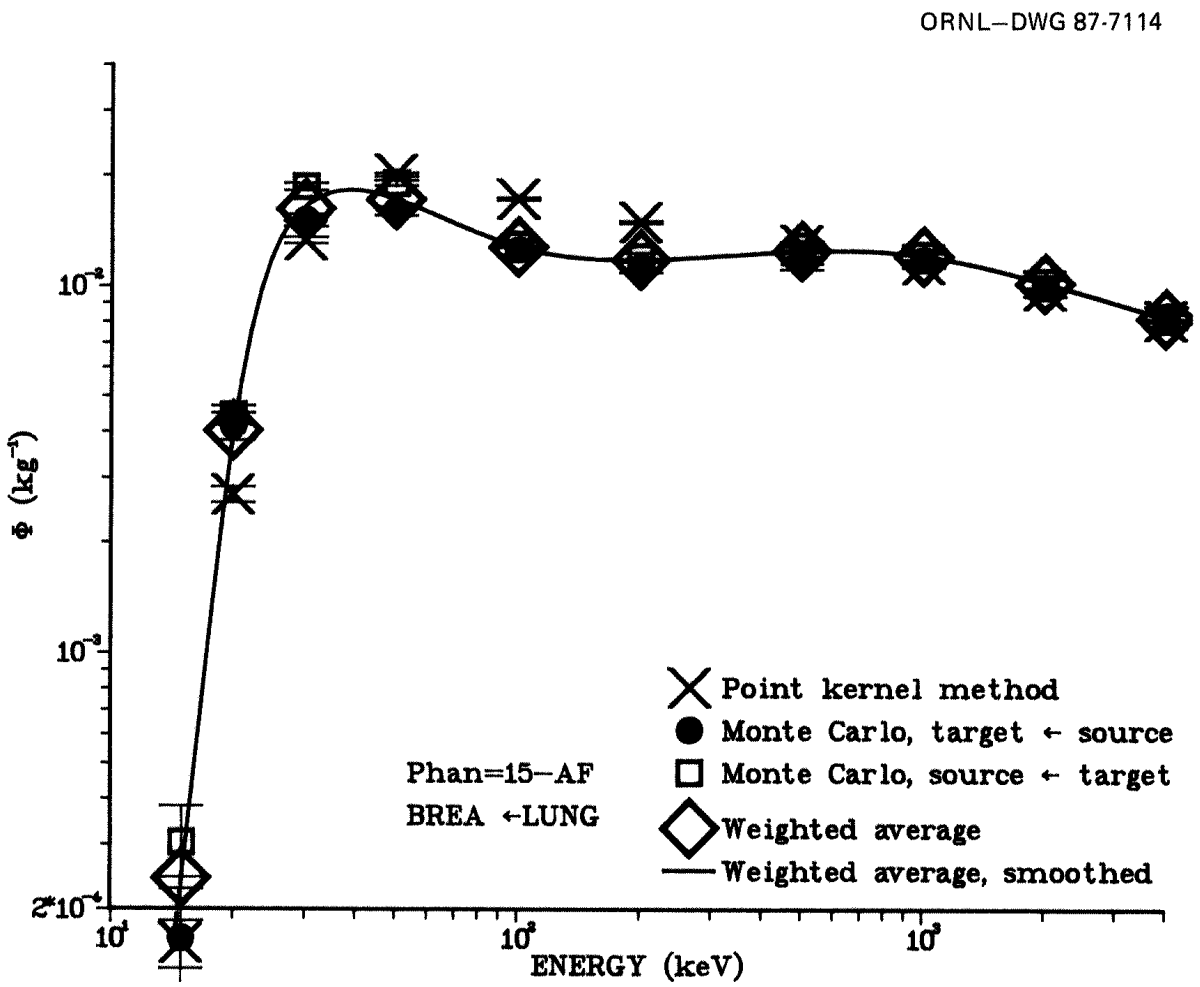

Fig. IV-6. Φ vs energy for source = lungs and target = breasts in the age-15-male/adult-female phantom.

In Fig. IV-7 the source is also in the lungs. Here the converse estimate, again corrected at energies below 100 keV, contributed heavily to the weighted average.

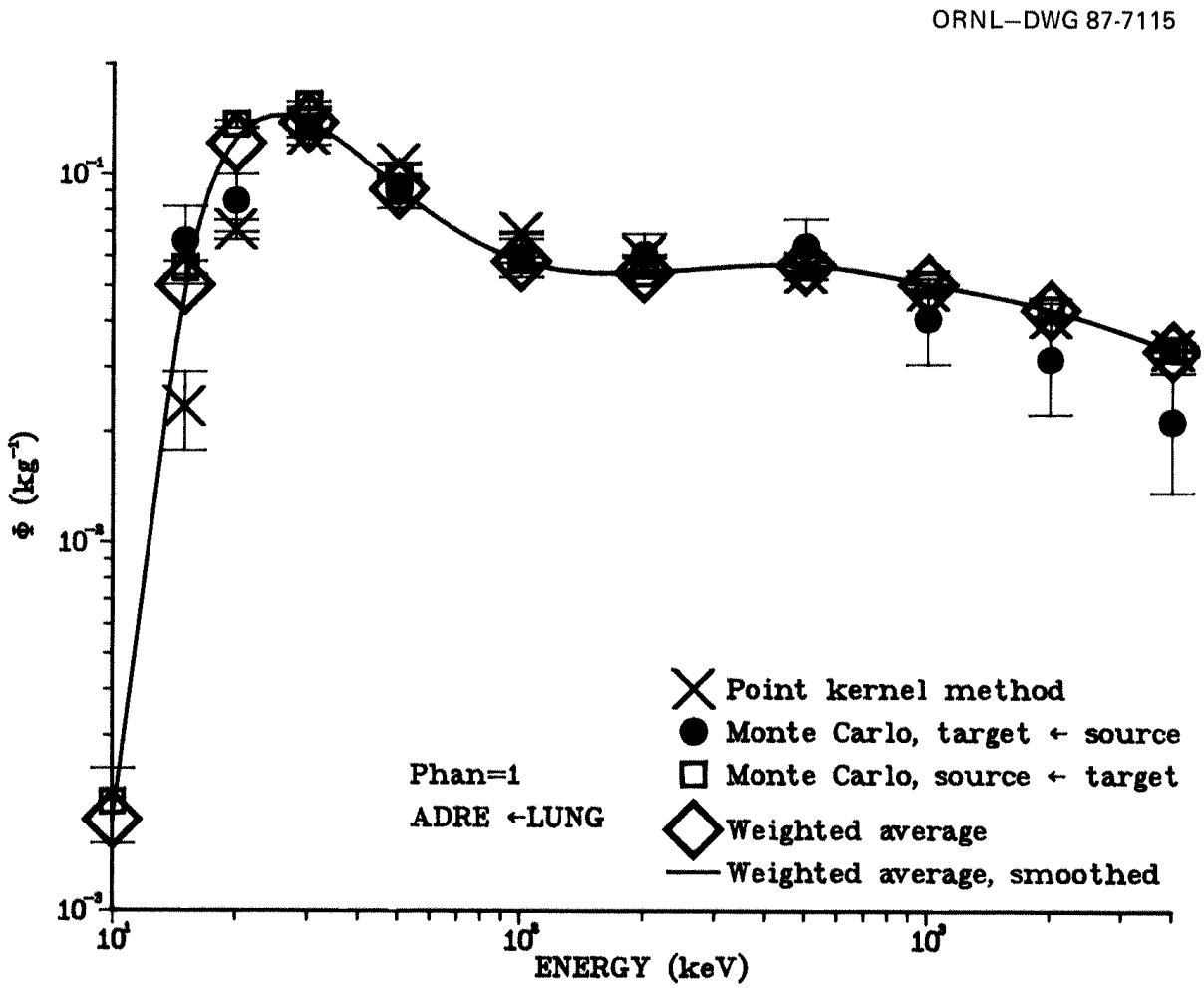

Fig. IV-7. Φ vs energy for source = lungs and target = adrenals in the age 1 phantom.

In Figs. IV-8 to IV-10 the source organ is the skeleton or the active marrow, another case in which the reciprocity principle breaks down and correction factors must be used. In Fig. IV-8 the target organ is the liver, a large organ, and the C.V.'s of the direct Monte Carlo estimates were reasonably small, except at low energies. However, the C.V.'s of the converse estimates were even smaller, and they were somewhat more important in determining the weighted average. At 10 keV, the converse estimate was the only acceptable estimate. In Figs. IV-9 and IV-10 are shown similar cases, except that the target organs are small. Here the statistics of the direct Monte Carlo estimates were poorer, and the corrected converse estimates were weighted heavily. Note that at 15 and 30 keV in Fig. IV-8 and at 30-100 keV in Fig. IV-10 the weighted average is smaller than both Monte Carlo estimates because the corrected converse estimates are largely determining the weighted average and they happen to be smaller than the direct estimates.

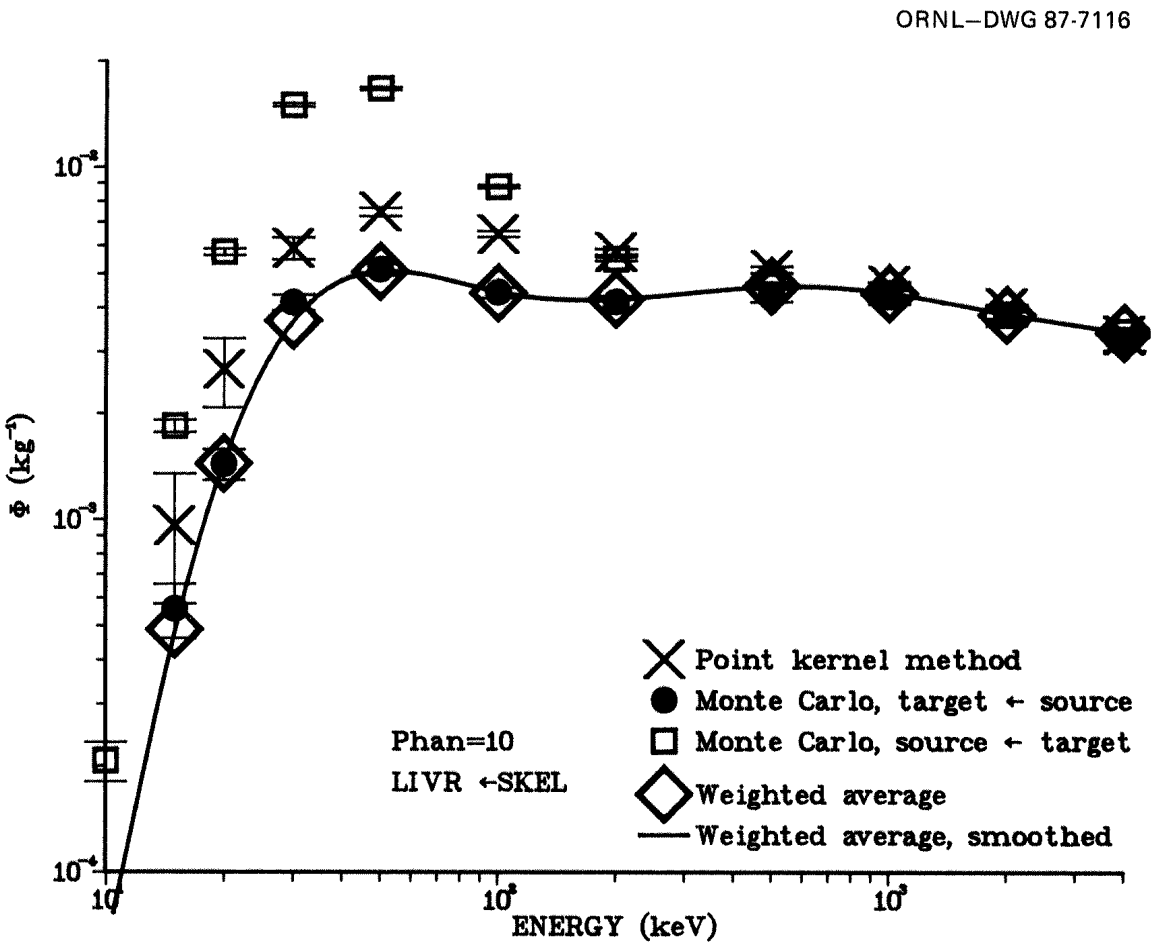

Fig. IV-8. Φ vs energy for source = whole skeleton and target = liver in the age 10 phantom.

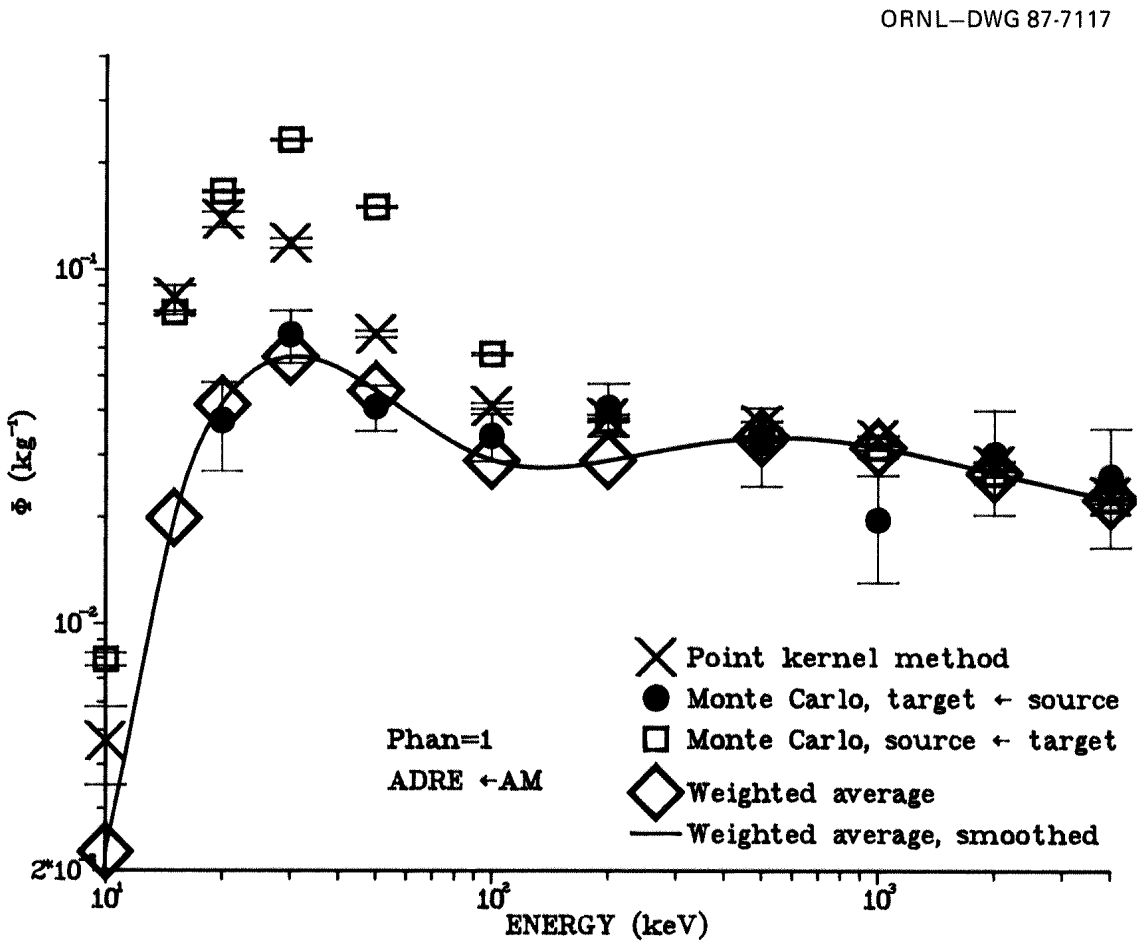

Fig. IV-9. Φ vs energy for source = active marrow and target = adrenals in the age 1 phantom. The converse Monte Carlo estimate, Φ(active marrow ←adrenals), is that calculated by the old way in the Monte Carlo computer program (see footnote in Table III-1 for further explanation).

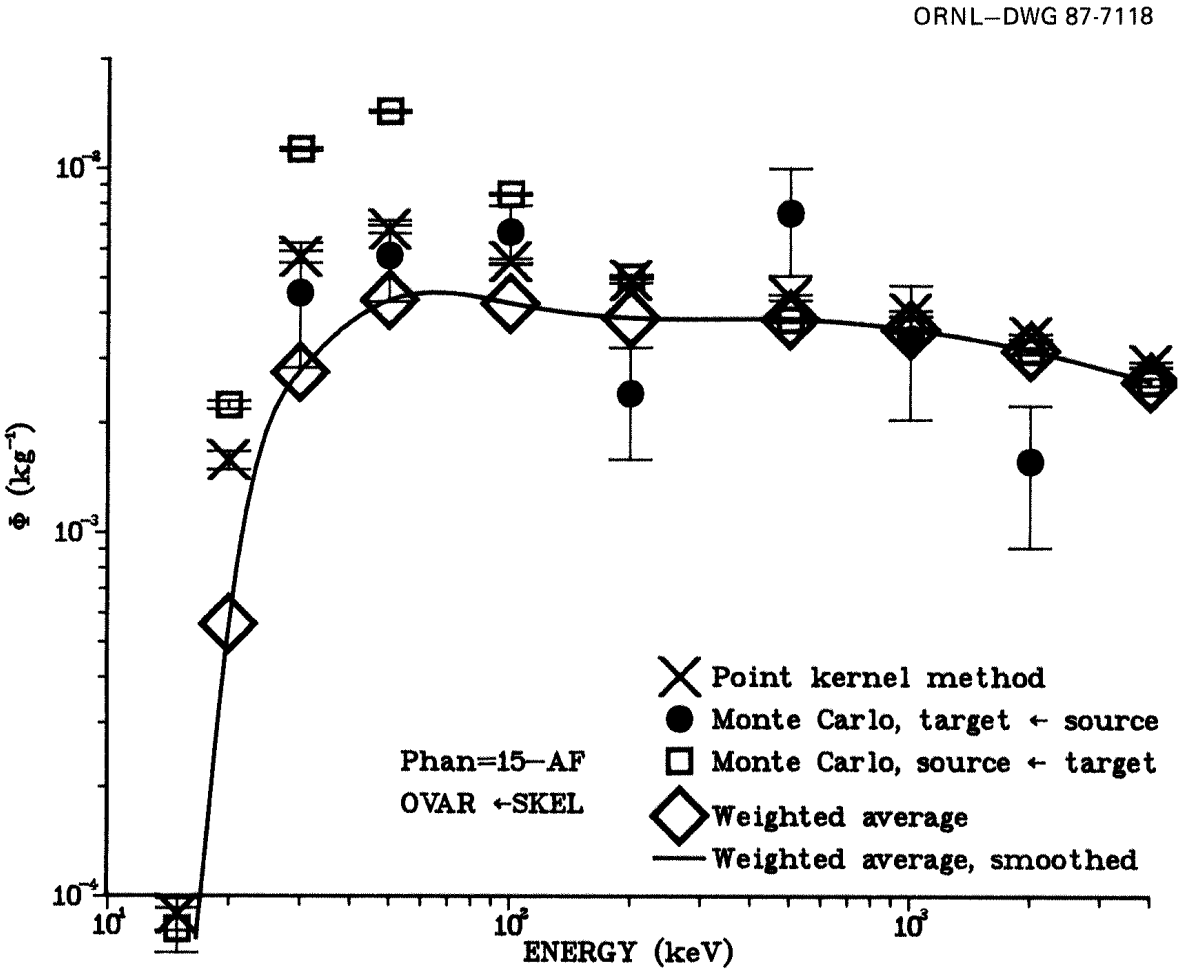

Fig. IV-10. Φ vs energy for source = whole skeleton and target = ovaries in the age-15-male/adult-female phantom.

In Fig. IV-l1 the smoothing spline technique worked poorly. The fit at 200-4000 keV was judged to be poor—the oscillation is probably an artifact of the cubic spline technique. To obtain recommended values, we smoothed this curve by hand in the offending region.

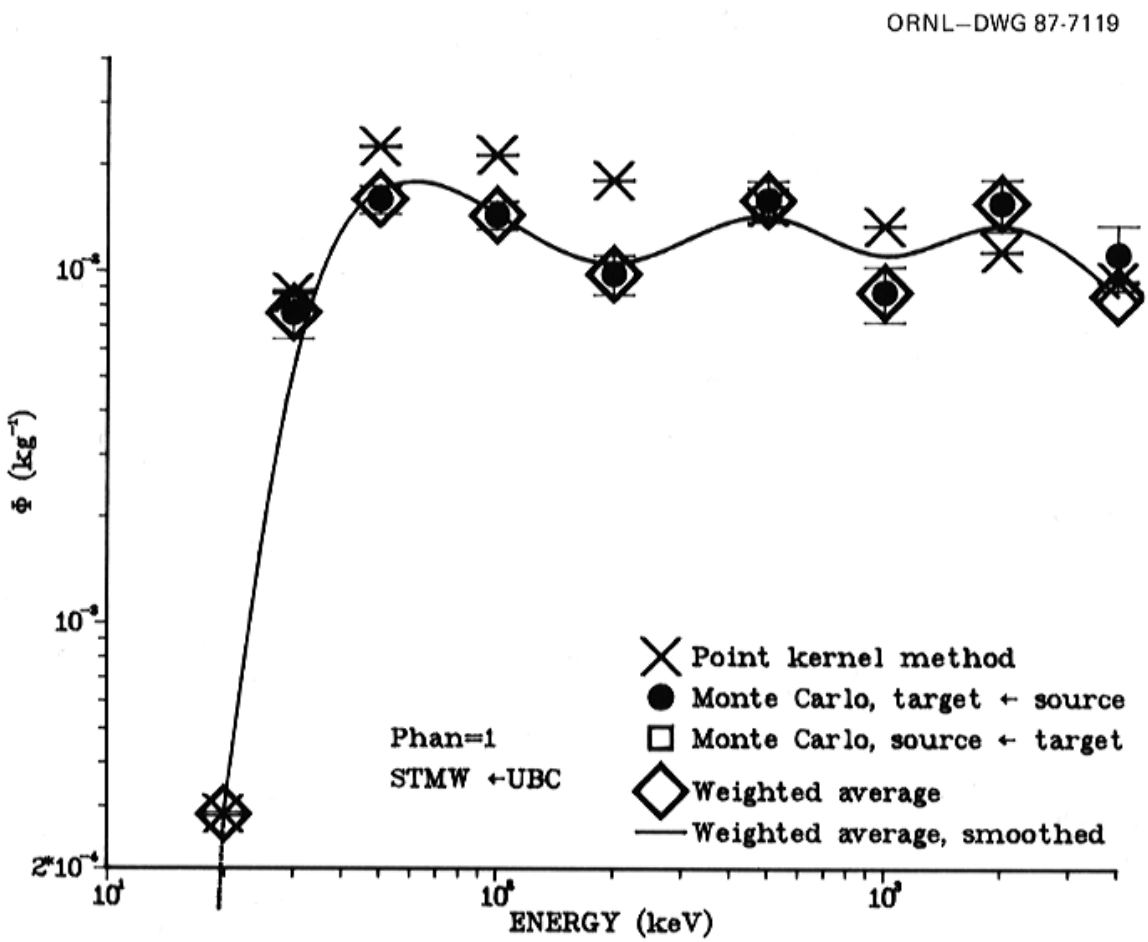

Fig. IV-11. Φ vs energy for source = urinary bladder contents and target = stomach wall in the age 1 phantom. The figure illustrates an oscillation in the fit by the smoothing spline technique at the higher energies; for our purposes, this oscillation is an artifact.

In Fig. IV-12 neither organ was run as a source organ with the Monte Carlo radiation transport computer program. Only point-source kernel estimates were available, and no correction factors have been developed for this situation. We make no recommendations here, but the raw data are tabulated in the companion volumes (Cristy and Eckerman 1987a-f).

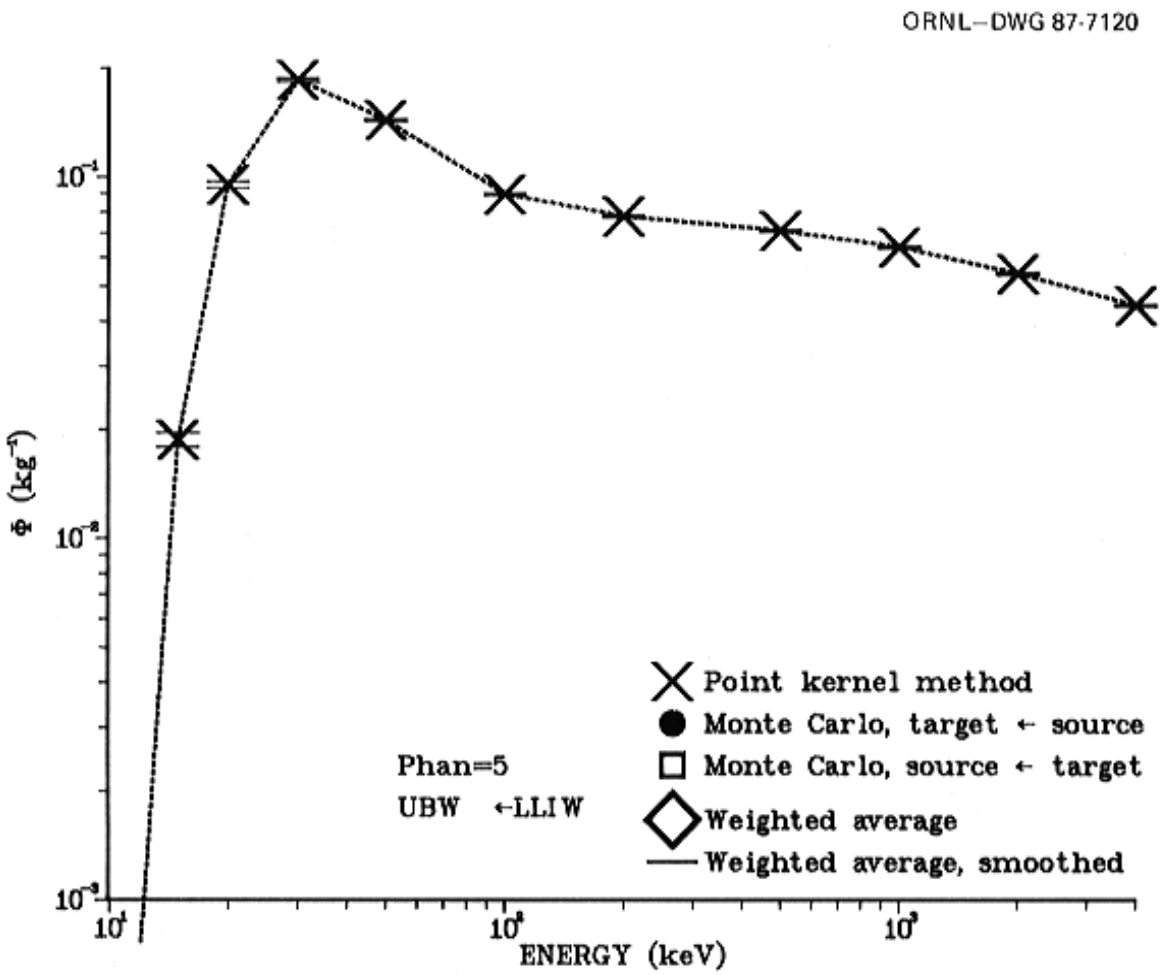

Fig. IV-12. Φ vs energy for soorce = lower large intestine wall aad target = urinary bladder wall in the age 5 phantom. Neither organ was a source organ in the Monte Carlo computer runs, and thus only point-source kernel estimates were available.

Approximate Methods for Remaining Tissue Compartment (Used for Muscle)

The "remaining tissue" compartment (*RT*) of each phantom is the tissue that remains after all the target organs specifically defined are excluded. Since muscle tissue and fat tissue are not explicitly defined in the phantoms and since these tissues are distributed approximately as *RT* is distributed, Snyder et al. (1974, 1978) used the specific absorbed fractions for *RT* to approximate the specific absorbed fractions for muscle or fat. We have also used this approximation for muscle. (See Snyder et al., 1978, p.13, for a more complete discussion. Their terminology for *RT* is "other tissues.")

Furthermore, since the *RT* compartment has not been used as a source organ in the Monte Carlo computer program, the value of $\Phi(X \leftarrow RT)$ itself must be approximated either by reciprocity (if *X* is an organ run as a source organ) or by additivity (if *X* is not such an organ—see Table IV-1). In the former case, the procedures described at the beginning of this chapter apply. In the latter case, the "method of difference" is applied, i.e.,

$$\Phi(X \leftarrow RT) = \frac{m_{WB}\Phi(X \leftarrow WB) - \sum_Y m_Y \Phi(X \leftarrow Y) - m_X \Phi(X \leftarrow X)}{m_{WB} - \sum_Y m_Y - m_X} ,$$

where *WB* is the whole body, *Y* is an organ *Y* run as a source in the Monte Carlo computer program, and m_{WB}, m_Y, and m_X are the masses of the whole body, organ *Y*, and organ *X*, respectively. This is the same equation used by Snyder et al. (1974, 1978), except that the last term in the numerator and the last term in the denominator above do not appear in their equation. (If *X* is *RT*, these new terms do not apply.) These new terms improve the approximation by 10-20% at higher energies and up to ten times at energies of 10-20 kev (Cristy, unpublished data). The value of $\Phi(X \leftarrow X)$ used in the equation above for a given phantom is obtained by interpolating between ($m_{X,\text{newborn}}$, $\ln \Phi(X \leftarrow X)_{\text{newborn}}$) and ($m_{X,\text{adult male}}$, $\ln \Phi(X \leftarrow X)_{\text{adult male}}$).

Snyder et al. (1978, p. 13) emphasized (and we repeat) that these methods "should be considered approximate at best."

Special Problems

Several special problems occurred:

(1) Occasionally both Monte Carlo estimates and the point-source kernel estimate were unreliable (C.V.'s >50%) at 10 keV or at both 10 and 15 keV. Then an extrapolation of the *ln*(Φ – *weighted average*) vs *ln*(*energy*) curve was performed, as shown in Fig. IV-13. Judging from other curves where reliable data were available at 10 and 15 keV, we claim that this log-log extrapolation is conservative (i.e., more likely to yield a Φ-value too large than too small), but not as strikingly conservative as the linear extrapolation employed by Snyder et al. (1974).

(2) When the source was in the whole skeleton or the active marrow and the target was the whole body, none of the correction factors in Tables III-1 and III-2 applied. Here, however, the direct Monte Carlo estimate was always reliable, and it was used as the "weighted average" in the procedures above.

When the source was in the inactive marrow, however, the converse estimate was necessary, because the inactive marrow was not run as a source organ with the Monte Carlo computer program. Consequently, correction factors for this special case were developed from the data Φ(whole skeleton←whole body), Φ(whole body←whole skeleton), Φ(active marrow←whole body), and Φ(whole body←active marrow). These correction factors are 1.08, 1.25, 1.50, 1.88, 2.05, 1.55, 1.13, 1.00, 1.00, 1.00, and 1.00 at 10, 15, 20, 30, 50, 100, 200, 500, 1000, 2000, and 4000 keV, respectively, and are defined as the ratio Φ(inactive marrow←whole body) : Φ(whole body←inactive marrow).

(3) When the target organ was the inactive marrow, no recommendations were made.

(4) When the source organ was the whole body, the specific absorbed fraction in a target organ was sometimes greater than the limiting value l/(mass of target organ) at low energies, because of poor statistics. When this occurred, the Φ-value was reduced to the limiting value.

(5) When the source was in the contents of an organ, e.g., stomach contents, and the target was the whole body, a spuriously high value of Φ was computed by the Monte Carlo computer program, because the contents itself was counted as part of the whole body. This extra contribution has been subtracted from the recommended values but not from the raw data tabulated in the companion volumes (Cristy and Eckerman 1987a-f).

(6) When the source was in the small intestine (contents) and the target was the small intestine (wall) or whole body, a spuriously high value of Φ was computed by the Monte Carlo computer program, because the contents and wall of the small intestine are not modeled separately in the phantoms. The relative magnitude of this overestimate was estimated from the data for the upper and lower large intestine and corrections were made for the the recommended values but not for the raw data tabulated in the companion volumes (Cristy and Eckerman 1987a-f).

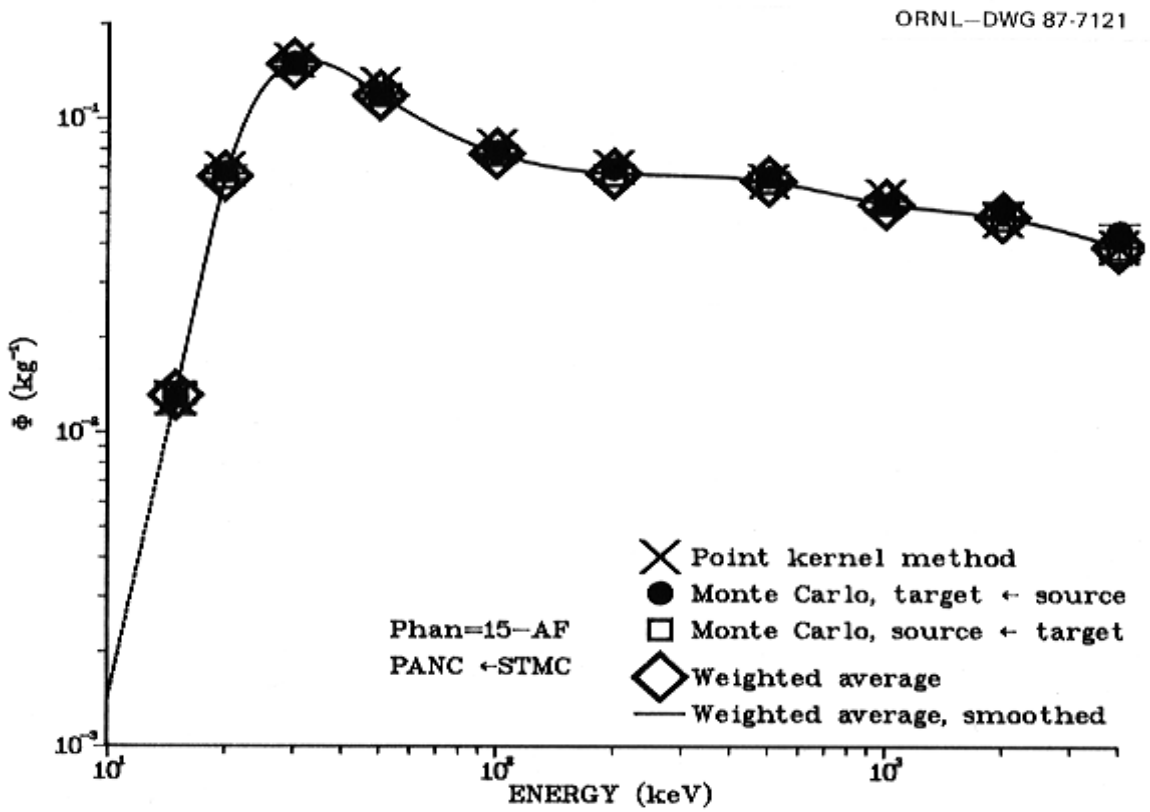

Fig. IV-13. Φ vs energy for source = stomach contents and target = pancreas in the age-15-male/adult-female phantom. The dashed line illustrates the log-log extrapolation employed when no reliable estimates of Φ were available at 10 keV.

REFERENCES FOR CHAPTER IV

Cristy, M., and Eckerman, K.F. 1987a. *Specific absorbed fractions of energy at various ages from internal photon sources. II. One-year-old.* Oak Ridge National Laboratory Rep. ORNL/TM-8381:Vol. 2.

— 1987b. *Specific absorbed fractions of energy at various ages from internal photon sources. III. Five-year-old.* Oak Ridge National Laboratory Rep. ORNL/TM-8381:Vol. 3.

— 1987c. *Specific absorbed fractions of energy at various ages from internal photon sources. IV. Ten-year-old.* Oak Ridge National Laboratory Rep. ORNL/TM-8381:Vol. 4.

— 1987d. *Specific absorbed fractions of energy at various ages from internal photon sources. V. Fifteen-year-old male and adult female.* Oak Ridge National Laboratory Rep. ORNL/TM-838 1:Vol. 5.

— 1987e. *Specific absorbed fractions of energy at various ages from internal photon sources. VI. Newborn.* Oak Ridge National Laboratory Rep. ORNL/TM-8381:Vol. 6.

— 1987f. *Specific absorbed fractions of energy at various ages from internal photon sources. VII. Adult male*. Oak Ridge National Laboratory Rep. ORNL/TM-8381:Vol. 7.

de Boor, C. 1978. *A practical guide to splines*, pp. 235-249. New York: Springer Verlag.

Snyder, W.S., Ford, M.R., Warner, G.G., and Watson, S.B. 1974. *A tabulation of dose equivalent per microcurie-day for source and target organs of an adult for various radionuclides: Part I.* Oak Ridge National Laboratory Rep. ORNL-5000.

Snyder, W.S., Ford, M.R., and Warner, G.G. 1978. *Estimates of specifk absorbed fractions for photon sources uniformly distributed in various organs of a heterogeneous phantom*. MIRD Pamphlet No. 5, Revised. New York: Society of Nuclear Medicine.

APPENDIX A

DESCRIPTION OF THE MATHEMATICAL PHANTOMS

INTRODUCTION

The mathematical phantoms used in our work are designed like the adult phantom of Snyder et al. (1974) and have different densities and chemical compositions for lung, skeletal, and soft tissues. (The term "soft tissues" will be used herein for all near-unit-density tissues, i.e., density $\simeq$ 1 g/cm^3.) These phantoms have been described by Cristy (1980), but several changes have been made in our phantoms since the 1980 report and are summarized in the following paragraphs.

One major change has been made: the age 15 phantom has been modified to represent both a 15-year-old male and an adult female, following the observation that the body weight and dimensions of a reference adult female (ICRP 1975) are approximately the same as those in the age 15 phantom. The breasts, the ovaries, and the uterus in the age 15 phantom were modified to be appropriate for an adult female. Also, the size of the liver was changed slightly, and the position of the gall bladder was changed so as not to overlap the new liver. These changes are noted in the description of these organs. This phantom is labeled "15-AF" in the tables of parametric values below.

The phantom labeled "Adult male" in the descriptions below is the Snyder adult phantom (Snyder et al. 1974), with certain organs modified as described by Cristy (1980). In brief, these modifications were the following: Female breast tissue was added to the trunk (this phantom, like all the others, is hermaphroditic and could represent a larger than average adult female), and the improved heart model of Coffey (1978) was fitted into the trunk. The lungs had to be redesigned to accommodate the new heart; the difference in size between right and left lungs—not represented in the Snyder phantom—was incorporated into the new design. The head was redesigned to incorporate the ideas of Hwang, Shoup, and Poston (1976), including a change in position of the thyroid. The gall bladder of Hwang et al. (1976) was added. A modification of the descending colon was made to eliminate a small overlap with the pelvic skeleton and to make the wall thickness uniform. Other minor changes were made so that the "Adult male" phantom would be consistent with the manner in which certain organs were fitted into the pediatric phantoms: the position of the adrenals, the position of the gall bladder, the size of the pancreas, and the shape and position of the thymus were all changed for this reason.

Two additional modifications to the "Adult male" phantom have been made here. The volumes of the breasts and the uterus have been changed slightly to be consistent with the "15-AF" phantom.

Another noteworthy change has been made: the chemical composition and density of each type of tissue in the phantoms (skeletal, lung, and soft tissues) have been modified slightly. Also, compositions of the skeletal and soft tissues of the newborn are now different from those at other ages. The new chemical compositions and densities are given in Tables A-l and A-4. As a consequence of this change, there are minor changes in the organ masses and whole-body masses from those listed in Cristy (1980). The new organ masses are listed in Appendix B.

Centroids of the organs are given in Appendix C.

DESCRIPTION OF THE MATHEMATICAL PHANTOMS

The phantom descriptions will follow the format of Snyder et al. (1974) and Cristy (1980) and even include language and diagrams used therein (without formal attribution in many cases) so that

the reader will not have to refer to those publications constantly to fill in missing information. However, the descriptions of the methods used to develop the phantoms and the references to anatomical data that were given in Cristy (1980) are omitted here. References to anatomical data are given wherever changes to the phantoms have been made.

Each phantom consists of three major sections: (1) an elliptical cylinder representing the trunk and arms; (2) two truncated circular cones representing the legs and feet; and (3) an elliptical cylinder capped by half an ellipsoid representing the head and neck. Attached to the legs section is a small region with a planar front surface to contain the testes. Attached to the trunk are portions of two ellipsoids representing the female breasts.

The exterior of the "Adult male" phantom is depicted in Fig. A-l. The arms are not separated from the trunk, and minor appendages such as fingers, feet, chin, and nose are omitted. Drawings depicting the external features of all the phantoms and some of the internal structures are shown in Fig. A-2.

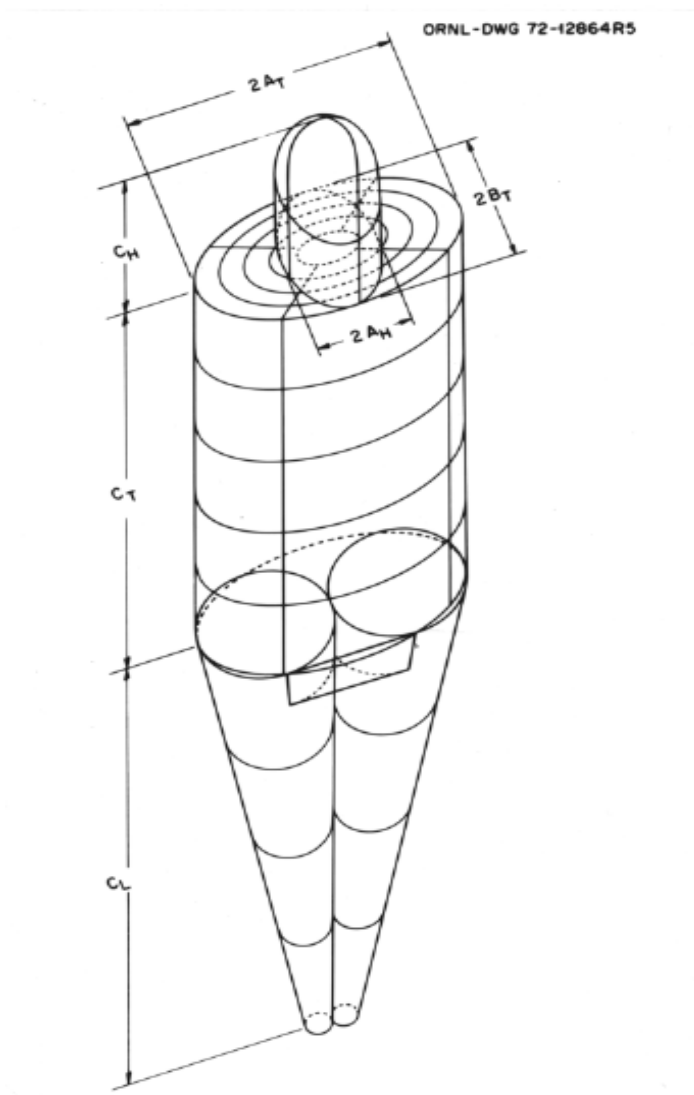

Fig. A-l. The "Adult male" phantom. Breasts are not shown.

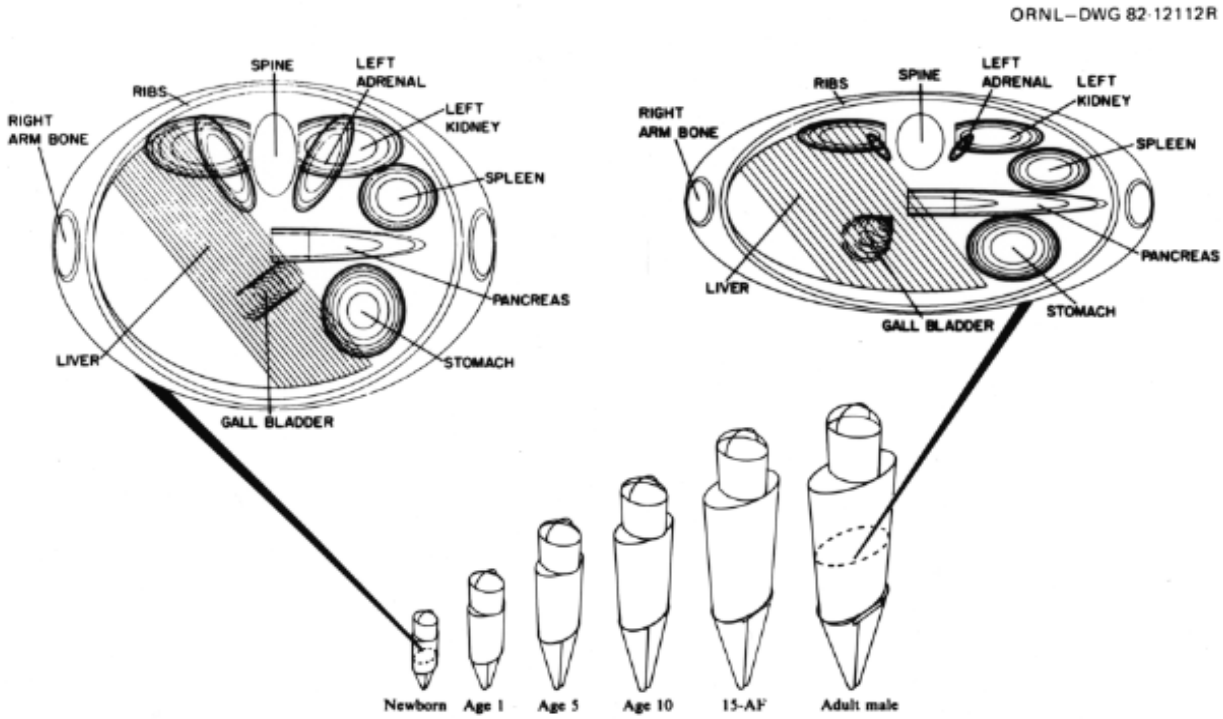

Fig. A-2. External views of the phantoms and superimposed cross-sections within the middle trunk of the newborn and adult male phantoms, depicting the space from the bottom of the liver to the top of the liver. In the younger phantoms, the head is relatively larger, the legs are relatively smaller, and the trunk is relatively thicker. The geometry of the organs may change dramatically from birth to adulthood. The "1 5-AF" and the "Adult male" phantoms have breasts appropriate for a reference adult female, which are not shown.

Elemental composition of the tissues

The Monte Carlo radiation transport code (Ryman, Warner and Eckerman 1987) recognizes three tissue types: skeletal, lung, and all other tissue (called "soft tissue" here). The elemental composition of each tissue type (for all phantoms except the newborn) is given in Table A-l. The compositions were derived from data in ICRP Publication 23 (ICRP 1975); they differ slightly from the compositions given by Snyder et al. (1974) for their adult phantom, because ICRP's revision of the P content of the body was included (see Addendum of ICRP 1980) and the minor elements F and Si were included. The value of μ/p for each tissue in Table A-l differs trivially from the value for the corresponding tissue as defined by Snyder et al.

On the basis of data in Table 105 of ICRP Publication 23, the densities of skeletal and soft tissues were changed slightly from those given by Snyder et al. Compared with the densities assigned by Snyder et al., the new densities have been changed from 1.4862 to 1.4 g/cm^3 for skeletal tissue and from 0.9869 to 1.04 g/cm^3 for soft tissue. The lung density is unchanged but was rounded to three significant digits.

These elemental compositions were derived from information on adults and are used for all phantoms except the newborn.

Newborn

It is generally acknowledged that the elemental composition and specific gravity of the newborn are different from those of the adult. A higher water content and lower bone mineral content are the most prominent differences. The specific gravity of the newborn is about 1.02 g/cm^3 compared

Table A-l. Elemental composition of the tissues for all phantoms except the newborn

Element	Percent by weight		
	Soft tissue	Skeleton	Lung
H	10.454	7.337	10.134
C	22.663	25.475	10.238
N	2.490	3.057	2.866
O	63.525	47.893	75.752
F	0	0.025	0
Na	0.112	0.326	0.184
Mg	0.013	0.112	0.007
Si	0.030	0.002	0.006
P	0.134	5.095	0.080
S	0.204	0.173	0.225
Cl	0.133	0.143	0.266
K	0.208	0.153	0.194
Ca	0.024	10.190	0.009
Fe	0.005	0.008	0.037
Zn	0.003	0.005	0.001
Rb	0.001	0.002	0.001
Sr	0	0.003	0
Zr	0.001	0	0
Pb	0	0.001	0
Density	1.04 g/cm^3	1.4 g/cm^3	0.296 g/cm^3

with about 1.07 for the adult male (ICRP 1975). Composition and tissue density are important parameters in determining the transport of photons in the body. Of particular concern is the influence of the less mineralized skeleton of the newborn.

Skeleton. The skeleton of the newborn contains more water, less fat, and less mineral than the adult skeleton. Furthermore, the distinction of two bone types, cortical and trabecular bone, is not evident in the newborn skeleton, and the marrow of the skeleton is all active. Thus it is clear that the elemental composition of the adult skeleton cannot be used when evaluating radiation transport in the newborn.

The newborn skeleton is wetter than the adult skeleton. The water content of the newborn skeleton has been estimated as 56% by Swanson and Iob (1940) and 62% by Klose (1914). Dickerson (1962) obtained a value of 64% from measurements of a whole femur.

The skeleton of the newborn contains approximately 28 g of calcium (Widdowson and Spray 1951, Mitchell et al. 1945). Assuming that the skeletal mass is 350 g (ICRP 1975) and that 38.8% of the bone ash is calcium (Holtzman 1962), we calculate that 20.6% of the skeleton is mineral.

Dickerson (1962) found the nitrogen content of the whole femur to be 2.71%. This corresponds to 16.9% protein with use of the factor 6.25 given by Fomon (1966).

The fat content was estimated as about 1% by Swanson and Iob (1940). Dickerson (1962) found 0.14% fat in the whole femur. Klose (1914) estimated the fat content as 2.6%.

With the above data in mind, we propose the following composition for the newborn skeleton; for reference we show also the adult values:

Material	Percent by weight	
	Newborn	Adult
Water	61	33
Protein	17	19
Mineral	21	28
Fat	1	19

The Ca:P ratio in the newborn skeleton is about 2.1:1 (Dickerson 1962, Swanson and Iob 1940). Hence the P content is approximately 13 g. The Mg content of bone ash is about 0.7% at all ages (see Forbes 1952). Thus the Mg content of the newborn skeleton is about 0.5 g. For all other trace elements we have assumed a content corresponding to the adult values in the 12-element approximation of Kerr (1982).

In Table A-2 the elemental composition of the newborn skeleton is presented. The RMCOMP/BAS computer program of Kerr (1982) was used to generate this table. The higher water content of the newborn skeleton and its lower mineral content, as compared with the adult skeleton (see Table A-l), are evident in the increased H and O content and decreased Ca content, respectively.

Table A-2. Elemental composition of the newborn skeleton

Element	Mass (g)	% by wt.
H	28.0	7.995
C	34.0	9.708
N	9.5	2.712
O	234.0	66.812
Na	1.1	0.314
Mg	0.5	0.143
P	13.0	3.712
S	1.1	0.314
Cl	0.49	0.140
K	0.52	0.148
Ca	28.0	7.995
Fe	0.028	0.008

Lung. Little information on the composition of the newborn lung is presented in the Reference Man Report (ICRP 1975). Thus we have used the composition of the adult lung in the radiation transport calculations for the newborn.

Whole body. Fomon (1966) has suggested a gross composition for the newborn whole body. That composition reflects a higher water and lower mineral content as noted above. We have adopted the following gross composition, with the composition of the adult shown for reference:

Material	Percent by weight	
	Newborn	Adult
Water	75.1	60.0
Fat	11.0	19.0
Protein	11.4	15.0
Bone ash	2.5	3.9

The elemental composition of the newborn is given in Table A-3. Data for the trace elements were derived by assuming the soft tissue composition of the adult (Kerr 1982). For reference the adult values for the whole body given by Kerr are also shown.

Table A-3. Elemental composition of the newborn and adult whole body

Element	Newborn		Adult
	Mass (g)	% by wt.	% by wt.
H	381.0	10.376	10.052
C	528.0	14.387	22.922
N	66.0	1.797	2.442
O	2622.0	71.407	61.289
Na	3.6	0.099	0.144
Mg	1.1	0.030	0.027
P	18.9	0.515	0.835
S	9.1	0.247	0.216
Cl	3.2	0.087	0.137
K	10.5	0.285	0.202
Ca	28.1	0.765	1.728
Fe	0.18	0.005	0.006

Soft tissue and summary. Data for soft tissue are obtained by subtracting the skeletal and lung compositions from the whole-body composition. In Table A-4 are summarized the elemental compositions of each tissue; these are the elemental compositions we have used with radiation transport calculations in the newborn phantom. The values for the specific gravity of each tissue type are also given in Table A-4. With these data the specific gravity of the newborn whole body is calculated to be 1.02 g/cm^3, consistent with observed measurements (ICRP 1975).

Description of the Body Regions and Organs

The pediatric phantoms were designed to form a developmentally consistent family with the existing Snyder adult phantom. The exterior of each phantom has approximately the form of the human body; but, as in their adult phantom, there has been no attempt to introduce small variations which would be presumed to have only a small effect on the scattering of photons. Similarly,

Table A-4. Elemental composition of the tissues of the newborn

Element	Percent by weight		
	Soft tissue	Skeleton	Lung[a]
H	10.625	7.337	10.134
C	14.964	9.708	10.238
N	1.681	2.712	2.866
O	71.830	66.811	75.752
Na	0.075	0.314	0.184
Mg	0.019	0.143	0.007
P	0.179	3.712	0.080
S	0.240	0.314	0.225
Cl	0.079	5.140	0.266
K	0.301	0.148	0.194
Ca	0.003	7.995	0.009
Fe	0.004	0.008	0.037
Density	1.04 g/cm^3	1.4 g/cm^3	0.296 g/cm^3

[a] The lung tissue also contains trace amounts of Si, Zn, and Rb—see Table A-l.

the description of the interior organs, while approximately correct as to size, shape, position, composition and density, are simplified to provide formulas which are readily calculated on a digital computer. The exact specifications of the phantom and the internal organs are given below. See Fig. A-3 for a schematic view of the principal organs.

Body regions

The body is represented as erect with the position z-axis directed upward toward the head. The *x*-axis is directed to the phantom's left (the reader's right in Fig. A-l), and the *y*-axis is directed toward the posterior side of the phantom. The origin is taken at the center of the base of the trunk section of the phantom.

In general, the dimensions (in centimeters) are given to two decimal places. The use of two decimal places does not imply that the average dimensions in some human population are known to such precision. This use is for convenience in designing the organs with correct volumes and spatial relationships.

Trunk. The trunk, exclusive of the female breasts, is represented by a solid elliptical cylinder specified by.

$$\left(\frac{x}{A_T}\right)^2 + \left(\frac{y}{B_T}\right)^2 \leq 1 \text{ and } 0 \leq z \leq C_T \quad .$$

The values of A_T, B_T, and C_T for each phantom are given in the table below.

Phantom	Length (cm)			Volume (cm^3)	Mass (g)
	A_T	B_T	C_T		
Newborn	6.35	4.90	21.60	2,110	2,100
Age 1	8.80	6.50	30.70	5,520	5,530
Age 5	11.45	7.50	40.80	11,000	11,000
Age 10	13.90	8.40	50.80	18,600	18,700
15-AF	17.25	9.80	63.10	33,500	34,500
Adult male	20.00	10.00	70.00	44,000	44,800

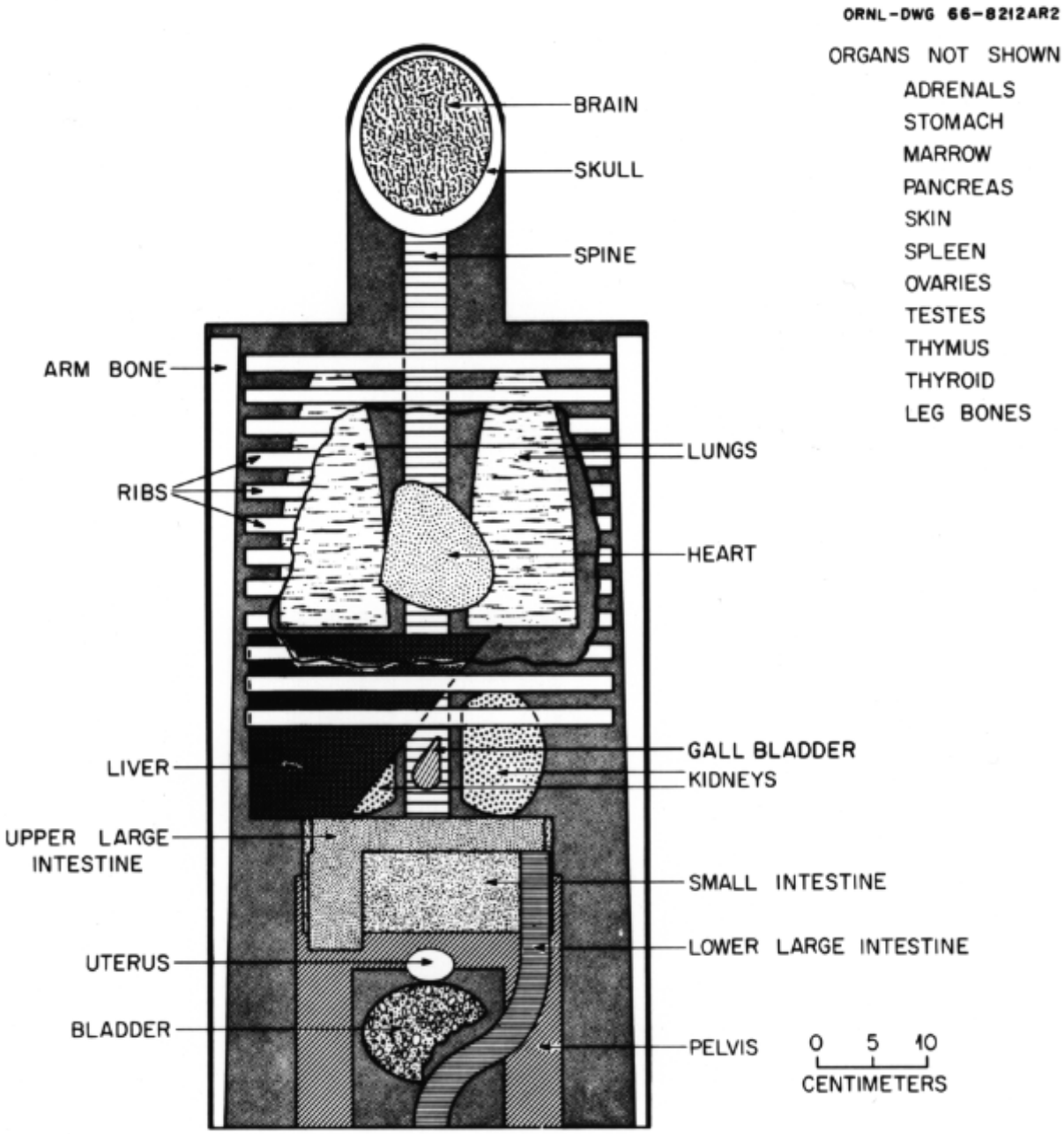

Fig. A-3. Anterior view of the principal organs in the head and trunk of the adult phantom developed by Snyder et al. (1974). Although the heart and head have been modified in this report, this schematic illustrates the simplicity of the geometries of the organs.

The trunk section includes the arms and the pelvic region to the crotch. The female breasts are appended to the outside of the trunk section. The volumes and masses for the trunk given above do not include the breasts.

Head. The head section is a right elliptical cylinder topped by half an ellipsoid. The locus is specified by

$$\left(\frac{x}{A_H}\right)^2 + \left(\frac{y}{B_H}\right)^2 \le 1 \text{ and } C_T \le z \le C_T + C_{H1} \ ,$$

or

$$\left(\frac{x}{A_H}\right)^2 + \left(\frac{y}{B_H}\right)^2 + \left(\frac{z - \left[C_T + C_{H1}\right]}{C_{H2}}\right)^2 \le 1 \text{ and } z > C_T + C_{H1} \ .$$

Phantom	Length (cm)				Volume (cm^3)	Mass (g)
	A_H	B_H	C_{H1}	C_{H2}		
Newborn	4.52	5.78	9.10	3.99	965	1,020
Age 1	6.13	7.84	12.35	5.41	2,410	2,580
Age 5	7.13	9.05	13.91	6.31	3,670	4,000
Age 10	7.43	9.40	15.19	6.59	4,300	4,710
15-AF	7.77	9.76	15.97	6.92	4,900	5,410
Adult male	8.00	10.00	16.85	7.15	5,430	6,040

The values of C_T have been given previously in the table of trunk values.

Legs. The legs region of each phantom consists of the frustrums of two circular cones specified by

$$x^2 + y^2 \le \ \pm \ x\left(A_T + \frac{A_T}{C_L} z\right)$$

$$\text{and} \quad -C_L \le z \le 0 \ ,$$

where the "±" sign is taken as plus for the left leg and minus for the right leg.

Phantom	Length (cm)		Volume (cm^3)	Mass (g)
	C_L	C_L		
Newborn	16.8	21.6	451	480
Age 1	26.5	37.1	1,470	1,600
Age 5	48.0	65.0	4,380	4,780
Age 10	66.0	90.0	8,930	9,740
15-AF	78.0	100.0	15,400	16,800
Adult male	80.0	100.0	20,800	22,600

The values of AT have been given previously in the table of trunk values.

Male genitalia. The male genitalia region of each phantom consists of the region specified by

$$\begin{gathered} z_1 \le z \le 0, \\ -r \le x \le r, \\ -r \le y \le 0, \\ \text{and } \left(x \pm r\right)^2 + y^2 \ge r^2 \ . \end{gathered}$$

The last inequality must hold for either choice of sign (i.e., the genitalia region lies outside both legs). The value of r is given by the expression $0.5A_T(1 + z/C'_L)$, where A_T is the trunk dimension and C'_L is the legs dimension defined previously. The value of z_1 is given by the expression $-(2c + S)$, where c is the value defined for the testes and S is the skin thickness. Thus, all of the parametric values are defined elsewhere, and only the volumes are given here.

Phantom	Volume (cm^3)
Newborn	5.48
Age 1	12.1
Age 5	23.2
Age 10	36.2
15-AF	109
Adult male	196

Mass of whole body. See discussion and Table B-2 in Appendix B.

Note: In the equations of the organs, which follow, the body section parameters A_T, B_T, C_T, A_H, B_H, C_{H1}, C_{H2}, C_L, and C'_L and the skin thickness S will be used without further explanation or denotation. Symbols for other parameters, usually lower case letters, will have meaning only for the organ being defined. The symbol "a," for example, is used in defining many different organs.

Organs

In the text below, each organ is explicitly defined and the volume is given. The mass determined by this volume and the appropriate density is given in Appendix B.

Skeletal system. The skeletal system consists of the 13 parts described below. A view of the whole skeleton is shown in Fig. A-4.

Leg bones. Each leg bone is the frustrum of a circular cone. In the defining inequalities below, the "+" sign is taken as minus for the left leg bone and plus for the right:

$$\left(x \pm \left[\frac{A_T}{2} + \frac{kz}{C_L - S}\right]\right)^2 + y^2 \quad \le \quad \left(R_1 + \left[\frac{R_1 - R_2}{C_L - S}\right]z\right)^2 ,$$

$$\text{and} \quad -(C_L - S) \le z \le 0 ,$$

in which

$$k = \frac{A_T}{2}\left(1 - \frac{C'_L - C_L}{C'_L}\right),$$

$$R_1 = 0.175\, A_T ,$$

$$\text{and } R_2 = \frac{A_T}{4}\left(\frac{C'_L - C_L}{C'_L}\right).$$

Phantom	Volume (cm^3)
Newborn	61.4
Age 1	207
Age 5	610
Age 10	1250
15-AF	2100
Adult male	2800

ORNL–DWG 70-4810R2A

DISTRIBUTION OF ACTIVE MARROW IN ADULT PHANTOM

SKELETAL REGION DEFINED IN PHANTOM	– OF SNYDER et al. (1974)	– OF THIS REPORT
SKULL	13.1%	8.3%
SPINE	28.4	29.9
RIBS	10.2	19.2
SCAPULAE	4.8	2.9
ARM BONES – UPPER PORTION	1.9	2.3
CLAVICLES	1.6	0.8
LEG BONES – UPPER PORTION	3.8	3.4
PELVIS	36.2	33.3
TOTAL AMOUNT OF ACTIVE BONE MARROW:	1500g	1120g

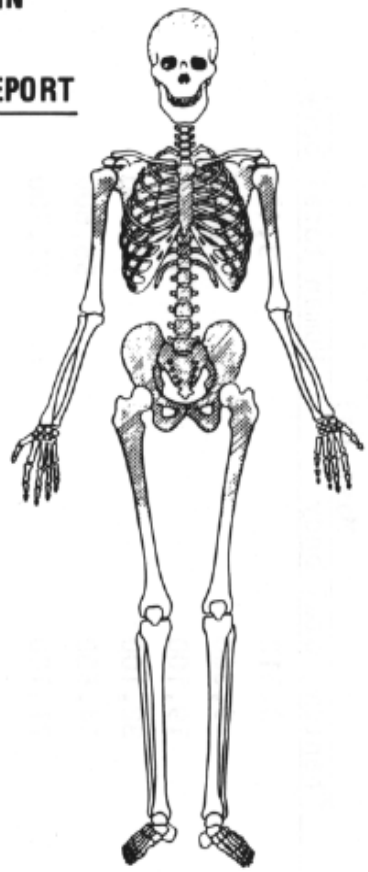

ACTIVE BONE MARROW

Fig. A-4. For the adult phantom of Snyder et al. (1974), the idealized model of the skeleton for computer calculations is shown on the left and a more realistic representation is shown on the right. The shaded areas indicate where the active bone marrow is located in the adult (from Hashimoto, 1960). The amount of active marrow in given bones, expressed as the percentage of the active marrow in the body, is also given for the adult. The values given in this report differ from those given by Snyder et al. (1974), and both sets of values are given above for comparison. Clavicles and scapulae are not shown in the phantom. The skull has been changed from that shown here to include a separate facial skeleton.

Arm bones. Each arm bone is the frustrum of an elliptical cone and is defined by

$$\left[\frac{\left(\frac{a}{2z_2}\right)(z-z_2)+(x-x_0)}{a}\right]^2+\left(\frac{y}{b}\right)^2 \le \left[\frac{2z_2+(z-z_2)}{2z_2}\right]^2$$

$$\text{and} \qquad 0 \le z \le z_2 .$$

In the table below, positive values of x_0 are used for the left arm bone, and negative for the right.

Phantom	a	b	x_0	z_0	Volume (both) (cm^3)
Newborn	0.44	1.32	±5.84	21.29	45.3
Age 1	0.62	1.76	±8.10	30.26	121
Age 5	0.80	2.03	±10.53	40.22	239
Age 10	0.97	2.27	±12.79	50.07	404
15-AF	1.21	2.65	±15.87	62.20	731
Adult male	1.40	2.70	±18.40	69.00	956

Pelvis. The pelvis is a portion of the volume between two nonconcentric elliptical cylinders. The inequalities defining the pelvis are

$$\left(\frac{x}{a_2}\right)^2+\left(\frac{y-y_{02}}{b_2}\right)^2 \le 1 ,$$

$$\left(\frac{x}{a_1}\right)^2+\left(\frac{y-y_{01}}{b_1}\right)^2 \le 1 ,$$

$$y \ge y_{02} ,$$

$$0 \le z \le z_2 ,$$

$$\text{and} \quad y \le y_1 \quad \text{if} \quad z \le z_1 .$$

Phantom	a_1	b_1	a_2	b_2	y_{01}	y_{02}	y_1	z_1	z_2	Volume (cm^3)
Newborn	3.59	5.54	3.81	5.88	-1.86	-1.47	2.45	4.32	6.79	28.9
Age 1	4.97	7.35	5.28	7.80	-2.47	-1.95	3.25	6.14	9.65	76.0
Age 5	6.47	8.48	6.87	9.00	-2.85	-2.25	3.75	8.16	12.82	151
Age 10	7.85	9.49	8.34	10.08	-3.19	-2.52	4.20	10.16	15.97	258
15-AF	9.75	11.07	10.35	11.76	-3.72	-2.94	4.90	12.62	19.83	460
Adult male	11.30	11.30	12.00	12.00	-3.80	-3.00	5.00	14.00	22.00	606

Spine. The spine is an elliptical cylinder given by

$$\left(\frac{x}{a}\right)^2+\left(\frac{y-y_0}{b}\right)^2 \le 1 \quad \text{and} \quad z_1 \le z \le z_4 .$$

It is divided into 3 portions—an upper, middle, and lower—such that dose and absorbed fractions can be estimated separately for each portion. These divisions are formed by the planes $z = z_2$ and $z = z_3$.

Phantom	a	b	y_0	z_1	z_2	z_3	z_4	Volume (cm^3)
Newborn	0.64	1.23	2.70	6.79	10.83	21.60	27.02	50.0
Age 1	0.88	1.63	3.58	9.65	15.39	30.70	38.01	128
Age 5	1.15	1.88	4.13	12.82	20.46	40.80	48.83	245
Age 10	1.39	2.10	4.62	15.97	25.47	50.80	59.89	403
15-AF	1.73	2.45	5.39	19.83	31.64	63.10	72.91	707
Adult male	2.00	2.50	5.50	22.00	35.10	70.00	80.54	920

Skull. The skull comprises the cranium and the facial skeleton. The cranium is represented by the volume between two concentric ellipsoids defined by

$$\left(\frac{x}{a}\right)^a + \left(\frac{y}{b}\right)^2 + \left(\frac{z - \left[C_T + C_{H1}\right]}{c}\right)^2 \geq 1$$

and $$\left(\frac{x}{a+d}\right)^2 + \left(\frac{y}{b+d}\right)^2 + \left(\frac{z - \left[C_T + C_{H1}\right]}{c+d}\right)^2 \leq 1 .$$

The values a, b, and c are the same as the values a, b, and c given in the statements and table for the brain.

Phantom	d	Volume (cm^3)
Newborn	0.20	49.8
Age 1	0.30	139
Age 5	0.56	339
Age 10	0.67	434
15-AF	0.76	508
Adult male	0.90	618

The facial skeleton is represented by a portion of the volume between two concentric elliptical cylinders. The portion of the volume that intersects the cranium and brain is excluded. The inequalities are

$$\left(\frac{x}{a_1}\right)^2 + \left(\frac{y}{b_1}\right)^2 \leq 1 ,$$

$$\left(\frac{x}{a_1 - d}\right)^2 + \left(\frac{y}{b_1 - d}\right)^2 \geq 1 ,$$

$$y \leq 0 ,$$

$$C_T + z_1 \leq z \leq C_T + z_5 ,$$

$$\text{and} \qquad \left(\frac{x}{a_2}\right)^2 + \left(\frac{x}{b_2}\right)^2 + \left(\frac{z - \left[C_T + C_{H1}\right]}{c_2}\right)^2 > 1 \,.$$

The variables a_2, b_2, and c_2 correspond in numerical values with the variable expressions (a + b), (b + d), and (c + d), respectively, in the statements defining the cranium and hence are not given below.

Phantom	a_1	b_1	d	z_1	z_5	Volume (cm^3)
Newborn	4.17	5.43	0.07	2.16	8.18	6.13
Age 1	5.73	7.44	0.14	2.93	11.18	22.8
Age 5	6.68	8.60	0.58	3.30	12.57	114
Age 10	6.93	8.90	0.74	3.61	13.73	161
15-AF	6.92	8.91	1.10	3.79	14.05	234
Adult male	7.00	9.00	1.40	4.00	14.73	305

Rib cage. The rib volume is a series of bands between two concentric, right-vertical, elliptical cylinders. This region is sliced by a series of equispaced horizontal planes into slabs, every other slice being a rib. The statements that must be satisfied are

$$\left(\frac{x}{a}\right)^2 + \left(\frac{y}{b}\right)^2 \le 1 \,,$$

$$\left(\frac{x}{a-d}\right)^2 + \left(\frac{x}{b-d}\right)^2 \le 1 \,,$$

$$z_1 \le z \le z_2 \,,$$

$$\text{and Integer} \left(\frac{z - z_1}{c}\right) \text{is even.}$$

The function Integer (u) is the integral part of u [e.g., Integer (3.67) = 3]. Thus, the statement "Integer [($z - z_1$)/c] is even" amounts to requiring that

$$0 \le \frac{z - z_1}{c} < 1 \quad \text{or} \quad 2 \le \frac{z - z_1}{c} \le 3 \quad \text{or} \quad 4 \le \frac{z - z_1}{c} < 5, \text{ etc.}$$

Phantom	a	b	d	z_1	z_2	c	Volume (cm^3)
Newborn	5.40	4.80	0.21	10.86	20.75	0.43	34.0
Age 1	7.48	6.37	0.28	15.44	29.47	0.61	87.4
Age 5	9.73	7.35	0.34	20.53	39.16	0.81	174
Age 10	11.82	8.23	0.39	25.43	48.89	1.02	295
15-AF	14.66	9.60	0.47	31.67	60.65	1.26	531
Adult male	17.00	9.80	0.50	35.10	67.30	1.40	694

Clavicles. The clavicles are represented as two portions of a torus which lies along the circular arc $x^2 + (y - y_0)^2 = R^2$ at $z = z_1$ and has a smaller radius of r. The clavicles include only the

portion of the torus between the planes $y_0 - y = |x| \cot \theta_1$ and $y_0 - y = |x| \cot \theta_2$. (The absolute value sign on x allows for both a right and a left clavicle.) These equations can be reduced to the form

$$(z - z_1)^2 + \left(R - \sqrt{x^2 + (y - y_0)^2}\right)^2 \le r^2 ,$$

$$\cot \theta_2 \le \frac{y_0 - y}{|x|} \le \cot \theta_1, \quad \text{and} \quad y < 0.$$

Phantom	y_0	z_1	R	r	$\cot \theta_1$	$\cot \theta_2$	Volume (both) (cm^3)
Newborn	0.73	21.06	5.07	0.2833	5.5868	0.38510	2.62
Age 1	1.38	29.93	7.14	0.3930	5.6814	0.43161	6.85
Age 5	3.14	39.78	9.80	0.4491	5.9977	0.56391	13.7
Age 10	4.93	49.53	12.40	0.5981	6.2581	0.65708	23.2
15-AF	7.22	61.52	15.93	0.7274	6.4852	0.73137	41.6
Adult male	11.10	68.25	20.00	0.7883	7.0342	0.89415	54.7

The clavicles lie slightly inside the cylinder defining the rib cage and just about the top rib.

Scapulae. The scapulae are defined as part of the volume between two concentric elliptical cylinders. For each scapula, the volume is bounded by the planes $z = z_1$, $z = z_2$, $y = m_1 |x|$, and $y = m_2|x|$. (The absolute value sign on x allows for both a right and a left scapula.) The defining inequalities are

$$\left(\frac{x}{a_2}\right)^2 + \left(\frac{y}{b}\right)^2 \le 1 ,$$

$$\left(\frac{x}{a_1}\right)^2 + \left(\frac{y}{b}\right)^2 \le 1 ,$$

$$z_1 \le z \le_2 .$$

$$y > 0 ,$$

$$\text{and} \quad m_1 < \frac{y}{|x|} < m_2 .$$

Phantom	a_1	a_2	b	z_1	z_2	m_1	m_2	Volume (both) (cm^3)
Newborn	5.40	6.04	4.80	15.71	20.77	0.39	1.23	9.64
Age 1	7.48	8.36	6.37	22.32	29.52	0.37	1.18	25.3
Age 5	9.73	10.88	7.35	29.67	39.23	0.33	1.05	50.4
Age 10	11.82	13.20	8.23	36.94	48.84	0.30	0.97	85.7
15-AF	14.66	16.36	9.60	45.88	60.67	0.28	0.91	154
Adult male	17.00	19.00	9.80	50.90	67.30	0.25	0.80	202

Bone marrow. On the right in Fig. A-4 is shown an adult skeleton, with the areas containing active marrow cross-hatched. On the left is shown the idealized skeleton used for the "Adult male" phantom with the corresponding areas cross-hatched.

The regional distributions of the active (hematopoietic) bone marrow and the inactive (fatty) marrow vary greatly with age. The approximate weights of the total (active plus inactive) marrow, the active marrow, and the inactive marrow as a function of age are given in Table A-5. Data from Hudson (1965), Custer (1974), ICRP (1975), and Woodard and Holodny (1960) were used to estimate the weight of the total marrow. The weights of active and inactive marrow in Table A-5 were calculated from the total marrow values by the method of Cristy (1981).

Table A-5. Weights of total marrow, active marrow, and inactive marrow in the body as a function of age

Phantom	Total marrow (g)	Active marrow (g)	Inactive marrow (g)
Newborn	47	47	0
Age 1	170	150	20
Age 5	460	320	140
Age 10	1200	610	590
15-AF	2600	1050	1550
Adult male	3500	1120	2380

The active marrow in individual bones, parts of bones, or bone groups of the phantoms, expressed as the percentage of active marrow in the body, are given in Table A-6. The weight of active marrow in a given bone or bone group may be found by using Tables A-5 and A-6 together. Similarly, in Table A-7 are given the inactive (fatty) marrow percentages, and the weights of inactive marrow may be found by using Tables A-5 and A-7 together. The weights of active and inactive marrow in individual bones are given in Appendix B.

The marrow, active or inactive, is assumed to be distributed uniformly in the bone regions defined. In calculating an absorbed fraction for active and for inactive marrow in these regions by the Monte Carlo computer program, it is assumed that the marrow absorbs energy per gram as efficiently as does bone. This assumption is not grossly in error at energies of 200 keV or more; but it is increasingly inaccurate at energies below 100 keV, where the photoelectric effect dominates the photon interaction process. The effect is to overestimate the dose to marrow and to underestimate the dose to the bone mineral component of the mixture. It is difficult to program the intricate microscopic intermixture of bone and marrow spaces in a more realistic fashion in the macroscopic characterization used in photon transport. As a consequence, another method of calculating this absorbed fraction was developed, as described in the section "Special Case: Active Marrow and Endosteal Tissues as Target Organs" in Chapter II.

The marrow from the lumbar vertebra L_5 and 50% of the upper half of the femora were assigned to the pelvis of each phantom (Tables A-6 and A-7). This assignment occurs because of the simplicity of the skeleton in the phantoms. For example, approximately the upper quarter of the femora is adjacent to the os coxae of the pelvis in humans, but in the phantoms the leg bones begin below the pelvis.

The total mass of the skeleton in each phantom is given in the following table.

Phantom	Mass of whole skeleton (g)
Newborn	351
Age 1	1,140
Age 5	2,710
Age 10	4,630
15-AF	7,650
Adult male	10,000

Table A-6. Active marrow in individual bones, parts of bones, or bone groups expressed as the percentage of active marrow in the body (derived from Cristy, 1981)

Phantom skeletal region	Corresponding skeletal region(s)	Percentage at various ages					
		0	1	5	10	15	Adult[a]
Skull (cranium + facial skeleton)[b]	Skull (cranium + mandible)[b]	29.50	27.47	17.44	12.72	10.12	8.32
Scapulae	Scapulae	2.70	2.73	2.72	2.89	3.26	2.85
Clavicles	Clavicles	0.80	0.83	0.85	0.89	0.98	0.79
Ribs	Ribs + sternum	9.20	9.61	10.58	13.02	16.27	19.22
Spine (upper portion[c])	Cervical vertebrae C_1-C_5	2.30	1.88	1.46	1.80	2.25	2.66
Spine (middle portion[c])	Cervical vertebrae C_6-C_7 + all thoracic vertebrae	9.40	9.27	9.58	11.79	14.75	17.41
Spine (lower portion[c])	Lumbar vertebrae L_1-L_4	1.90	3.37	5.39	6.63	8.29	9.79
Pelvis	Sacrum + os coxae + lumbar vertebra L_5 + 50% of upper 1/2 femora	11.66	16.47	23.33	28.73	33.60	33.31
Leg bones (upper portion[d])	50% of upper 1/2 femora	1.87	2.07	3.41	4.72	4.60	3.35
Leg bones (middle portion[d])	Lower 1/2 femora	3.73	3.88	6.28	6.14	2.04	0
Leg bones (lower portion[d])	Tibiae, fibulae, patellae + ankle and foot bones	16.24	13.40	11.55	5.51	0	0
Arm bones (upper portion[e])	Upper 1/2 humeri	2.32	2.41	2.36	2.49	3.14	2.29
Arm bones (middle portion[e])	Lower 1/2 humeri	2.32	2.25	2.18	1.62	0.70	0
Arm bones (lower portion[e])	Radii and ulnae + wrist and hand bones	6.07	4.36	2.88	1.06	0	0

[a]Age 40 values from Cristy (1981) were used for the "Adult male" phantom.

[b]In column 1, cranium does not include the facial skeleton, but in column 2, cranium includes all the facial skeleton except the mandible.

[c]The upper, middle, and lower portions of the spine are defined in the section on the spine.

[d]The upper portion of the leg bones is defined as the upper 14% of the length of the bones; the lower portion is defined as the lower 57%; and the middle portion is the rest. The unevenness of these numbers results from the assignment of part of the marrow in the upper femora to the pelvis.

[e]The upper portion of the arm bones is defined as the upper 25% of the length of the bones; the lower portion is defined as the lower 50%; and the middle portion is the rest.

Table A-7. Inactive marrow in individual bones, parts of bones, or bone groups expressed as the percentage of inactive marrow in the body (derived from Cristy, 1981)

Phantom skeletal region	Corresponding skeletal region(s)	Percentage at various ages					
		0	1	5	10	15	Adult[a]
Skull (cranium + facial skeleton)[b]	Skull (cranium + mandible)[b]	0	11.33	10.17	7.16	5.63	6.35
Scapulae	Scapulae	0	1.06	1.60	1.64	1.82	2.17
Clavicles	Clavicles	0	0.35	0.53	0.53	0.61	0.75
Ribs	Ribs + sternum	0	3.90	4.32	3.42	3.70	3.86
Spine (upper portion[c])	Cervical vertebrae C_1-C_5	0	0.78	0.61	0.47	0.51	0.53
Spine (middle portion[c])	Cervical vertebrae C_6-C_7 + all thoracic vertebrae	0	3.82	3.95	3.10	3.34	3.50
Spine (lower portion[c])	Lumbar vertebrae L_1-L_4	0	1.40	2.21	1.74	1.90	1.97
Pelvis	Sacrum + os coxae + lumbar vertebra L_5 + 50% of upper 1/2 femora	0	6.79	13.28	11.87	13.28	16.07
Leg bones (upper portion[d])	50% of upper 1/2 femora	0	0.84	2.36	3.31	3.83	4.70
Leg bones (middle portion[d])	Lower 1/2 femora	0	3.72	5.95	10.08	12.53	12.53
Leg bones (lower portion[d])	Tibiae, fibulae, patellae + ankle and foot bones	0	45.35	39.29	40.05	36.66	32.05
Arm bones (upper portion[e])	Upper 1/2 humeri	0	0.97	1.63	1.74	2.62	3.21
Arm bones (middle portion[e])	Lower 1/2 humeri	0	2.21	2.06	2.64	4.29	4.29
Arm bones (lower portion[e])	Radii and ulnae + wrist and hand bones	0	17.45	12.04	12.25	9.28	8.02

[a]Age 40 values from Cristy (1981) were used for the "Adult male" phantom.

[b]In column 1, cranium does not include the facial skeleton, but in column 2, cranium includes all the facial skeleton except the mandible.

[c]The upper, middle, and lower portions of the spine are defined in the section on the spine.

[d]The upper portion of the leg bones is defined as the upper 14% of the length of the bones; the lower portion is defined as the lower 57%; and the middle portion is the rest. The unevenness of these numbers results from the assignment of part of the marrow in the upper femora to the pelvis.

[e]The upper portion of the arm bones is defined as the upper 25% of the length of the bones; the lower portion is defined as the lower 50%; and the middle portion is the rest.

Adrenals. Each adrenal is half an ellipsoid atop a kidney, defined by

$$\left(\frac{x_1}{a}\right)^2 + \left(\frac{y_1}{b}\right)^2 + \left(\frac{z_1}{c}\right)^2 \le 1 \quad \text{and} \quad z_1 \ge 0 \,,$$

where the (x_1,y_1,z_1)-coordinate system is related to the phantom's (x,y,z)-coordinate system by the following rotation-translation equations, given in matrix form:

$$\begin{bmatrix} x_1 \\ y_1 \\ z_1 \end{bmatrix} = \begin{bmatrix} \cos\theta & \sin\theta & 0 \\ -\sin\theta & \cos\theta & 0 \\ 0 & 0 & 1 \end{bmatrix} \begin{bmatrix} x - x_0 \\ y - y_0 \\ z - z_0 \end{bmatrix} .$$

In the following table of parametric values, x_0 and θ are both taken as positive for the left adrenal, and both negative for the right.

Phantom	a	b	c	x_0	y_0	z_0	θ	Volume (both) (cm^3)
Newborn	1.61	0.54	1.54	±1.41	2.45	11.73	±63.3°	5.61
Age 1	1.05	0.35	2.20	±1.54	3.25	16.66	±62.2	3.39
Age 5	1.12	0.37	2.92	±2.00	3.75	22.14	±59.3	5.07
Age 10	1.17	0.39	3.63	±2.43	4.20	27.58	±57.2	6.94
15-AF	1.30	0.43	4.30	±3.02	4.90	34.26	±55.6	10.1
Adult male	1.50	0.50	5.00	±3.50	5.00	38.00	±52.0	15.7

Brain. The brain is an ellipsoid given by

$$\left(\frac{x}{a}\right)^2 + \left(\frac{y}{b}\right)^2 + \left(\frac{z - [C_t + C_{H1}]}{c}\right)^2 \le 1 \,.$$

Phantom	a	b	c	Volume (cm^3)
Newborn	4.14	5.40	3.61	338
Age 1	5.63	7.34	4.91	850
Age 5	6.34	8.26	5.52	1210
Age 10	6.51	8.48	5.67	1310
15-AF	6.58	8.57	5.73	1350
Adult male	6.60	8.60	5.75	1370

Breasts. The female breasts are represented by portions of two ellipsoids attached to the trunk, given by

$$\left(\frac{x - x_0}{a}\right)^2 + \left(\frac{y - y_0}{b}\right)^2 + \left(\frac{z - z_0}{c}\right)^2 \le 1$$

$$\text{and} \quad \left(\frac{x}{A_T}\right)^2 + \left(\frac{y}{B_T}\right)^2 > 1 \,,$$

$$\text{where} \quad y_0 = -B_T\sqrt{1-\left(\frac{x_0}{A_T}\right)^2}\,.$$

The positive values of x_0 in the table below are taken for the left breast; and the negative values, for the right breast.

Since the outer thickness S is counted as skin, the breast tissue is represented by

$$\left(\frac{x-x_0}{a-S}\right)^2+\left(\frac{y-y_0}{b-S}\right)^2+\left(\frac{z-z_0}{c-S}\right)^2 \le 1$$

$$\text{and} \quad \left(\frac{x}{A_T}\right)^2+\left(\frac{y}{B_T}\right) > 1\,.$$

The breasts in the age-15-male/adult-female phantom have been changed from those given by Cristy (1980) for the age 15 phantom. The latter were designed to represent adolescent breasts. Note also that the breasts in the "Adult male" phantom as described in Cristy (1980) are modified slightly here to be consistent with the age-15-male/adult-female phantom. (The "Adult male" phantom is hermaphroditic, like all the other phantoms, and can be used for larger-than-average females.)

There has been some disagreement between Kramer and co-workers (Kramer and Drexler 1981; Kramer, Williams, and Drexler 1982) and Cristy (1980, 1982) on the appropriate size of the breast for a reference adult female. Cristy (1982) recommends a volume of 190-200 ml for the size of a single breast, in accord with the 180 g mass recommended by the ICRP (1975). Kramer and co-workers first recommended a volume of about 365 ml (Kramer and Drexler 1981) and later changed their recommendation to 260-270 ml (Kramer et al. 1982). The present difference in recommended representative breast sizes (~195 ml vs. ~265 ml) is similar to the difference between the median (193 ml) and the mean (238 ml) in one study (Katch et al. 1980; and see Cristy, 1982), and the standard deviation of the mean is large (50%).

Cristy (1984) argues that this difference in breast size does not yield important differences in estimates of dose to the breast from either internal or external sources of photons, except at energies well below 0.025 MeV. At such low energies the phantoms may be too simple in design to give meaningful estimates of dose to the breasts for either internal or external sources—e.g., the distribution of the radiosensitive glandular tissue within the breast could become important here. Thus, this disagreement may be academic.

Phantom	a	b	c	x_0	z_0	Volume (both) (cm^3)	
						Including skin	Excluding skin
Newborn	0.36	0.36	0.36	±3.18	16.05	0.197	0.103
Age 1	0.63	0.63	0.63	±4.40	22.81	1.06	0.704
Age 5	0.79	0.79	0.79	±5.73	30.31	2.09	1.45
Age 10	0.94	0.94	0.94	±6.95	37.73	3.51	2.50
15-AF	4.95	4.35	4.15	±8.63	46.87	391	347
Adult male	4.95	4.35	4.15	±10.00	52.00	388	337

Gall bladder and contents. For the the age 1, the age 5, the age 10, the age-15-male/adult-female, and the adult male phantoms, the gall bladder is represented by the frustrum of a cone capped with a hemisphere. For the newborn phantom, the gall bladder is cylindrical. The gall bladder is defined as a walled organ.

The equations are given below in $(x_1,y_1,z_1,)$-coordinates which are related to (x,y,z)-coordinate system by the following rotation-translation equations:

$$\begin{bmatrix} x_1 \\ y_1 \\ z_1 \end{bmatrix} = \begin{bmatrix} \alpha_1 & \beta_1 & \gamma_1 \\ \alpha_2 & \beta_2 & \gamma_2 \\ \alpha_3 & \beta_3 & \gamma_3 \end{bmatrix} \begin{bmatrix} x - x_0 \\ y - y_0 \\ z - z_0 \end{bmatrix}.$$

The walls are specified as follows:

(hemispherical part)

$$x_1^2 + y_1^2 + z_1^2 \le r_2^2,$$
$$x_1^2 + y_1^2 + z_1^2 \ge r_1^2,$$
$$\text{and} \quad z_1 < 0;$$

and (conical part)

$$x_1^2 + y_1^2 \le (r_2 - sz_1)^2,$$
$$x_1^2 + y_1^2 \ge (r_1 - sz_1)^2,$$
$$\text{and} \quad 0 \le z_1 \le h.$$

The contents are specified as follows:

(hemispherical part)

$$x\frac{2}{1} + y\frac{2}{1} + z\frac{2}{2} < r\frac{2}{1}$$

$$\text{and} \quad z_1 < 0;$$

and (conical part)

$$x\frac{2}{1} + y\frac{2}{1} < (r_1 - sz_1)^2$$

$$\text{and} \quad 0 \le z_1 \le h.$$

To obtain the equations for the newborn gall bladder wall and contents, set $s = 0$ and ignore the hemispherical part.

The value of x_0 in the age-15-male/adult-female phantom has been changed from that given for the age 15 phantom in Cristy (1980). This change was made to avoid overlap with the liver, whose volume was changed.

Phantom	α_1	β_1	γ_1	α_2	β_2	γ_2	α_3	β_3	γ_3
Newborn	0.9292	0	-0.3695	-0.1018	0.9613	-0.2559	0.3553	0.2754	0.8933
Age 1	0.9770	0	-0.2132	-0.0348	0.9866	-0.1594	0.2105	0.1632	0.9639
Age 5	0.9814	0	-0.1921	-0.0291	0.9884	-0.1490	0.1898	0.1518	0.9700
Age 10	0.9722	0	-0.2342	-0.0400	0.9853	-0.1661	0.2307	0.1709	0.9579
15-AF	0.9550	0	-0.2964	-0.0606	0.9789	-0.1952	0.2903	0.2044	0.9349
Adult male	0.9615	0	-0.2748	-0.0574	0.9779	-0.2008	0.2687	0.2090	0.9403

Phantom	r_1	r_2	s	h	x_0	y_0	z_0
Newborn	0.458	0.500	0	3.10	-0.67	-1.75	8.68
Age 1	0.884	0.937	0.2275	3.54	-0.71	-2.08	13.16
Age 5	1.414	1.499	0.2275	5.66	-0.59	-2.40	17.49
Age 10	1.768	1.874	0.2275	7.07	-1.69	-2.69	21.77
15-AF	1.916	2.031	0.2275	7.66	-3.98	-3.14	27.04
Adult male	2.000	2.120	0.2275	8.00	-4.50	-3.20	30.00

Phantom	Volume (cm^3)		
	Wall	Contents	Wall + Contents
Newborn	0.392	2.04	2.43
Age 1	0.875	4.62	5.50
Age 5	3.59	18.9	22.5
Age 10	7.00	37.0	44.0
15-AF	8.92	47.1	56.0
Adult male	10.1	53.6	63.7

Gastrointestinal tract and contents. Stomach. The stomach wall is represented by the volume between two concentric ellipsoids. The contents are represented by the volume within the inner ellipsoid. The wall is defined by

$$\left(\frac{x-x_0}{a}\right)^2+\left(\frac{y-y_0}{b}\right)^2+\left(\frac{z-z_0}{c}\right)^2 \le 1$$

$$\text{and} \quad \left(\frac{x-x_0}{a-d}\right)^2+\left(\frac{y-y_0}{b-d}\right)^2+\left(\frac{z-z_0}{c-d}\right)^2 \ge 1.$$

The contents are defined by

$$\left(\frac{x-x_0}{a-d}\right)^2+\left(\frac{y-y_0}{b-d}\right)^2+\left(\frac{z-z_0}{c-d}\right)^2 < 1.$$

Phantom	a	b	c	d	x_0	y_0	z_0
Newborn	1.20	1.39	2.34	0.22	2.54	-1.96	10.80
Age 1	1.85	2.05	3.51	0.33	3.52	-2.70	15.35
Age 5	2.55	2.40	4.66	0.45	4.58	-3.15	20.40
Age 10	3.14	2.74	5.81	0.53	5.56	-3.51	25.40
15-AF	3.43	2.92	7.16	0.56	6.90	-3.92	31.55
Adult male	4.00	3.00	8.00	0.613	8.00	-4.00	35.00

Phantom	Volume-wall (cm^3)	Volume-contents (cm^3)
Newborn	6.17	10.2
Age 1	20.9	34.8
Age 5	47.2	72.2
Age 10	81.8	128
15-AF	113	187
Adult male	152	250

The stomach represented here is a "full" stomach, and the average dose rate, even for the same activity present, probably varies greatly depending on the degree of extension of the stomach, presence of air spaces, etc.

Small intestine. The small intestine does not seem to remain in any "standard position" except the ends, which are relatively fixed. Thus, the small intestine is to be regarded as occupying a volume within which it is free to move. No attempt to determine a specific configuration is made here, and thus the wall and contents are not distinguished for estimation of photon dose.

The small intestine and contents are represented by a section of an elliptical cylinder, defined by

$$\left(\frac{x}{a}\right)^2 + \left(\frac{y - y_0}{b}\right)^2 \le 1,$$
$$y_1 \le y \le_2,$$
$$\text{and} \quad z_1 \le z \le z_2.$$

The portion of the large intestine within this region is excluded.

Phantom	a	b	y_0	y_1	y_2	z_1	z_2	Volume (cm^3)
Newborn	3.59	5.54	-1.86	-2.39	1.08	5.25	8.33	50.9
Age 1	4.97	7.35	-2.47	-3.16	1.43	7.46	11.84	132
Age 5	6.47	8.48	-2.85	-3.65	1.65	9.91	15.74	265
Age 10	7.85	9.49	-3.19	-4.08	1.85	12.34	19.59	447
15-AF	9.75	11.07	-3.72	-4.76	2.16	15.32	24.34	806
Adult male	11.30	11.30	-3.80	-4.86	2.20	17.00	27.00	1060

Upper large intestine. The upper large intestine consists of an ascending colon and a transverse colon.

The ascending colon wall is defined by the space between two coaxial elliptical cylinders:

$$\left(\frac{x - x_0}{a}\right)^2 + \left(\frac{y - y_0}{b}\right)^2 \le 1,$$
$$\left(\frac{x - x_0}{a - d}\right)^2 + \left(\frac{y - y_0}{b - d}\right)^2 \ge 1,$$
$$\text{and} \quad z_1 \le z \le z_2.$$

The contents are defined by the space within the inner cylinder,

$$\left(\frac{x - x_0}{a - d}\right)^2 + \left(\frac{y - y_0}{b - d}\right)^2 < 1$$
$$\text{and} \quad z_1 \le z \le z_2.$$

Phantom	a	b	d	x_0	y_0	z_1	z_2	Volume (cm^3)	
								Wall	Contents
Newborn	0.79	1.23	0.27	-2.70	-1.16	4.46	7.41	4.38	4.63
Age 1	1.10	1.63	0.37	-3.74	-1.53	6.34	10.53	11.5	12.1
Age 5	1.43	1.88	0.46	-4.87	-1.77	8.42	13.99	22.9	24.1
Age 10	1.74	2.10	0.54	-5.91	-1.98	10.49	17.42	38.8	40.8
15-AF	2.16	2.45	0.65	-7.33	-2.31	13.03	21.63	69.5	73.4
Adult male	2.50	2.50	0.7085	-8.50	-2.36	14.45	24.00	91.2	96.3

The transverse colon wall is also defined by the space between two coaxial elliptical cylinders:

$$\left(\frac{y - y_0}{b}\right)^2 + \left(\frac{z - z_0}{c}\right)^2 \le 1,$$

$$\left(\frac{y - y_0}{b - d}\right)^2 + \left(\frac{z - z_0}{c - d}\right)^2 \ge 1,$$

$$\text{and} \quad -x_1 \le x \ge x_1.$$

The contents are defined by the space within the inner cylinder,

$$\left(\frac{y - y_0}{b - d}\right)^2 + \left(\frac{z - z_0}{c - d}\right)^2 < 1$$

$$\text{and} \quad -x_1 \le x \le x_1.$$

Phantom	b	c	d	y_0	z_0	x_1	Volume (cm^3)	
							Wall	Contents
Newborn	1.23	0.46	0.18	-1.16	7.87	3.33	5.69	6.15
Age 1	1.63	0.65	0.26	-1.53	11.18	4.62	15.2	15.5
Age 5	1.88	0.87	0.33	-1.77	14.86	6.01	30.2	31.6
Age 10	2.10	1.08	0.40	-1.98	18.51	7.30	51.0	53.0
15-AF	2.45	1.35	0.49	-2.31	22.99	9.06	92.3	96.0
Adult male	2.50	1.50	0.527	-2.36	25.50	10.50	121	127

Lower large intestine. The lower large intestine consists of a descending colon and a sigmoid colon.

The descending colon wall is defined by the space between two coaxial elliptical cylinders. The axis of the cylinders is at a slight angle with the z-axis of the phantom, but the ends of the descending colon are defined by horizontal planes ($z = z_1$ and $z = z_2$). The wall is specified by

$$\left(\frac{x - x_0}{a}\right)^2 + \left(\frac{y - y_0}{b}\right)^2 \le 1,$$

$$\left(\frac{x - x_0}{a - d}\right)^2 + \left(\frac{y - y_0}{b - d}\right)^2 \ge 1,$$

$$\text{and} \quad z_1 \le z \le z_2,$$

where

$$x_0 = x_1 + \frac{m_x(z - z_2)}{z_2 - z_1}$$

$$\text{and} \quad y_0 = \frac{m_y(z_1 - z)}{z_2 - z_1}.$$

The contents of the descending colon are defined by the space within the inner cylinder, i.e.,

$$\left(\frac{x - x_0}{a - d}\right)^2 + \left(\frac{y - y_0}{b - d}\right)^2 < 1,$$

$$\text{and} \quad z_1 \le z \le z_2 .$$

Phantom	a	b	d	x_1	m_x	m_y	z_1	z_2	Volume (cm^3)	
									Wall	Contents
Newborn	0.60	1.04	0.20	2.94	0.2477	1.225	2.69	7.41	4.27	4.98
Age 1	0.83	1.38	0.27	4.07	0.3432	1.625	3.82	10.53	11.0	13.1
Age 5	1.08	1.60	0.34	5.30	0.4466	1.875	5.08	13.99	22.3	26.1
Age 10	1.31	1.79	0.40	6.43	0.5421	2.100	6.33	17.42	37.6	44.1
15-AF	1.62	2.09	0.49	7.98	0.6728	2.450	7.86	21.63	68.3	78.2
Adult male	1.88	2.13	0.54	9.25	0.7800	2.500	8.72	24.00	89.9	102

The sigmoid colon plus contents is represented by portions of two flattened tori; that is, the axis of each torus is circular but the cross-section is elliptical. The wall is defined as follows:

(portion of upper torus)

$$\left(\frac{\sqrt{(x - x_0)^2 + (z - z_0)^2} - R_1}{a}\right)^2 + \left(\frac{y}{b}\right)^2 \le 1,$$

$$\left(\frac{\sqrt{(x - x_0)^2 + (z - z_0)^2} - R_1}{a - d}\right)^2 + \left(\frac{y}{b - d}\right)^2 \ge 1,$$

$$x \ge x_0, \quad \text{and} \quad z \le z_0;$$

and (portion of lower torus)

$$\left(\frac{\sqrt{(x - x_0)^2 + z^2} - R_2}{a}\right)^2 + \left(\frac{y}{b}\right)^2 \le 1,$$

$$\left(\frac{\sqrt{(x - x_0)^2 + z^2} - R_2}{a - d}\right)^2 + \left(\frac{y}{b - d}\right)^2 \ge 1,$$

$$x \le x_0, \quad \text{and} \quad z \ge 0.$$

The contents of the sigmoid colon are defined as follows:

(portion of upper torus)

$$\left(\frac{\sqrt{(x - x_0)^2 + (z - z_0)^2} - R_1}{a - d}\right)^2 + \left(\frac{y}{b - d}\right)^2 < 1,$$

$$x \ge x_0, \quad \text{and} \quad z \le z_0;$$

and (portion of lower torus)

$$\left(\frac{\sqrt{(x - x_0) + z^2} - R_2}{a - d}\right)^2 + \left(\frac{y}{b - d}\right)^2 < 1,$$

$$x \le x_0, \quad \text{and} \quad z \ge 0.$$

Phantom	a	b	d	x_0	z_0	R_1	R_2	Volume (cm^3)	
								Wall	Contents
Newborn	0.50	0.77	0.25	0.95	2.69	1.77	0.92	3.39	1.73
Age 1	0.69	1.02	0.34	1.32	3.82	2.51	1.31	8.78	4.49
Age 5	0.88	1.21	0.42	1.72	5.08	3.33	1.75	17.6	9.11
Age 10	0.96	1.50	0.48	2.09	6.33	4.15	2.18	29.7	15.3
15-AF	1.18	1.76	0.59	2.59	7.86	5.16	2.70	53.8	26.8
Adult male	1.57	1.57	0.66	3.00	8.72	5.72	3.00	70.4	35.6

Heart and contents. The heart model developed by Coffey for the adult phantom has been employed (Coffey 1978; Coffey, Cristy, and Warner 1981). The outer surface of the heart is represented by four quarter-ellipsoids. Within this space, the heart is divided into regions representing the muscular walls and the four chambers. The equations are given below in (x_1,y_1,z_1)-coordinates, which are related to the (x,y,z)-coordinate system by the following rotation-translation equations:

$$\begin{bmatrix} x_1 \\ y_1 \\ z_1 \end{bmatrix} = \begin{bmatrix} \alpha_1 & \beta_1 & \gamma_1 \\ \alpha_2 & \beta_2 & \gamma_2 \\ \alpha_3 & \beta_3 & \gamma_3 \end{bmatrix} \begin{bmatrix} x - x_0 \\ y - y_0 \\ z - z_0 \end{bmatrix}.$$

In the equations below, the variable names *VX*, *AVY*, *LAVZ*, *RAVZ*, *AX*, *TLVW*, *TRVW*, and *TAW* are acronyms in which the letters *L* and *R* refer to left and right, *A* and *V* to atrium and ventricle, *T* to thickness, *W* to wall, and *X*, *Y*, and *Z* to dimensions in the x_1, y_l, and z_1 directions. Thus, *AVY* is a dimension common to the atria and ventricles in the y_1 direction.

The left ventricle (wall + contents) is represented by half an ellipsoid. The wall is defined by the inequalities

$$\left(\frac{x_1}{VX}\right)^2 + \left(\frac{y_1}{AVY}\right)^2 + \left(\frac{z_1}{LAVZ}\right)^2 \le 1,$$

$$\left(\frac{x_1}{VX - TLVW}\right)^2 + \left(\frac{y_1}{AVY - TLVW}\right)^2 + \left(\frac{z_1}{LAVZ - TLVW}\right)^2 \ge 1,$$

$$\text{and} \quad x_1 \ge 0.$$

The contents of the left ventricle are defined by the volume within the inner of the two half-ellipsoids given above, i.e.,

$$\left(\frac{x_1}{VX - TLVW}\right)^2 + \left(\frac{y_1}{AVY - TLVW}\right)^2 + \left(\frac{z_1}{LAVZ - TLVW}\right)^2 < 1,$$

$$\text{and} \quad x_1 \ge 0.$$

The right ventricle (wall + contents) is represented by a quarter-ellipsoid that wraps around half of the left ventricle. The wall is defined by the inequalities

$$\left(\frac{x_1}{VX}\right)^2 + \left(\frac{y_1}{AVY}\right)^2 + \left(\frac{z_1}{RAVZ}\right)^2 \le 1,$$

$$\left(\frac{x_1}{VX - TRVW}\right)^2 + \left(\frac{y_1}{AVY - TRVW}\right)^2 + \left(\frac{z_1}{RAVZ - TRVW}\right)^2 \geq 1,$$

$$x_1 \geq 0, \quad \text{and} \quad z_1 < 0.$$

The volume common to the left and right ventricle walls is considered part of the left ventricle wall and is excluded here.

The contents of the right ventricle are defined by the inequalities

$$\left(\frac{x_1}{VX - TRVW}\right)^2 + \left(\frac{y_1}{AVY - TRVW}\right)^2 + \left(\frac{z_1}{RAVZ - TRVW}\right)^2 < 1,$$

$$x_1 \geq 0, \quad \text{and} \quad z_1 < 0.$$

The portion of the left ventricle within this space is excluded, i.e., the inequality

$$\left(\frac{x_1}{VX}\right)^2 + \left(\frac{y_1}{AVY}\right)^2 + \left(\frac{z_1}{LAVZ}\right)^2 > 1$$

must also hold.

The left atrium (wall + contents) is represented by two adjacent quarter-ellipsoids. The left atria1 wall is defined as follows:

(part 1)

$$\left(\frac{x_1}{AX}\right)^2 + \left(\frac{y_1}{AVY}\right)^2 + \left(\frac{z_1}{LAVZ}\right)^2 \leq 1,$$

$$\left(\frac{x_1}{AX - TAW}\right)^2 + \left(\frac{y_1}{AVY - TAW}\right)^2 + \left(\frac{z_1}{LAVZ - TAW}\right)^2 \leq 1,$$

$$x_1 < 0, \quad \text{and} \quad z_1 \geq 0;$$

and (part 2)

$$\left(\frac{x_1}{AX}\right)^2 + \left(\frac{y_1}{AVY}\right)^2 + \left(\frac{z_1}{LAVZ - TLVW + TAW}\right)^2 \leq 1,$$

$$\left(\frac{x_1}{AX - TAW}\right)^2 + \left(\frac{y_1}{AVY - TAW}\right)^2 + \left(\frac{z_1}{LAVZ - TLVW}\right)^2 \geq 1,$$

$$x_1 < 0, \quad \text{and} \quad z_1 < 0.$$

The contents of the left atrium are represented by the volume within these walls, i.e., by

(part 1)

$$\left(\frac{x_1}{AX - TAW}\right)^2 + \left(\frac{y_1}{AVY - TAW}\right)^2 + \left(\frac{z_1}{LAVZ - TAW}\right)^2 < 1,$$

$$x_1 < 0, \quad \text{and} \quad z_1 \geq 0;$$

and (part 2)

$$\left(\frac{x_1}{AX - TAW}\right)^2 + \left(\frac{y_1}{AVY - TAW}\right)^2 + \left(\frac{z_1}{LAVZ - TLVW}\right)^2 < 1,$$

$$x_1 < 0, \quad \text{and} \quad z_1 < 0.$$

The right atrium (wall + contents) is represented by a quarter-ellipsoid that wraps around part of the left atrium. The wall is defined by the inequalities

$$\left(\frac{x_1}{AX}\right)^2 + \left(\frac{y_1}{AVY}\right)^2 + \left(\frac{z_1}{RAVZ}\right)^2 \le 1,$$

$$\left(\frac{x_1}{AX - TAW}\right)^2 + \left(\frac{y_1}{AVY - TAW}\right)^2 + \left(\frac{z_1}{RAVZ - TAW}\right)^2 \ge 1,$$

$$x_1 < 0, \quad \text{and} \quad z_1 < 0.$$

The volume common to the left and right atria1 walls is considered part of the left atria1 wall and is excluded here.

The contents of the right atrium are defined by the inequalities

$$\left(\frac{x_1}{AX - TAW}\right)^2 + \left(\frac{y_1}{AVY - TAW}\right)^2 + \left(\frac{z_1}{RAVZ - TAW}\right)^2 < 1,$$

$$x_1 < 0, \quad \text{and} \quad z_1 < 0.$$

The portion of the left atrium within this space is excluded, i.e., the inequality

$$\left(\frac{x_1}{AX}\right)^2 + \left(\frac{y_1}{AVY}\right)^2 + \left(\frac{z_1}{LAVZ - TLVW - TAW}\right)^2 > 1$$

must also hold.

The age-dependent values of all the heart parameters are given in the tables below. The volumes are given in cubic centimeters.

Phantom	α_1	β_1	γ_1	α_2	β_2	γ_2	α_3	β_3	γ_3
Newborn	0.5942	-0.6421	-0.4845	-0.3291	0.3556	-0.8748	0.7340	0.6792	0
Age 1	0.6009	-0.6216	-0.5025	-0.3493	0.3613	-0.8646	0.7190	0.6950	0
Age 5	0.6237	-0.5721	-0.5327	-0.3926	0.3601	-0.8463	0.6760	0.7369	0
Age 10	0.6345	-0.5370	-0.5559	-0.4243	0.3591	-0.8312	0.6460	0.7633	0
15-AF	0.6453	-0.5134	-0.5658	-0.4428	0.3523	-0.8245	0.6226	0.7825	0
Adult male	0.6751	-0.4727	-0.5664	-0.4640	0.3249	-0.8241	0.5736	0.8191	0

Phantom	*VX*	*AVY*	*LAVZ*	*RAVZ*	*AX*	*TLVW*	*TRVW*	*TAX*	x_0	y_0	z_0
Newborn	3.71	2.16	1.34	3.02	2.33	0.56	0.26	0.13	0.42	-1.08	16.05
Age 1	4.67	2.72	1.68	3.80	2.93	0.71	0.33	0.16	0.54	-1.67	22.43
Age 5	5.72	3.33	2.06	4.66	3.59	0.86	0.40	0.20	0.77	-1.70	29.60
Age 10	6.73	3.92	2.43	5.48	4.23	1.02	0.47	0.23	0.80	-1.70	36.60
15-AF	7.86	4.57	2.83	6.40	4.94	1.19	0.55	0.27	0.86	-2.10	45.10
Adult male	8.60	5.00	3.10	7.00	5.40	1.30	0.60	0.30	1.00	-1.80	50.00

Phantom	Volume			
	Left ventricle		Right ventricle	
	Wall	Contents	Wall	Contents
Newborn	14.3	8.23	5.42	8.68
Age 1	28.5	16.2	10.9	17.3
Age 5	52.0	30.2	19.8	32.0
Age 10	85.4	48.9	32.3	52.0
15-AF	135	77.4	51.4	82.9
Adult male	177	102	67.2	108

Phantom	Volume			
	Left ventricle		Right ventricle	
	Wall	Contents	Wall	Contents
Newborn	2.55	9.31	2.21	8.91
Age 1	4.96	18.5	4.32	18.0
Age 5	9.31	34.0	8.09	32.7
Age 10	14.9	55.8	12.9	53.8
15-AF	23.7	88.3	20.7	85.5
Adult male	31.6	115	27.4	111

Phantom	Volume-total heart walls	Volume-total heart contents
Newborn	24.4	35.1
Age 1	48.7	69.9
Age 5	89.3	129
Age 10	145	210
15-AF	231	334
Adult male	303	437

Kidneys. Each kidney is an ellipsoid cut by a plane, given by the following:

$$\left(\frac{x - x_0}{a}\right)^2 + \left(\frac{y - y_0}{b}\right)^2 + \left(\frac{z - z_0}{c}\right)^2 \le 1$$

$$\text{and} \quad |x| \ge x_1.$$

In the following table, x_0 is taken as positive for the left kidney, and negative for the right.

Phantom	a	b	c	x_0	y_0	z_0	z_1	Volume (both) (cm^3)
Newborn	1.79	0.93	1.70	±1.91	2.94	10.03	0.71	22.0
Age 1	2.61	1.25	2.41	±2.64	3.90	14.25	0.95	60.5
Age 5	3.20	1.40	3.20	±3.44	4.50	18.94	1.31	111
Age 10	3.66	1.47	3.99	±4.17	5.04	23.59	1.74	166
15-AF	4.05	1.53	4.96	±5.18	5.88	29.30	2.48	238
Adult male	4.50	1.50	5.50	±6.00	6.00	32.50	3.00	288

Liver. The liver is defined by an elliptical cylinder cut by a plane as follows:

$$\left(\frac{x}{a}\right)^2 + \left(\frac{y}{b}\right)^2 \le 1,$$

$$\frac{x}{x_m} + \frac{y}{y_m} - \frac{z}{z_m} \le -1,$$

$$\text{and} \quad z_1 \le z \le z_2 .$$

The liver in the age-15-male/adult-female phantom has been changed slightly from that given for the age 15 phantom in Cristy (1980) to match the data for a reference adult female (ICRP 1975).

Phantom	a	b	x_m	y_0	z_m	z_1	z_2
Newborn	5.19	4.25	8.45	10.90	13.27	8.33	13.27
Age 1	7.20	5.47	12.83	16.55	18.86	11.84	18.86
Age 5	9.39	6.30	16.27	20.34	25.06	15.74	25.06
Age 10	11.43	6.83	21.98	29.67	31.21	19.59	31.21
15-AF	14.19	7.84	31.51	44.75	38.76	24.34	38.76
Adult male	16.50	8.00	35.00	45.00	43.00	27.00	43.00

Phantom	Volume (cm^3)
Newborn	117
Age 1	281
Age 5	562
Age 10	853
15-AF	1350
Adult male	1830

Lungs. Each lung is represented by half an ellipsoid with a section removed. Note that the section removed from the left lung is larger than that removed from the right lung because of the position of the heart. The right lung is defined as follows:

$$\left(\frac{x + x_0}{a}\right)^2 + \left(\frac{y}{b}\right)^2 + \left(\frac{z - z_0}{c}\right)^2 \le 1$$

$$\text{and} \quad z \ge z_0 ;$$

if $z_{1R} \le z \le z_{2R}$ and $y < y_{2R}$, then $x \le x_{1R}$ must also hold.

The statements for the left lung are similar, but replace ($x + x_0$) with ($x - x_0$), and z_{1R}, z_{2R}, and y_{2R} with z_0, z_{2L}, and y_{2L}, respectively; and replace the inequality ($x \le x_{1R}$) with ($x \ge x_{1L}$). The letters *R* and *L* refer to right and left.

Phantom	a	b	c	x_0	z_0
Newborn	1.89	3.68	7.41	2.70	13.42
Age 1	2.68	4.88	10.53	3.74	19.08
Age 5	3.47	5.63	13.99	4.87	25.35
Age 10	3.82	6.30	17.42	5.91	31.57
15-AF	4.09	6.98	20.55	7.33	39.21
Adult male	5.00	7.50	24.00	8.50	43.50

Phantom	x_{1R}	y_{1R}	z_{1R}	z_{2R}	x_{1L}	y_{1L}	z_{2L}
Newborn	-2.30	0.75	14.15	17.85	+3.00	0.30	17.90
Age 1	-2.90	0.70	20.10	24.60	+3.90	0.40	24.80
Age 5	-3.50	1.00	26.90	32.30	+5.00	0.50	32.60
Age 10	-4.10	1.30	33.40	39.60	+5.90	0.75	40.00
15-AF	-5.00	1.20	41.60	48.50	+7.00	0.70	49.00
Adult male	-5.40	1.50	46.00	54.00	+8.00	1.00	55.00

Phantom	Volume (cm^3)		
	Left lung	Right lung	Both lungs
Newborn	79.1	91.9	171
Age 1	225	259	484
Age 5	454	526	980
Age 10	709	821	1530
15-AF	1020	1180	2200
Adult male	1560	1810	3380

Ovaries. Each ovary is an ellipsoid and is given by

$$\left(\frac{x - x_0}{a}\right)^2 + \left(\frac{y}{b}\right)^2 + \left(\frac{z - z_0}{c}\right)^2 \le 1.$$

The values of x_0 in the table below are taken as positive for the left ovary, and negative for the right ovary.

The ovaries in the age-15-male/adult-female phantom have been changed from those in the age 15 phantom in Cristy (1980), to represent an adult female rather than an adolescent female. There is a small intersection of the right ovary (as defined above) with the wall of the ascending colon and a small intersection of the left ovary (as defined above) with the wall of the descending colon in this phantom. These regions of intersection are defined as colon walls only in the computer codes. These regions are also excluded in the computations of volume and mass of the ovaries given below and in Appendix B.

The ovaries in the "adult male" phantom have not been modified from those of Snyder et al. (1974) and are smaller than those in the "15-AF" phantom. For recommended values of specific absorbed fractions in the companion volumes, values of Φ(ovaries←ovaries) derived from the "15-AF" phantom are tabulated for both the "age 15 male or adult female" and the "adult male or large adult female."

Phantom	a	b	c	x_0	z_0	Volume (both) (cm^3)
Newborn	0.30	0.22	0.57	±1.91	4.63	0.315
Age 1	0.38	0.28	0.77	±2.64	6.58	0.686
Age 5	0.53	0.35	1.07	±3.44	8.74	1.66
Age 10	0.66	0.40	1.36	±4.17	10.89	3.01
15-AF	1.17	0.58	1.80	±5.18	13.52	10.1
Adult male	1.00	0.50	2.00	±6.00	15.00	8.38

Pancreas. The pancreas is half an ellipsoid with a section removed. It is defined by

$$\left(\frac{x - x_0}{a}\right)^2 + \left(\frac{y}{b}\right)^2 + \left(\frac{z - z_0}{c}\right)^2 \le 1,$$

$$x \ge x_0,$$

$$\text{and} \quad z \ge z_0 \quad \text{if} \quad x > x_1.$$

Phantom	a	b	c	x_0	z_0	x_1	Volume (cm^3)
Newborn	4.32	0.50	0.87	-0.09	11.42	0.99	0.315
Age 1	6.85	0.71	1.41	-0.43	16.23	1.32	0.686
Age 5	9.16	0.90	1.92	-0.57	21.57	1.72	1.66
Age 10	10.09	0.92	2.17	-0.38	26.85	2.15	3.01
15-AF	13.32	1.14	2.87	-0.72	33.35	2.61	10.1
Adult male	16.00	1.20	3.30	-1.00	37.00	3.00	8.38

Skin. Skin is represented as a layer of thickness S extending over the exterior of the phantom, including the exposed top of the trunk and the bottom of the legs, but excluding the exposed bottom of the trunk, top of the legs, and bottom of the head. The part of the legs covered by the male genitalia region has skin, but the part of the trunk covered by the female breasts does not.

This layer corresponds to the dermis as well as the epidermis. Greater thicknesses in places such as the back have been ignored.

Phantom	S	Volume of skin (cm^3)				
		Head	Trunk	Legs	Male Gentalia	Total
Newborn	0.07	30.2	54.6	28.3	0.741	114
Age 1	0.08	63.6	121	75.0	1.48	261
Age 5	0.09	94.3	225	195	2.64	517
Age 10	0.10	117	370	363	4.05	854
15-AF	0.17	217	958	866	13.5	2050
Adult male	0.20	274	1410	1190	23.4	2890

Spleen. The spleen is represented by the ellipsoid

$$\left(\frac{x - x_0}{a}\right)^2 + \left(\frac{y - y_0}{b}\right)^2 + \left(\frac{z - z_0}{c}\right)^2 \leq 1.$$

Phantom	a	b	c	x_0	y_0	z_0	Volume (cm^3)
Newborn	1.13	1.00	1.85	3.54	1.42	11.42	8.76
Age 1	1.65	1.35	2.63	4.94	1.85	16.23	24.5
Age 5	2.09	1.52	3.49	6.40	2.25	21.57	46.4
Age 10	2.43	1.68	4.35	7.65	2.52	26.85	74.4
15-AF	2.90	1.88	5.19	9.49	2.94	33.35	119
Adult male	3.50	2.00	6.00	11.00	3.00	37.00	176

Testes. The testes are represented by the ellipsoids

$$\left(\frac{x \pm a}{a}\right)^2 + \left(\frac{y - y_0}{b}\right)^2 + \left(\frac{z + c}{c}\right)^2 \leq 1,$$

where the "±" sign is taken as positive for the right testis and negative for the left testis.

Phantom	a	b	c	y_0	Volume (both) (cm^3)
Newborn	1.13	1.00	1.85	1.42	8.76
Age 1	1.65	1.35	2.63	1.85	24.5
Age 5	2.09	1.52	3.49	2.25	46.4
Age 10	2.43	1.68	4.35	2.52	74.4
15-AF	2.90	1.88	5.19	2.94	119
Adult male	3.50	2.00	6.00	3.00	176

Thymus. The thymus is represented by an ellipsoid, given by

$$\left(\frac{x}{a}\right)^2 + \left(\frac{y - y_0}{b}\right)^2 + \left(\frac{z - z_0}{c}\right)^2 \leq 1.$$

Phantom	a	b	c	y_0	z_0	Volume (cm^3)
Newborn	1.76	0.70	2.10	-3.60	19.30	10.8
Age 1	1.75	1.00	3.00	-4.75	27.00	22.0
Age 5	1.85	1.05	3.50	-5.48	35.00	28.5
Age 10	1.85	1.00	3.90	-6.13	43.00	30.2
15-AF	1.75	0.93	4.00	-7.15	52.00	27.3
Adult male	1.50	0.80	4.00	-7.30	57.00	20.1

Thyroid. The lobes of the thyroid lie between two concentric cylinders and are formed by a cutting surface. The statements defining this organ are

$$x^2 + (y - y_0)^2 \le R^2,$$

$$x^2 + (y - y_0)^2 \ge r^2,$$

$$y \le y_0$$

$$C_T \le z \le C_T + c,$$

$$\text{and} \quad [(y - y_0) - |x|]^2 \ge 2[x^2 + (y - y_0)^2]\tau^2,$$

in which

$$\tau = \left(\frac{\sqrt{2} - 2}{2}\right)\left(\frac{z - C_T}{0.25c}\right) + 1 \quad \text{for} \quad 0 \le z - C_T \le 0.25c$$

$$\text{and} \quad \tau = \left(\frac{2 - \sqrt{2}}{2}\right)\left(\frac{z - C_T}{0.75c}\right) + \frac{2\sqrt{2} - 1}{3} \quad \text{for} \quad 0.25c \le z - C_T \le c.$$

Phantom	R	r	c	y_0	Volume (cm^3)
Newborn	0.87	0.40	2.00	-2.14	1.24
Age 1	0.97	0.44	2.21	-2.87	1.71
Age 5	1.21	0.55	2.76	-3.31	3.32
Age 10	1.60	0.73	3.63	-3.56	7.62
15-AF	1.85	0.83	4.20	-3.91	11.9
Adult male	2.20	1.00	5.00	-4.00	19.9

It was stated in Cristy (1980, p. 94) that, when compared with the adult phantom of Snyder et al. (1974), the "thyroid has been moved closer to the front surface of the body, after Hwang, Shoup, and Poston [19761. The thyroid had been located too deeply within the neck-and-head region for external dose calculations (Kerr 1979). The new position is better for external sources anterior to the body, but it will remain unsuitable for external sources from the back or sides until a separate neck region is added to the phantom design. This difficulty is unimportant for internal emitters."

There are several errors in this quoted paragraph. While Kerr (1979) did move the thyroid closer to the front surface of the neck-and-head region for his studies of doses from external irradiation, Hwang et al. (1976, p.3) moved the thyroid "slightly back towards the center of the lower head section and in[to] a more natural position." The thyroid as given here and in Cristy (1980) was moved backwards deeper into the neck-and-head region, like Hwang et al. but unlike Kerr. The position as given here is better for internal dosimetry but worse for external dosimetry.

Cristy (1985) has recently modified the neck-and-head region in developing a Japanese adult phantom for the A-bomb dose reassessment study, with the purpose of making the neck and thyroid region suitable for either external or internal dosimetry. However, the parameters as given therein will probably be changed and parameters for our Western phantoms have not been finalized. Note that this is a problem for external dosimetry only.

Urinary bladder and contents. The bladder wall is represented by the volume between two concentric ellipsoids. The contents are represented by the volume within the inner ellipsoid. The wall is defined by

$$\left(\frac{x}{a}\right)^2 + \left(\frac{y - y_0}{b}\right)^2 + \left(\frac{z - z_0}{c}\right)^2 \le 1$$

$$\text{and } \left(\frac{x}{a-d}\right)^2 + \left(\frac{y-y_0}{b-d}\right)^2 + \left(\frac{z-z_0}{c-d}\right)^2 \geq 1.$$

The contents are defined by

$$\left(\frac{x}{a-d}\right)^2 + \left(\frac{y-y_0}{b-d}\right)^2 + \left(\frac{z-z_0}{c-d}\right)^2 \geq 1.$$

Phantom	a	b	c	d	y_0	z_0	Volume-wall (cm^3)	Volume-contents (cm^3)
Newborn	1.69	1.82	1.14	0.10	-2.21	2.47	2.77	11.9
Age 1	2.35	2.42	1.64	0.14	-2.93	3.51	7.41	31.7
Age 5	3.04	2.77	2.16	0.17	-3.38	4.66	14.0	62.2
Age 10	3.61	3.04	2.63	0.20	-3.78	5.81	22.3	98.6
15-AF	4.27	3.38	3.11	0.23	-4.41	7.21	34.5	154
Adult male	4.958	3.458	3.458	0.252	-4.50	8.00	45.7	203

Dose to the bladder wall from a photon emitter present in the urine will vary greatly, depending on the degree of filling even for the same concentration or amount of activity present. The specific absorbed fraction, *(bladder wall - contents), will vary by approximately an order of magnitude in the adult, according to the calculations of Snyder, Ford, and Warner (1970). Thus, the reader should be aware that specific absorbed fractions calculated using these phantoms are appropriate only for one size of bladder. The variation in the specific absorbed fraction to bladder walls of different sizes from other source organs outside the bladder is generally small (Snyder 1970).

Uterus. The uterus is an ellipsoid cut by a plane and is given by

$$\left(\frac{x}{a}\right)^2 + \left(\frac{y-y_0}{b}\right)^2 + \left(\frac{z-z_0}{c}\right)^2 \leq 1$$

$$\text{and } \; y \geq y_1.$$

The uterus in the age-15-male/adult-female phantom has been changed from that in the age 15 phantom of Cristy (1980), to represent an adult female rather than an adolescent. The volume was calculated from data given in ICRP Publication 23 (ICRP 1975).

The uterus in the "Adult male" phantom was also modified to be consistent with the change in the "15-AF" phantom. The shapes are slightly different because of differences in trunk shape in the two phantoms. Generally organ shapes were allowed to change according to change in trunk shape, unless there was information to the contrary (see Cristy, 1980).

Phantom	a	b	c	y_0	z_0	y_1	Volume (cm^3)
Newborn	0.83	2.57	0.49	-0.98	4.32	-2.27	3.70
Age 1	0.61	1.80	0.36	-1.30	6.14	-2.20	1.40
Age 5	0.78	2.00	0.47	-1.50	8.16	-2.51	2.60
Age 10	0.91	2.17	0.57	-1.68	10.16	-2.78	4.00
15-AF	2.47	5.61	1.55	-1.96	12.62	-4.77	76.0
Adult male	2.62	5.22	1.57	-2.00	14.00	-4.62	76.0

REFERENCES FOR APPENDIX A

Coffey, J.L. 1978. *A revised mathematical model of the heart for use in radiation absorbed dose calculations.* MS. thesis, Univ. Tenn., Knoxville.

Coffey, J.L., Cristy, M., and Warner, G.G. 1981. Specific absorbed fractions for photon sources uniformly distributed in the heart chambers and heart wall of a heterogeneous phantom. MIRD Pamphlet No. 13. J. Nucl. Med 22: 65-71.

Cristy, M. 1980. *Mathematical phantoms representing children of various ages for use in estimates of internal dose.* U.S. Nuclear Regulatory Commission Rep. NUREG/CR-1159 (also Oak Ridge National Laboratory Rep. ORNL/NUREG/TM-367).

Cristy, M. 1981. Active bone marrow distribution as a function of age in humans. *Phys. Med. Biol*. 26: 389-400.

Cristy, M. 1982. Representative breast size of reference female. *Health Phys.* 43: 930-932.

Cristy, M. 1984. Calculation of annual limits of intake of radionuclides by workers: significance of breast as an explicitly represented tissue. *Health Phys.* 46: 283-291.

Cristy, M. 1985. *Mathematical phantoms for use in reassessment of radiation doses to Japanese A-bomb survivors.* Oak Ridge National Laboratory Rep. ORNL/TM-9487.

Custer, R.P. 1974. *An atlas of the blood and bone marrow*, 2nd ed. Philadelphia: W. B. Saunders.

Dickerson, J.W.T. 1962. Changes in the composition of the human femur during growth. *Biochem. J.* 82: 56-61.

Fomon, S.J. 1966. Body composition of the infant: I. The male "reference infant. " In *Human development*, ed. F. Falkner, pp. 239-245. Philadelphia: W. B. Saunders.

Forbes, G.B. 1952. Chemical growth in man. *Pediatrics* 9: 58.

Hashimoto, M. 1960. The distribution of active marrow in the bones of normal adult. *Kyushu J. Med. Sci*. 11: 103-l 11.

Holtzman, R.B. 1962. Desirability of expressing concentrations of mineral-seeking constituents of bone as a function of ash weight. *Health Phys.* 8: 315-319.

Hudson, G. 1965. Bone-marrow volume in the human foetus and newborn. *Brit. J. Haemat.* 11: 446-452.

Hwang, J.M.L., Shoup, R.L., and Poston, J.W. 1976. *Modifications and additions to the pediatric and adult mathematical phantoms.* Oak Ridge National Laboratory Rep. ORNL/TM-5454.

International Commission on Radiological Protection. 1975. *Report of the task group on Reference Man*. ICRP Publication 23. Oxford: Pergamon Press.

International Commission on Radiological Protection. 1980. Limits for intake of radionuclides by workers. ICRP Publication 30, Part 2. *Annals of the ICRP* 4: No. 3/4.

Katch, V.L., Campaigne, B., Freedson, P., Sady, S., Katch, F.I., and Behnke, A.R. 1980. Contribution of breast volume and weight to body fat distribution in females. *Am. J. Phys. Anthropol.* 53: 93-100.

Kerr, G.D. 1979. Organ dose estimates for the Japanese atomic-bomb survivors. *Health Phys.* 37: 487-508.

Kerr, G.D. 1982. *Photon and neutron fluence-to-kerma conversion factors for ICRP-1975 Reference Man using improved elemental compositions for bone and marrow of the skeleton.* Oak Ridge National Laboratory Rep. ORNL/TM-83 18.

Klose, E. 1914. Zur Kenntnis der Körperzusammensetzung bei Ernährungsstörungen. *Jahrb. f. Kinderh*. 80: 154187.

Kramer, R., and Drexler, G. 1981. Representative breast size of reference female. *Health Phys.* 40: 913-914.

Kramer, R., Williams, G., and Drexler, G. 1982. Reply to M. Cristy. *Health Phys.* 43: 932-935.

Mitchell, H.H., Hamilton, T.S., Steggerda, F.R., and Beam, H.W. 1945. The chemical composition of the adult human body and its bearing on the biochemistry of growth. *J. Biol. Chem.* 158: 625-637.

Ryman, J.C., Warner, G.G., and Eckerman, K.F. 1987. *ALGAMP--A Monte Carlo radiation transport code for calculating speci'c absorbed fractions of energy from internal or external photon sources. Oak* Ridge National Laboratory Rep. ORNL/TM-8377 (in preparation).

Snyder, W.S. 1970. Estimation of absorbed fraction of energy from photon sources in body organs. In *Medical radionuclides: radiation dose and effects, proc. symp. held at the Oak Ridge Associated Universities, December 8-11, 1969.* CONF-691212, pp. 33-49.

Snyder, W.S., Ford, M.R., and Warner, G.G. 1970. Estimation of dose and dose commitment to bladder wall from a radionuclide present in urine. *Health Phys. Div. Annu. Prog. Rep. July 31, 1970.* Oak Ridge National Laboratory Rep. ORNL-4584, pp. 206-208.

Snyder, W.S., Ford, M.R., Warner, G.G., and Watson, S.B. 1974. *A tabulation of dose equivalent per microcurie-day for source and target organs of an adult for various radionuclides: Part 1*. Oak Ridge National Laboratory Rep. ORNL-5000.

Swanson, W.W., and Iob, V. 1940. Growth and chemical composition of the human skeleton, *Am. J. Dis. Child.* 59: 107-l 11.

Widdowson, E.M., and Spray, C.M. 1951. Chemical development *in utero. Arch. Dis. Child*. 26: 205-214.

Woodard, H.Q., and Holodny, E. 1960. A summary of the data of Mechanik on the distribution of human bone marrow. *Phys. Med. Biol.* 5: 57-59.

APPENDIX B

SUMMARY OF ORGAN MASSES IN ALL PHANTOMS

The organ masses now used with the phantom series and given in Table B-3 are slightly different from the values initially given by Cristy (1980). This is a result of changes in the tissue densities assumed for the three tissue types (lung, skeleton, and soft tissue) considered in the Monte Carlo calculations. Cristy used the density values of Snyder, Ford, Warner, and Watson (1974) when he tabulated the organ mass values in his report. We have since examined the density data (see Appendix A) and, noting the design approach of Cristy, have made some minor changes in the organ density values. It should be appreciated that the assumed density values not only determine the mass of the organ from its geometric volume but also the linear cross-sections for photon interaction in the organs.

It is important to understand that Cristy viewed the design of the phantom series as a geometry problem where volume, not mass, values were of prime interest. Consider, for example, the design of a particular organ in the phantom whose mass (*M*) and specific gravity or density (*d*) are available from ICRP Publication 23 (ICRP 1975). A volume of *M/d* is thus associated with the organ. Note that the value of d cited in ICRP Publication 23 for the specific organ under consideration was used to derive the organ volume, a volume which Cristy refers to as the "targeted volume" in that the design was targeted to this volume.

In the Monte Carlo calculations only three tissue densities are considered. During the course of preparing the data for these calculations it became apparent that the density values of Snyder et al. were not consistent with the design approach of Cristy. Although these differences were minor, we felt that this inconsistency should be removed prior to undertaking the calculations for the entire series. In Table B-l are given the density values of the adult phantom of Snyder et al. and the newer values.

Review of the data in ICRP Publication 23 (see Appendix A) indicates that a soft tissue density of approximately 1.04 g/cm^3 is representative of soft tissue organs. Further we noted that a skeletal density of 1.4 g/cm^3 is in agreement with the Reference Man data. The lung density value was not changed, other than to carry fewer significant figures into the calculations. These density values result in a total body density of about 1.07 g/cm^3, which is in good agreement with the literature.

We have changed the density of the skeleton to 1.4 g/cm^3, which reduces the mass of the skeleton by about 7%. Also, note that ICRP Publication 23 lists no data for skeletal weights except for the newborn and adults. The graph of skeletal weights vs age (ICRP 1975, p. 63) was generated from the observation that "Jackson . . . has indicated that the weight of the skeleton as % W [% of body weight] is approximately constant during the postnatal period". Cristy incorporated this observation into his phantom design procedure as meaning that the skeletal volume as % of body volume was approximately constant. With the imprecision inherent in the skeletal mass estimates of ICRP Publication 23, a change of 7% is unimportant.

Table B-l. Tissue densities in g/cm^3

Tissue	Adult phantom of Snyder et al.	Phantoms of this report (except newborn)	Newborn phantom
Skeletal	1.4862	1.4	1.22
Lung	0.2958	0.296	0.296
Soft	0.9869	1.04	1.04

For the purpose of estimating specific absorbed fractions from photons, too much attention to small differences between derived and reference mass values of ICRP Publication 23 is not warranted. As mentioned above, the construction of the phantoms is a volume problem; furthermore, Cristy (1981) has shown that if the design approach had been to obtain correct (numerical value) masses at the expense of correct (numerical) volumes, the errors in the specific absorbed fraction would have been larger than with his approach. Thus the approach taken is more accurate than the alternate method with a phantom having accurate organ masses but poorer volume descriptions. We should also remember that, numerically, the differences in masses introduced by the revised density values are trivial, certainly small in relation to normal variations within a population.

For the purpose of estimating specific absorbed fractions from photons, we view the adult male phantom simply as a model for the 70-kg Reference Man, the fifteen-year-old-male/adult-female phantom as a model for either the 58-kg Reference Woman or a 55-kg fifteen-year-old male, the age 10 phantom as a model for a 32-to-33-kg male or female child, and so on, even though the masses of organs in the phantoms and the masses of the phantoms themselves may be slightly different from values in ICRP Publication 23 (1975). A comparison of whole-body masses between the phantoms and humans is given in Table B-2. In Table B-3 in the identifying heading we give the nominal value of whole-body mass from Table B-2 rather than the actual mass of the phantom; the actual mass of each phantom is given in the body of the table. We recommend use of the organ masses from ICRP Publication 23 (1975), especially for the 70-kg adult male, for all other purposes, e.g., for computing Φ-values from non-penetrating radiations. If masses of organs in children are not available, the masses in the phantoms could be used with little error.

Table B-2. Comparison of whole-body masses

Phantom	Whole-body mass of phantom (kg)		Age	Whole-body mass of human (kg)[e]	
	Actual	Nominal		Female	Male
Newborn	3.6	3.4	Newborn	3.4	3.4[f]
Age 1	9.7	9.8	1 year	9.5	10.1
Age 5	19.8	19	5 years	18.6	18.8
Age 10	33.2	32	10 years	31.9	32.7
15-AF[a]	56.8[b]	55-58[d]	15 years	51.6	54.5
Adult male	73.7[c]	70	Adult	56.7 (58)[g]	71.7 (70)[g]

[a]Age-15-male/adult-female phantom.

[b]56.4 kg without the female breasts.

[c]73.3 kg without the female breasts.

[d]55 kg for age 15 male and 58 kg for adult female.

[e]Data for ages newborn to 15 years are from Watson and Lowrey (1967). Data for adults are from ICRP Publication 23, p, 13.

[f]3.5 kg for newborn male is given in ICRP Publication 23.

[g]Reference whole-body masses were rounded to 58 and 70 kg for adult females and males in ICRP Publication 23.

Table B-3. Summary of organ masses in all phantoms

Organ	Mass (g) of organ in each phantom					
	Newborn 3.4kg	Age 1 9.8 kg	Age 5 19 kg	Age 10 32 kg	15-AF 55-58 kg	Adult male 70 kg
Skeletal system—active marrow	47.0	150	320	610	1050	1120
Leg bones—upper portion[a]	0.879	3.11	10.9	28.8	48.3	37.5
Leg bones—middle portion[a]	1.75	5.82	20.1	37.5	21.4	0
Leg bones—lower portion[a]	7.63	20.1	37.0	33.6	0	0
Arm bones—upper portion[a]	1.09	3.62	7.55	15.2	33.0	25.7
Arm bones—middle portion[a]	1.09	3.38	6.98	9.88	7.35	0
Arm bones—lower portion[a]	2.85	6.54	9.22	6.47	0	0
Pelvis	5.48	24.7	74.7	175	353	373
Spine—upper portion[b]	1.08	2.82	4.67	11.0	23.6	29.8
Spine—middle portion[b]	4.42	13.9	30.7	71.9	155	195
Spine—lower portion[b]	0.893	5.06	17.2	40.4	87.0	110
Skull—cranium	12.3	35.4	41.8	56.6	72.8	62.4
Skull—facial skeleton	1.52	5.81	14.0	21.0	33.5	30.8
Ribs	4.32	14.4	33.9	79.4	171	215
Clavicles	0.376	1.25	2.72	5.43	10.3	8.85
Scapulae	1.27	4.10	8.70	17.6	34.2	31.9
Skeletal system—active marrow	0	20.0	140	590	1550	2380
Leg bones—upper portion[a]	0	0.168	3.30	19.5	59.4	112
Leg bones—middle portion[a]	0	0.744	8.33	59.5	194	298
Leg bones—lower portion[a]	0	9.07	55.0	236	568	763
Arm bones—upper portion[a]	0	0.194	2.28	10.3	40.6	76.4
Arm bones—middle portion[a]	0	0.442	2.88	15.6	66.5	102
Arm bones—lower portion[a]	0	3.49	16.9	72.3	144	191
Pelvis	0	1.36	18.6	70.0	206	382
Spine—upper portion[b]	0	0.156	0.854	2.77	7.91	12.6
Spine—middle portion[b]	0	0.764	5.53	18.3	51.8	83.3
Spine—lower portion[b]	0	0.280	3.09	10.3	29.5	46.9
Skull—cranium	0	1.95	10.7	30.8	59.8	101
Skull—facial skeleton	0	0.320	3.57	11.4	27.5	50.0
Ribs	0	0.780	6.05	20.2	57.4	91.9
Clavicles	0	0.070	0.742	3.13	9.46	17.9
Scapulae	0	0.212	2.24	9.68	28.2	51.6
Skeletal system—active marrow	351	1140	2710	4630	7650	10000
Leg bones—upper portion[a]	20.1	70.9	217	440	792	1090
Leg bones—middle portion[a]	29.9	111	332	667	1180	1590
Leg bones—lower portion[a]	24.8	108	304	628	969	1240
Arm bones—upper portion[a]	20.9	63.9	126	213	386	505
Arm bones—middle portion[a]	15.7	48.0	95.0	160	290	379
Arm bones—lower portion[a]	18.8	57.5	114	192	347	454
Pelvis	35.2	106	212	361	645	849
Spine—upper portion[b]	16.4	46.1	76.4	117	183	232
Spine—middle portion[b]	32.5	96.6	193	325	586	767
Spine—lower portion[b]	12.2	36.2	72.6	122	220	288
Skull—cranium	60.8	194	475	607	712	865
Skull—facial skeleton	7.47	31.9	159	226	327	427
Ribs	41.5	122	243	413	744	972
Clavicles	3.20	9.59	19.2	32.4	58.3	76.5
Scapulae	11.8	35.4	70.6	120	216	283

Table B-3 (continued)

Organ	Mass (g) of organ in each phantom					
	Newborn 3.4kg	Age 1 9.8 kg	Age 5 19 kg	Age 10 32 kg	15-AF 55-58 kg	Adult male 70 kg
Adrenals	5.83	3.52	5.27	7.22	10.5	16.3
Brain	352	884	1260	1360	1410	1420
Breasts—including skin	0.205	1.10	2.17	3.65	407	403
Breasts—excluding skin	0.107	0.732	1.51	2.60	361	351
Gall bladder contents	2.12	4.81	19.7	38.5	49.0	55.7
Gall bladder wall	0.408	0.910	3.73	7.28	9.27	10.5
GI tract						
—LLI[c] contents	6.98	18.3	36.6	61.7	109	143
—LLI[c] wall	7.96	20.6	41.4	70.0	127	167
—SI[c] contents and wall	52.9	138	275	465	838	1100
—stomach contents	10.6	36.2	75.1	133	195	260
—stomach wall	6.41	21.8	49.1	85.1	118	153
—ULI[c] contents	11.2	28.7	57.9	97.5	176	232
—ULI[c] wall	10.5	27.8	55.2	93.4	168	220
Heart contents	36.5	72.7	134	219	347	454
Heart wall	25.4	50.6	92.8	151	241	316
Kidneys	22.9	62.9	116	173	248	299
Liver	121	292	584	887	1400	1910
Lungs	50.6	143	290	453	651	1000
Ovaries	0.328	0.714	1.73	3.13	10.5	8.71[e]
Pancreas	2.80	10.3	23.6	30.0	64.9	94.3
Remaining tissue[d]	2360	6400	13300	23100	40000	51800
Skin	118	271	538	888	2150	3010
Spleen	9.11	25.5	48.3	77.4	123	183
Testes	0.843	1.21	1.63	1.89	15.5	39.1
Thymus	11.3	22.9	29.6	31.4	28.4	20.9
Thyroid	1.29	1.78	3.45	7.93	12.4	20.7
Urinary bladder contents	12.4	32.9	64.7	103	160	211
Urinary bladder wall	2.88	7.70	14.5	23.2	35.9	47.6
Uterus	3.85	1.45	2.70	4.16	79.0	79.0
Whole body —actual mass	3.60 kg	9.72 kg	19.8 kg	33.2 kg	56.8 kg[f]	73.7 kg[g]
Whole body —nominal mass	3.4 kg	9.8 kg	19 kg	32 kg	55-58 kg	70 kg

[a]The upper, middle, and lower portions of the leg bones and arm bones are defined in Table A-6 of Appendix A.

[b]The upper, middle, and lower portions of the spine are defined in the section of Appendix A defining the spine.

[c]LLI = lower large intestine, ULI = upper large intestine, and SI = small intestine.

[d]The "remaining tissue" compartment is that part of a phantom remaining when all the organs specifically defined have been removed. It is used to model muscle in the tables of specific absorbed fractions in the companion volumes.

[e]The ovaries in the "adult male" phantom have not been modified from those of Snyder et al. (1974) and are smaller than those in the "15-AF" phantom. For recommended values of specific absorbed fractions in the companion volumes, values of Φ(ovaries←ovaries) derived from the "15-AF" phantom are tabulated for both the "age 15 male or adult female" and the "adult male or large adult female."

[f]56.4 kg without the female breasts.

[g]73.3 kg without the female breasts.

REFERENCES FOR APPENDIX B

Cristy, M. 1980. *Mathematical phantoms representing children of various ages for use in estimates of internal dose.* U.S. Nuclear Regulatory Commission Rep. NUREG/CR-1159 (also Oak Ridge National Laboratory Rep. ORNL/NUREG/TM-367).

Cristy, M. 1981. Development of mathematical pediatric phantoms for internal dose calculations: designs, limitations, and prospects. In *Third International Radiopharmaceutical Dosimetry Symposium, proc. conf held at Oak Ridge, Tennessee, October 7-10, 1980*, eds. E.E. Watson, A.T. Schlafke-Stelson, J.L. Coffey, and R.J. Cloutier. HHS Publication FDA 81-8166.

International Commission on Radiological Protection. 1975. *Report of the task group on Reference Man.* ICRP Publication 23. Oxford: Pergamon Press.

Snyder, W.S., Ford, M.R., Warner, G.G., and Watson, S.B. 1974. *A tabulation of dose equivalent per microcurie-day for source and target organs of an adult for various radionuclides: Part 1*. Oak Ridge National Laboratory Rep. ORNL-5000.

Watson, E. H., and Lowrey, G. H. 1967. *Growth and development of children*, 5th ed. Chicago: Year Book Medical.

APPENDIX C

CENTROIDS OF ORGANS IN ALL PHANTOMS

The phantoms are designed to represent certain age classes, and the specific absorbed fractions are given according to these classes. However, some users of the data who are concerned with dose to individuals (as in nuclear medicine) may be interested in scaling the results according to body size rather than age. Since most organs are in the trunk, inter-organ distance varies most closely with trunk height. In Table C-l are given the trunk heights of the phantoms, which correspond to shoulder-to-crotch height.

In Table C-2 are given the centroids of the organs in each phantom. Users who have data on inter-organ distances in an individual for whom dose estimates are desired may wish to compare these distances with the corresponding distances in the phantoms as a further check.

Table C-l. Trunk heights of phantoms

Phantom	Trunk height (cm)
Newborn	21.6
Age 1	30.7
Age 5	40.8
Age 10	50.8
15-AF	63.1
Adult male	70.0

Table C-2. Centroids of organs

Organ	Centroid [(*x*, *y*, *z*) coordinates in cm] of organ in each phantom								
	Newborn			Age 1			Age 5		
Adrenals —left	1.41,	2.45,	12.31	1.54,	3.25,	17.49	2.00,	3.75,	23.24
Adrenals —right	-1.41,	2.45,	12.31	-1.54,	3.25,	17.49	-2.00,	3.75,	23.24
Brain	0.00,	0.00,	30.70	0.00	0.00,	43.05	0.00,	0.00,	54.71
Breasts—left[a]	3.22,	-4.34,	16.05	4.48,	-5.82,	22.81	5.82,	-6.74,	30.31
Breasts—right[a]	-3.22,	-4.34,	16.05	-4.48,	-5.82,	22.81	-5.82,	-6.74,	30.31
Gall bladder contents	-0.12,	-1.32,	10.06	-0.59,	-1.99,	13.70	-0.42,	-2.26,	18.37
Gall bladder wall	-0.12,	-1.32,	10.06	-0.55,	-1.96,	13.88	-0.36,	-2.22,	18.65
GI tract									
—LLI[b] contents	2.48,	-0.45,	4.06	3.44,	-0.61,	5.79	4.47,	-0.70,	7.67
—LLI[b] wall	2.23,	-0.34,	3.36	3.10,	-0.45,	4.78	4.04,	-0.52,	6.36
—SI[b] contents and wall	0.11,	-0.51,	6.64	0.16,	-0.67,	9.44	0.20,	-0.78,	12.54
—stomach contents	2.54,	-1.96,	10.80	3.52,	-2.70,	15.35	4.58,	-3.15,	20.40
—stomach wall	2.54,	-1.96,	10.80	3.52,	-2.70,	15.35	4.58,	-3.15,	20.40
—ULI[b] contents	-1.17,	-1.16,	7.04	-1.64,	-1.53,	10.00	-2.10,	-1.77,	13.28
—ULI[b] wall	-1.17,	-1.16,	7.04	-1.64,	-1.53,	10.00	-2.10,	-1.77,	13.28
Heart contents	-0.02,	-1.68,	15.97	-0.01,	-2.43,	22.33	0.16,	-2.68,	29.47
Heart wall	0.68,	-2.08,	15.55	0.89,	-2.91,	21.77	1.26,	-3.16,	28.75
Kidneys —left	2.02,	2.94,	10.03	2.82,	3.90,	14.25	3.64,	4.50,	18.94
Kidneys —right	-2.02,	2.94,	10.03	-2.82,	3.90,	14.25	-3.64,	4.50,	18.94
Liver	-2.40,	-1.23,	11.18	-3.45,	-1.53,	15.97	-4.60,	-1.63,	21.22
Lungs —left	2.93,	0.49,	16.46	4.03,	0.50,	23.40	5.23,	0.53,	31.08
Lungs —right	-2.87,	0.14,	16.25	-3.91,	0.12,	23.11	-5.06,	0.09,	30.68
Ovaries —left	1.91,	0.00,	4.63	2.64,	0.00,	6.58	3.44,	0.00,	8.74
Ovaries —right	-1.91,	0.00,	4.63	-2.64,	0.00,	6.58	-3.44,	0.00,	8.74
Pancreas	1.24,	0.00,	11.56	1.67,	0.00,	16.45	2.25,	0.00,	21.88
Spleen	3.54,	1.42,	11.42	4.94,	1.85,	16.23	6.40,	2.25,	21.57
Testes —left	0.36,	-2.58,	-0.64	0.41,	-3.73,	-0.72	0.45,	-4.98,	-0.80
Testes —right	-0.36,	-2.58,	-0.64	-0.41,	-3.73,	-0.72	-0.45,	-4.98,	-0.80
Thymus	0.00,	-3.60,	19.30	0.00,	-4.75,	27.00	0.00,	-5.48,	35.00
Thyroid	0.00,	-2.58,	22.50	0.00,	-3.36,	31.69	0.00,	-3.92,	42.04
Urinary bladder contents	0.00,	-2.21,	2.47	0.00,	-2.93,	3.51	0.00,	-3.38,	4.66
Urinary bladder wall	0.00,	-2.21,	2.47	0.00,	-2.93,	3.51	0.00,	-3.38,	4.66
Uterus	0.00,	-0.66,	4.32	0.00,	-1.08,	6.14	0.00,	-1.25,	8.16

Table C-2. Centroids of organs (continued)

Organ	Centroid [(*x*, *y*, *z*) coordinates in cm] of organ in each phantom								
	Age 10			15-AF			Adult male		
Adrenals —left	2.43,	4.20,	28.94	3.02,	4.90,	35.87	3.50,	5.00,	39.88
Adrenals —right	-2.43,	4.20,	28.94	-3.02,	4.90,	35.87	-3.50,	5.00,	39.88
Brain	0.00,	0.00,	65.99	0.00,	0.00,	79.07	0.00,	0.00,	86.85
Breasts—left[a]	7.05,	-7.57,	37.73	9.23,	-9.89,	46.86	10.54,	-10.09,	52.00
Breasts—right[a]	-7.05,	-7.57,	37.73	-9.23,	-9.89,	46.86	-10.54,	-10.09,	52.00
Gall bladder contents	-1.43,	-2.50,	22.85	-3.63,	-2.89,	28.18	-4.16,	-2.94,	31.19
Gall bladder wall	-1.35,	-2.44,	23.20	-3.51,	-2.81,	28.55	-4.05,	-2.85,	31.59
GI tract									
—LLI[b] contents	5.44,	-0.78,	9.57	6.76,	-0.91,	11.90	7.80,	-0.92,	13.14
—LLI[b] wall	4.93,	-0.59,	7.93	6.11,	-0.68,	9.83	7.05,	-0.70,	10.93
—SI[b] contents and wall	0.24,	-0.86,	15.61	0.29,	-1.00,	19.38	0.35,	-1.03,	21.50
—stomach contents	5.56,	-3.51,	25.40	6.90,	-3.92,	31.55	8.00,	-4.00,	35.00
—stomach wall	5.56,	-3.51,	25.40	6.90,	-3.92,	31.55	8.00,	-4.00,	35.00
—ULI[b] contents	-2.56,	-1.98,	16.54	-3.15,	-2.31,	20.55	-3.67,	-2.36,	22.80
—ULI[b] wall	-2.56,	-1.98,	16.54	-3.15,	-2.31,	20.55	-3.67,	-2.36,	22.80
Heart contents	0.12,	-2.87,	36.45	0.11,	-3.48,	44.92	0.27,	-3.37,	49.80
Heart wall	1.44,	-3.38,	35.55	1.65,	-4.03,	43.85	1.98,	-3.84,	48.64
Kidneys —left	4.40,	5.04,	23.59	5.43,	5.88,	29.30	6.28,	6.00,	32.50
Kidneys —right	-4.40,	5.04,	23.59	-5.43,	5.88,	29.30	-6.28,	6.00,	32.50
Liver	-5.94,	-1.56,	26.65	-7.68,	-1.65,	33.51	-8.92,	-1.62,	37.06
Lungs —left	6.30,	0.51,	38.70	7.72,	0.46,	47.55	9.00,	0.48,	53.23
Lungs —right	-6.08,	0.06,	38.20	-7.46,	0.03,	47.00	-8.64,	0.01,	52.60
Ovaries —left	4.17,	0.00,	10.89	5.18,	0.00,	13.52	6.00,	0.00,	15.00
Ovaries —right	-4.17,	0.00,	10.89	-5.18,	0.00,	13.52	-6.00,	0.00,	15.00
Pancreas	2.72,	0.00,	27.20	3.37,	0.00,	33.81	3.93,	0.00,	37.53
Spleen	7.65,	2.52,	26.85	9.49,	2.94,	33.35	11.00,	3.00,	37.00
Testes —left	0.47,	-6.15,	-0.84	0.96,	-7.10,	-1.69	1.30,	-8.00,	-2.30
Testes —right	-0.47,	-6.15,	-0.84	-0.96,	-7.10,	-1.69	-1.30,	-8.00,	-2.30
Thymus	0.00,	-6.13,	43.00	0.00,	-7.15,	52.00	0.00,	-7.30,	57.00
Thyroid	0.00,	-4.37,	52.43	0.00,	-4.84,	64.98	0.00,	-5.11,	72.25
Urinary bladder contents	0.00,	-3.78,	5.81	0.00,	-4.41,	7.21	0.00,	-4.50,	8.00
Urinary bladder wall	0.00,	-3.78,	5.81	0.00,	-4.41,	7.21	0.00,	-4.50,	8.00
Uterus	0.00,	-1.41,	10.16	0.00,	-1.26,	12.62	0.00,	-1.35,	14.00

[a]Excluding skin.
[b]LLI = lower large intestine, ULI = upper large intestine, and SI = small intestine.

APPENDIX D

DOSE-RESPONSE FUNCTIONS FOR SOFT TISSUES OF THE SKELETON

Calculations of absorbed dose to soft tissues within the skeleton have been hampered by difficulties in modeling the geometry of the bone/soft-tissue mixture. In this Appendix the absorbed dose in the soft tissue of the skeleton per unit photon fluence is formulated in terms of the physical and anatomical parameters governing the energy deposition. The resulting relationships are referred to as response functions, and we can estimate the absorbed dose by applying them to estimates of photon fluence in the skeleton derived from Monte Carlo transport calculations.

Absorbed Dose per Unit Fluence

Consider the trabeculation of a bone experiencing a fluence, $\psi(E)$, of photons of energy E. Let $m(TB)$, $m(AM)$, and $m(BS)$ denote the mass of trabecular bone (TB), active (red) marrow (AM), and endosteal tissue (or "bone surface," BS) adjacent to the surface of the trabeculae. If we index the type of interaction by i and the region in which it occurred by r, where $r = TB$ or AM, then the absorbed dose in active marrow, $D(AM)$, and in endosteal tissue, $D(BS)$, per unit fluence can be expressed as

$$\frac{D(AM)}{\Psi(E)} = \sum_r \frac{m(r)}{m(AM)} \sum_i \int_0^\infty \phi(AM \leftarrow r, T_i)\ (i/\rho)_r\ n_r(T_i)\ T_i\ dT_i \tag{D-1}$$

$$\frac{D(BS)}{\Psi(E)} = \sum_r \frac{m(r)}{m(BS)} \sum_i \int_0^\infty \phi(BS \leftarrow r, T_i)\ (i/\rho)_r\ n_r(T_i)\ T_i\ dT_i \tag{D-2}$$

where

$\varphi(AM \leftarrow r, T_i)$ is the absorbed fraction in AM from r for electrons of energy T_i,

$\varphi(BS \leftarrow r, T_i)$ is the absorbed fraction in BS from r for electrons of energy T_i,

$(i/\rho)_r$, $i=\tau$, σ, and κ, denotes the mass attenuation coefficients in medium r for the photoelectric, Compton, and pair-production interactions, respectively, and

$n_r(Ti)dTi$ denotes the number of electrons of energy between T_i and $T_i + dT_i$ liberated in region r per interaction i.

The mass ratios appearing in the above equations can be related to the mean chord lengths of the trabeculae, $<t>$, and marrow space, $<l>$, as measured by scanning the trabeculation in an isotropic manner (Beddoe, Darley, and Spiers 1976). Information on the mean chord lengths for various trabecular bones of the body as a function of age is given in Table D-l. Note that for all ages the parietal bone of the skull appears to be distinct from other trabecular bones, as indicated by the ratios of the mean chord-lengths. The mass ratios in Eq. (D-l) and (D-2) can be expressed in terms of the measured chord lengths:

$$\frac{m(TB)}{m(AM)} = \frac{\rho_{TB}}{\rho_{AM}} \frac{<t>}{<l>} \tag{D-3}$$

$$\frac{m(TB)}{m(BS)} = \frac{\rho_{TB}}{\rho_{AM}} \frac{<t>}{<4d>} \tag{D-4}$$

Table D-l. Mean chord- and ray-lengths (μm) for trabeculae and marrow cavities in various bones

Bones	Trabeculae[a]			Marrow cavities[a]			Ratio of mean chord lengths
	$<t>_\mu$	V_μ	$<t>_i$	$<l>_\mu$	V_μ	$<l>_i$	$<t>_\mu:<l>_\mu$
44-year-old male[b]							
Parietal	511	0.570	401	389	0.784	347	1.31
Cervical vertebra	279	0.719	240	910	0.894	861	0.307
Lumbar vertebra	247	1.11	260	1228	1.12	1299	0.201
Rib	265	1.49	330	1706	1.09	1786	0.155
Iliac crest	242	0.675	203	904	0.647	745	0.268
Femur head	232	0.665	193	1157	0.901	1099	0.200
Femur neck	314	0.914	301	1655	0.905	1576	0.190
9-year-old child[c]							
Parietal	539			306			1.76
Cervical vertebra	162			906			0.179
Lumbar vertebra	168			857			0.196
Rib	231			1133			0.204
Iliac crest	180			744			0.242
Femur head & neck	249			616			0.404
20-month-old child[b]							
Parietal	566	1.21	625	255	2.90	497	2.22
Lumbar vertebra	188	1.04	192	736	0.987	731	0.255
Rib	191	1.22	212	559	1.04	569	0.342
Iliac crest	181	1.31	209	575	0.869	535	0.315
Femur	197	0.865	184	788	1.13	839	0.250

[a]Notation: ($<t>\mu$, $V\mu$) and ($<l>\mu$,$V\mu$) denote the mean and the fractional variance under μ-randomness for the trabeculae and marrow cavities, respectively. $<t>_i$ and $<l>_i$ denote the mean ray-length for trabeculae and cavities, respectively. Lengths are in units of μm.

[b]Values were computed from the chord-length distributions of Whitwell (1973).

[c]See Tables 1 and 3 of Beddoe (1978).

$$\frac{m(AB)}{m(BS)} = \frac{<l>}{<4d>} \tag{D-5}$$

where ρ_{TB} and ρ_{AM} denote the density of bone and marrow and d is the distance over which the dose to endosteal tissue is averaged. We use a value for d of 10 μm from ICRP Publication 30 (1979).

About one-half of the mass of soft tissue within 10 μm of the surfaces of bone is associated with trabecular bone (ICRP 1975). The soft tissue of cortical bone is contained within small cavities (mostly the Haversian canals of about 50 μm diameter) within the bone matrix. The dose-response function for this component of the endosteal tissue is computed as the dose to a small tissue-filled cavity in an infinite extent of bone. The response function for the endosteal tissue of cortical bone is given as

$$\frac{D(BS)}{\Psi(E)} = \sum_i \int_0^\infty (i/\rho)_r \; n_r(T_i) \; T_i \; S(T_i) \, dT_i \quad , \tag{D-6}$$

where $S(T_i)$ denotes the ratio of the mass stopping power for soft tissue to that of bone at energy T_i. Stopping power data were computed with the procedures of Seltzer and Berger (1982a,b) and

the elemental composition of marrow and bone from Kerr (1982). The dose to endosteal tissues is taken as the average of that indicated by equations D-2 and D-3, since trabecular and cortical bone each contributes equally to the skeletal endosteal tissue.

Absorbed Fractions for Monoenergetic Electrons

Because the geometry of trabecular bone could not be described in simple terms, Spiers and co-workers (Spiers 1969; Whitwell and Spiers 1976; Spiers, Whitwell, and Beddoe 1978) introduced a method of calculating energy deposition using the path-lengths traversed by particles. These path-lengths are based on chord-length distributions for trabeculae and marrow cavities obtained by optically scanning the trabeculation (Beddoe et al. 1976). Absorbed fraction data for monoenergetic electrons, as required in Eq. (D-l), were computed (Eckerman 1986) following the methods outlined by Whitwell (1973) and Whitwell and Spiers (1976). Data for the parietal bone and lumbar vertebra of the skeleton of a 44-year-old male are shown in Fig. D-l and are tabulated in Table D-2; corresponding data for a child (age 20 months) are presented in Table D-3. In both subjects the

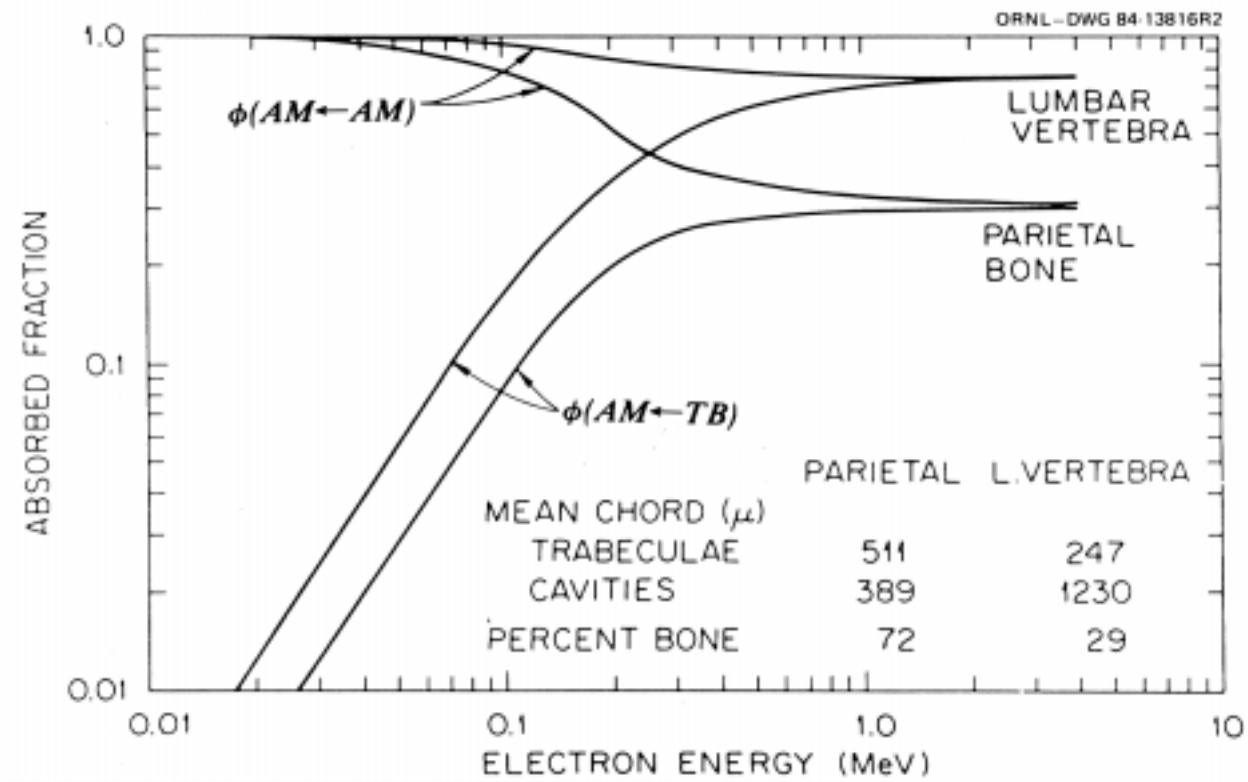

Fig. D-1. Absorbed fractions in active marrow *AM* from a source of monoenergetic electrons distributed uniformly in the trabeculae *TB* or the active marrow of the lumbar vertebra and parietal bone of the adult.

absorbed fraction data for other marrow sites were similar to that for the lumbar vertebra. Although some age dependence is indicated, it appears to be weak. (It should be remembered, however, that limited data are available for each kind of bone and for each age; it would be useful to have data from additional persons.)

Table D-2. Absorbed fraction, *φ*, in active marrow, *AM*, and bone surface, *BS*, from a uniformly distributed source of monoenergetic electrons in trabeculae, *TB*, and marrow of the parietal bone and lumbar vertebra of a 44-year-old male

Electron energy (MeV)	Parietal bone				Lumbar vertebra			
	$\varphi(AM \leftarrow TB)$	$\varphi(AM \leftarrow AM)$	$\varphi(BS \leftarrow AM)$	$\varphi(BS \leftarrow TB)$	$\varphi(AM \leftarrow TB)$	$\varphi(AM \leftarrow AM)$	$\varphi(BS \leftarrow AM)$	$\varphi(BS \leftarrow TB)$
0.010	1.95E-3	0.994	1.05E-1	1.95E-3	3.94E-3	0.999	3.87E-2	2.94E-3
0.015	3.29E-3	0.990	9.67E-2	3.29E-3	7.81E-3	0.997	3.77E-2	6.56E-3
0.020	5.77E-3	0.983	9.11E-2	5.77E-3	1.29E-2	0.996	3.51E-2	1.71E-2
0.030	1.23E-2	0.969	7.88E-2	1.14E-2	2.59E-2	0.991	3.06E-2	2.08E-2
0.040	1.98E-2	0.950	6.97E-2	1.54E-2	4.34E-2	0.985	2.82E-2	2.90E-2
0.050	2.94E-2	0.927	6.55E-2	1.85E-2	6.26E-2	0.979	2.75E-2	3.32E-2
0.060	4.03E-2	0.901	6.10E-2	2.04E-2	8.25E-2	0.971	2.68E-2	3.56E-2
0.080	6.34E-2	0.854	5.28E-2	2.18E-2	1.31E-1	0.953	2.51E-2	3.91E-2
0.10	8.80E-2	0.794	5.09E-2	2.37E-2	1.83E-1	0.935	2.58E-2	4.24E-2
0.15	1.53E-1	0.654	4.52E-2	2.65E-2	3.12E-1	0.888	2.82E-2	4.24E-2
0.20	1.99E-1	0.538	4.08E-2	2.84E-2	4.17E-1	0.848	2.78E-2	3.87E-2
0.30	2.58E-1	0.415	3.87E-2	2.98E-2	5.47E-1	0.808	2.84E-2	3.44E-2
0.40	2.71E-1	0.376	3.60E-2	2.96E-2	5.97E-1	0.793	2.90E-2	3.23E-2
0.50	2.76E-1	0.358	3.50E-2	3.00E-2	6.25E-1	0.779	2.86E-2	3.32E-2
0.60	2.82E-1	0.346	3.35E-2	3.05E-2	6.48E-1	0.767	2.85E-2	3.30E-2
0.80	2.88E-1	0.335	3.37E-2	3.09E-2	6.74E-1	0.765	2.87E-2	3.32E-2
1.0	2.93E-1	0.327	3.30E-2	3.09E-2	6.90E-1	0.757	2.88E-2	3.23E-2
2.0	2.97E-1	0.317	3.19E-2	3.11E-2	7.17E-1	0.747	2.94E-2	3.26E-2
3.0	3.00E-1	0.311	3.18E-2	3.11E-2	7.22E-1	0.747	2.90E-2	3.23E-2
4.0	3.01E-1	0.308	3.15E-2	3.11E-2	7.27E-1	0.744	2.88E-2	3.22E-2

Table D-3. Absorbed fraction, *φ*, in active marrow, *AM*, and bone surface, *BS*, from a uniformly distributed source of monoenergetic electrons in trabeculae, *TB*, and marrow of the parietal bone and lumbar vertebra of a 20-month-old child

Electron energy (MeV)	Parietal bone				Lumbar vertebra			
	$\varphi(AM \leftarrow TB)$	$\varphi(AM \leftarrow AM)$	$\varphi(BS \leftarrow TB)$	$\varphi(BS \leftarrow AM)$	$\varphi(AM \leftarrow TB)$	$\varphi(AM \leftarrow AM)$	$\varphi(BS \leftarrow TB)$	$\varphi(BS \leftarrow AM)$
0.01	1.62E-3	0.990	1.62E-3	1.40E-1	4.66E-3	0.997	4.66E-3	5.99E-2
0.015	3.44E-3	0.981	3.44E-3	1.33E-1	9.90E-3	0.995	9.90E-3	5.68E-2
0.02	6.09E-3	0.969	6.09E-3	1.21E-1	1.65E-2	0.992	1.65E-2	5.26E-2
0.03	1.24E-2	0.947	1.14E-2	1.01E-1	3.39E-2	0.984	3.16E-2	4.62E-2
0.04	1.91E-2	0.920	1.47E-2	9.04E-2	5.67E-2	0.973	4.24E-2	4.19E-2
0.05	2.80E-2	0.889	1.74E-2	7.98E-2	8.01E-2	0.962	4.83E-2	3.94E-2
0.06	3.46E-2	0.858	1.79E-2	6.97E-2	1.12E-2	0.949	5.37E-2	3.75E-2
0.08	5.12E-2	0.789	2.00E-2	6.28E-2	1.74E-1	0.922	5.83E-2	3.49E-2
0.10	7.09E-2	0.724	2.28E-2	5.73E-2	2.34E-1	0.892	5.68E-2	3.52E-2
0.15	1.06E-1	0.591	2.44E-2	4.67E-2	3.74E-1	0.829	5.30E-2	3.65E-2
0.20	1.30E-1	0.501	2.61E-2	4.21E-2	4.70E-1	0.786	4.78E-2	3.95E-2
0.30	1.54E-1	0.401	2.67E-2	3.76E-2	5.58E-1	0.750	4.37E-2	4.11E-2
0.40	1.68E-1	0.354	2.79E-2	3.49E-2	5.94E-1	0.730	4.20E-2	4.23E-2
0.50	1.76E-1	0.328	2.80E-2	3.34E-2	6.26E-1	0.722	4.16E-2	4.25E-2
0.60	1.79E-1	0.308	2.75E-2	3.26E-2	6.38E-1	0.718	4.12E-2	4.11E-2
0.80	1.81E-1	0.283	2.79E-2	3.18E-2	6.51E-1	0.706	4.09E-2	4.12E-2
1.0	1.88E-1	0.267	2.80E-2	3.09E-2	6.62E-1	0.708	4.18E-2	4.19E-2
2.0	1.96E-1	0.238	2.82E-2	2.96E-2	6.78E-1	0.698	4.12E-2	4.13E-2
3.0	1.99E-1	0.224	2.82E-2	2.92E-2	6.81E-1	0.696	4.12E-2	4.13E-2
4.0	2.01E-1	0.221	2.82E-2	2.89E-2	6.84E-1	0.696	4.09E-2	4.10E-2

Energy Distribution of Secondary Electrons

Photons transfer energy to electrons through three major interactions: the photoelectric effect, the Compton effect, and pair-production. Photon cross sections from Hubbell (1982) and elemental composition of tissue from Kerr (1982) were used in evaluating the energy transfer. Photoelectrons were assumed to be of discrete energy corresponding to the incident photon energy. The energy distribution of Compton electrons was calculated from the Klein-Nishina relationship (Evans 1969), and the positron-electron energy distribution was derived from the Bethe-Heitler theory of pair-production (Heitler 1964).

Dose per Unit Fluence

A complete set of dose-response functions for the active marrow of each trabecular bone of the adult is given in Table D-4. The contributions of electrons arising from photon interactions in bone

Table D-4. Absorbed dose in active marrow, *D(AM)*, per unit fluence, *Ψ(E)*, of monoenergetic photons in trabecular bones of the skeleton of a 44-year-old male

Photon energy (MeV)	*D(AM)/Ψ(E)*, Gy per photon/m^2						
	Parietal bone	Cervical vertebra	Lumbar vertebra	Rib	Iliac crest	Head of femur	Neck of femur
0.010	6.30E-16	6.16E-16	6.14E-16	6.12E-16	6.16E-16	6.13E-16	6.12E-16
0.015	2.71E-16	2.62E-16	2.61E-16	2.59E-16	2.63E-16	2.61E-16	2.59E-16
0.020	1.53E-16	1.45E-16	1.43E-16	1.41E-16	1.45E-16	1.43E-16	1.41E-16
0.030	7.49E-17	6.60E-17	6.44E-17	6.29E-17	6.61E-17	6.47E-17	6.31E-17
0.040	5.04E-17	4.27E-17	4.11E-17	3.99E-17	4.28E-17	4.14E-17	3.99E-17
0.050	4.18E-17	3.45E-17	3.31E-17	3.20E-17	3.45E-17	3.33E-17	3.21E-17
0.060	3.93E-17	3.26E-17	3.11E-17	3.01E-17	3.24E-17	3.13E-17	3.01E-17
0.080	4.15E-17	3.58E-17	3.45E-17	3.36E-17	3.57E-17	3.49E-17	3.37E-17
0.10	4.79E-17	4.33E-17	4.22E-17	4.14E-17	4.33E-17	4.25E-17	4.15E-17
0.15	7.16E-17	6.83E-17	6.74E-17	6.68E-17	6.83E-17	6.77E-17	6.70E-17
0.20	9.88E-17	9.63E-17	9.57E-17	9.52E-17	9.64E-17	9.59E-17	9.53E-17
0.30	1.57E-16	1.54E-16	1.54E-16	1.53E-16	1.54E-16	1.54E-16	1.53E-16
0.40	2.15E-16	2.12E-16	2.10E-16	2.10E-16	2.12E-16	2.11E-16	2.10E-16
0.50	2.72E-16	2.67E-16	2.66E-16	2.65E-16	2.68E-16	2.66E-16	2.65E-16
0.60	3.28E-16	3.20E-16	3.19E-16	3.17E-16	3.20E-16	3.18E-16	3.18E-16
0.80	4.28E-16	4.17E-16	4.15E-16	4.14E-16	4.17E-16	4.15E-16	4.14E-16
1.0	5.19E-16	5.06E-16	5.03E-16	5.01E-16	5.06E-16	5.04E-16	5.02E-16
1.5	7.13E-16	6.95E-16	6.91E-16	6.89E-16	6.94E-16	6.92E-16	6.90E-16
2.0	8.79E-16	8.56E-16	8.50E-16	8.47E-16	8.54E-16	8.51E-16	8.49E-16
3.0	1.17E-15	1.13E-15	1.12E-15	1.11E-15	1.13E-15	1.12E-15	1.12E-15
4.0	1.43E-15	1.37E-15	1.37E-15	1.35E-15	1.37E-15	1.36E-15	1.36E-15
5.0	1.67E-15	1.60E-15	1.59E-15	1.57E-15	1.60E-15	1.59E-15	1.58E-15
6.0	1.92E-15	1.82E-15	1.80E-15	1.78E-15	1.82E-15	1.80E-15	1.79E-15
8.0	2.41E-15	2.27E-15	2.23E-15	2.20E-15	2.26E-15	2.23E-15	2.22E-15
10.0	2.92E-15	2.71E-15	2.66E-15	2.62E-15	2.70E-15	2.67E-15	2.64E-15

and marrow to the absorbed dose in the active marrow are shown in Fig. D-2. The response function for the active marrow of the parietal bone is different from the response functions for the other sites. Considering the highly stylized model of the skeleton used in photon transport calculations, we recommend that the skull be treated as a separate bone region and data for the parietal bone in Table D-4 be applied to estimate marrow dose. The lumbar vertebra appears to be representative of other trabecular sites. Furthermore, we note that the age dependence in the microstructure of trabecular bone appears not to strongly influence the absorbed dose estimates for the active marrow. We thus recommend that the response functions of Table D-5 be used for all ages. These data can be applied to estimates of photon fluence from the Monte Carlo transport calculations in a phantom to estimate absorbed dose. Variations with incident photon energy in the ratio of absorbed dose in active marrow to the equilibrium dose (kerma) in soft tissue are indicated in Fig. D-3. The ratios are largest at photon energies to 50 to 60 keV and are higher for the thick trabeculae and small marrow cavities of the parietal bone than for the thinner trabeculae and larger marrow cavities of other bones. The ratios at low energies conform to the general features indicated by Spiers (1969). However, the parietal bone exhibits a substantially higher enhancement of the marrow dose than other trabecular bones. This enhancement should be considered in deriving skeletal average values for the diagnostic x-ray region. Enhancement of dose in the high-energy (pair-production) region is also indicated by our calculations. Enhancement is small, about 5%, for most trabecular sites but approaches 20% for the parietal bone.

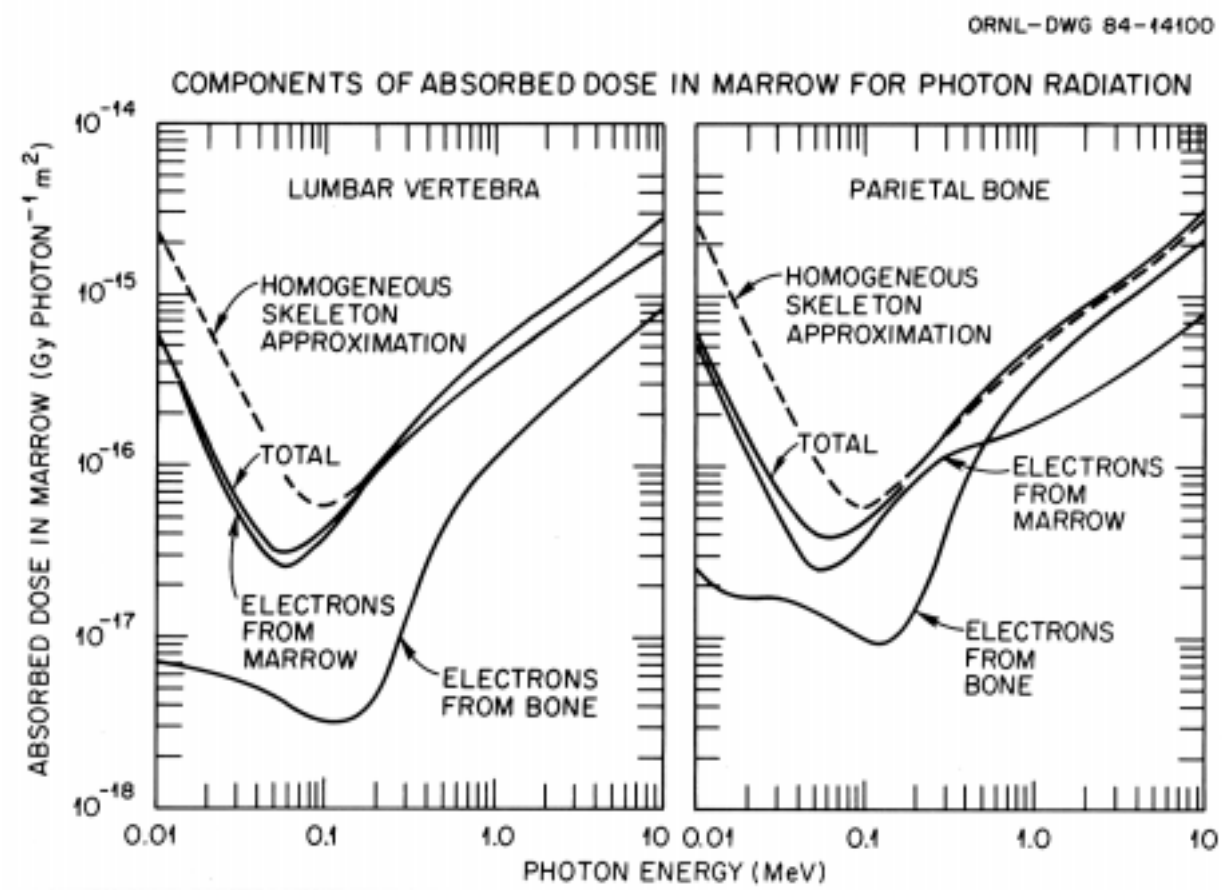

Fig. D-2. Components of the absorbed dose in marrow from photon radiations. The dotted curve shows the dose with the assumption that the active marrow absorbs energy per unit mass at the rate for the homogeneous skeleton approximation, as in Snyder et al. (1978).

Table D-5. Absorbed dose in active marrow, *D(AM)*, and in bone surface, *D(BS)*, per unit fluence, Ψ*(E)*, of monoenergetic photons in the skeleton

Photon energy (MeV)	*D(AM or BS)/Ψ(E)*, Gy per photon/m^2					
	Parietal bone		Lumbar vertebra		Cortical	Total[a]
	D(AM)	*D(BS)*	*D(AM)*	*D(BS)*	*D(BS)*	*D(BS)*
0.010	6.30E-16	8.47E-16	6.14E-16	9.43E-16	5.32E-15	3.13E-15
0.015	2.71E-16	4.17E-16	2.61E-16	4.98E-16	2.45E-15	1.47E-15
0.020	1.53E-16	2.98E-16	1.43E-16	3.39E-16	1.39E-15	8.65E-16
0.030	7.49E-17	2.00E-16	6.44E-17	2.12E-16	6.11E-16	4.12E-16
0.040	5.04E-17	1.42E-16	4.11E-17	1.51E-16	3.41E-16	2.46E-16
0.050	4.18E-17	1.09E-16	3.31E-17	1.10E-16	2.20E-16	1.65E-16
0.060	3.93E-17	8.75E-17	3.11E-17	8.69E-17	1.57E-16	1.22E-16
0.080	4.15E-17	6.61E-17	3.45E-17	7.03E-17	1.03E-16	8.67E-17
0.10	4.79E-17	6.32E-17	4.22E-17	6.76E-17	8.51E-17	7.64E-17
0.15	7.16E-17	7.96E-17	6.74E-17	8.90E-17	8.80E-17	8.85E-17
0.20	9.88E-17	1.05E-17	9.57E-17	1.22E-17	1.10E-16	1.16E-16
0.30	1.57E-16	1.65E-16	1.54E-16	1.98E-16	1.67E-16	1.83E-16
0.40	2.15E-16	2.26E-16	2.10E-16	2.65E-16	2.24E-16	2.45E-16
0.50	2.72E-16	2.85E-16	2.66E-16	3.30E-16	2.80E-16	3.05E-16
0.60	3.28E-16	3.38E-16	3.19E-16	3.94E-16	3.34E-16	3.64E-16
0.80	4.28E-16	4.37E-16	4.15E-16	5.09E-16	4.33E-16	4.71E-16
1.0	5.19E-16	5.29E-16	5.03E-16	6.12E-16	5.22E-16	5.67E-16
1.5	7.13E-16	7.23E-16	6.91E-16	8.37E-16	7.09E-16	7.73E-16
2.0	8.79E-16	8.89E-16	8.50E-16	1.03E-16	8.69E-16	9.49E-16
3.0	1.17E-15	1.18E-15	1.12E-15	1.36E-15	1.15E-15	1.26E-15
4.0	1.43E-15	1.44E-15	1.37E-15	1.65E-15	1.42E-15	1.54E-15
5.0	1.67E-15	1.70E-15	1.59E-15	1.93E-15	1.68E-15	1.81E-15
6.0	1.92E-15	1.95E-15	1.80E-15	2.20E-15	1.94E-15	2.07E-15
8.0	2.41E-15	2.46E-15	2.23E-15	2.74E-15	2.47E-15	2.61E-15
10.0	2.92E-15	2.99E-15	2.66E-15	3.28E-15	3.03E-15	3.16E-15

[a]Total represents the bone surface response of the skeleton and is computed as the average of the lumbar vertebra and cortical responses.